



TUTORIALS

Section Coordinator: F. Solana and S. Cicero
UNIVERSITY OF CANTABRIA - Spain

14 Tutorials

| | | |
|----------|--|----|
| 14.1 | Introduction | 3 |
| 14.2 | Fracture Tutorial: Failure Analysis of a Broken Forklift | 4 |
| 14.2.1 | Introduction | 4 |
| 14.2.2 | Inputs | 5 |
| 14.2.2.1 | Flaw information | 5 |
| 14.2.2.2 | Stresses | 6 |
| 14.2.2.3 | Material Properties | 7 |
| 14.2.3 | Assessment | 8 |
| 14.2.4 | References | 11 |
| 14.3 | Fracture Tutorial: Fracture Analysis of Mismatched Components | 12 |
| 14.3.1 | Introduction | 12 |
| 14.3.2 | Inputs | 12 |
| 14.3.2.1 | Flaw information | 12 |
| 14.3.2.2 | Stresses | 12 |
| 14.3.2.3 | Material Properties | 12 |
| 14.3.3 | Assessment | 14 |
| 14.3.4 | References | 20 |
| 14.4 | Fracture Tutorial: Embrittlement Effect on Fracture Assessments | 21 |
| 14.4.1 | Introduction | 21 |
| 14.4.2 | Inputs | 21 |
| 14.4.2.1 | Flaw information | 21 |
| 14.4.2.2 | Stresses | 21 |
| 14.4.2.3 | Material Properties | 22 |
| 14.4.3 | Assessment | 24 |
| 14.4.4 | References | 29 |
| 14.5 | Fatigue tutorial: Fatigue Analysis of a Scallop by using FITNET Fatigue Routes 1 and 2 [14.17] | 30 |
| 14.5.1 | Introduction | 30 |
| 14.5.2 | Inputs | 31 |
| 14.5.2.1 | Flaw Information | 31 |
| 14.5.2.2 | Stresses | 31 |
| 14.5.2.3 | Material Properties | 31 |
| 14.5.3 | Assessment | 32 |
| 14.5.3.1 | Route 1: Fatigue damage assessment using nominal stresses | 32 |
| 14.5.3.2 | Route 2: Fatigue damage assessment using structural or notch stresses | 34 |
| 14.5.4 | References | 35 |
| 14.6 | Fatigue tutorial: Application of Structural Stress Method on Welded Components [14.18] | 36 |
| 14.6.1 | Introduction | 36 |
| 14.6.2 | Inputs | 36 |
| 14.6.3 | Assessment | 36 |
| 14.6.4 | References | 39 |
| 14.7 | Creep tutorial: Flat Plate under Constant Tensile Load | 40 |
| 14.7.1 | Introduction | 40 |
| 14.7.2 | Inputs | 40 |
| 14.7.2.1 | Flaw information | 40 |
| 14.7.2.2 | Stresses | 40 |
| 14.7.2.3 | Material Properties | 40 |
| 14.7.3 | Assessment | 41 |
| 14.7.4 | References | 47 |
| 14.8 | Creep tutorial: Cylindrical Pipe with an Internal Crack under Cyclic Loading | 48 |
| 14.8.1 | Introduction | 48 |
| 14.8.2 | Inputs | 48 |
| 14.8.2.1 | Flaw information | 48 |
| 14.8.2.2 | Stresses | 48 |

| | |
|--|-----|
| 14.8.2.3 Material Properties | 48 |
| 14.8.3. Assessment..... | 49 |
| 14.8.4. References..... | 62 |
| 14.9. SCC tutorial: Failure Analysis of Different Pipes Containing an Internal Flaw | 63 |
| 14.9.1 Introduction | 63 |
| 14.9.2 Inputs | 63 |
| 14.9.2.1 Flaw information | 63 |
| 14.9.2.2 Stresses | 64 |
| 14.9.2.3 Material Properties | 65 |
| 14.9.3. Assessment..... | 65 |
| 14.10. LTA tutorial: Pipeline Local Thinned Area Assessment | 68 |
| 14.10.1. Introduction | 68 |
| 14.10.2. Inputs | 68 |
| 14.10.2.1 Flaw Information | 68 |
| 14.10.2.2 Stresses | 68 |
| 14.10.2.3 Material Properties | 68 |
| 14.10.3. Assessment..... | 68 |
| 14.10.3.1 Safe Working Pressure Estimate..... | 68 |
| 14.10.3.2 Allowable Remaining Wall Thickness for Internal Pressure | 69 |
| 14.11. Crossed tutorial: Failure Analysis of a Hip Implant | 70 |
| 14.11.1. Introduction | 70 |
| 14.11.2. Inputs | 70 |
| 14.11.2.1 Flaw information | 70 |
| 14.11.2.2 Stresses | 72 |
| 14.11.2.3 Material Properties | 73 |
| 14.11.3. Assessment..... | 73 |
| 14.11.4. References..... | 78 |
| 14.12. Crossed tutorial: Structural Integrity Assessment of Different Components of a Power Plant | 79 |
| 14.12.1. Introduction | 79 |
| 14.12.2. Failure analysis | 80 |
| 14.12.3. Proposed Solution, New Failures and Uncertainty | 81 |
| 14.12.4. Inputs | 81 |
| 14.12.4.1 Flaw information | 81 |
| 14.12.4.2 Stresses and working conditions | 83 |
| 14.12.4.3 Material Properties | 83 |
| 14.12.5. Assessment..... | 85 |
| 14.12.6. References..... | 87 |
| 14.13. Qualitative tutorial: Application of FITNET Philosophy to the Aeronautical Industry [14.42] | 88 |
| 14.13.1. List of abbreviations..... | 88 |
| 14.13.2. List of symbols | 89 |
| 14.13.3. Introduction | 91 |
| 14.13.4. FFS procedure for aeronautical application – general | 91 |
| 14.13.5. FFS procedure for pre-development/development/design phase | 92 |
| 14.13.6. FFS procedure for certification phase..... | 112 |
| 14.13.7. FFS procedure for in-service phase | 121 |
| 14.13.8. FFS procedure for in-service—Life extension phase | 129 |
| 14.13.9. Bibliography | 130 |

14.1 Introduction

FITNET Fitness-for-Service (FFS) Procedure consists of three volumes;

Volume I: FITNET FFS Procedure (Sections 1 to 12)

Volume II: Case Studies and Tutorials (Sections 13 and 14)

Volume III: FITNET FFS Annexes

This Volume II: Case studies and Tutorials, contains two Sections. **Section 13: Case studies and validation, Section 14: Tutorials.** First section aims to provide examples from validation works during the FITNET FFS Procedure development. Section 14 provides examples of the FFS applications in a more detailed manner. The materials used in Tutorials section was used in FITNET Training and Education Seminars which took place in Spain, Slovenia and Hungary during the project period.

This Volume presents the 7th version (MK7) of the FITNET FFS Procedure development work during the period of 2002 to 2006. It is called a “Final Draft”, implying for further revisions.

The FITNET FFS procedure has been validated in parallel with the development of the procedure. Numbers of case studies have been developed by the members and hence this section presents these case studies. The case studies themselves have been collected from a wide range of sources, such as international case benchmarks, integrity assessment trials, recent publications and works within the FITNET consortium etc., with the emphasis of covering the various aspects of the FITNET FFS procedure to produce verification of the different assessment modules.

Some well-documented examples presented in this Volume II have earlier been used in R6, BS7910 and SINTAP procedures. Therefore, this final draft has still tentative subsection and/or figure, equation numbers. They will be harmonised during the next revision.

Numbers of the case studies covered in this Section 13 are also presented in Section 14 (Tutorials) and covered in a much more detailed fashion to provide a clear and “step-by-step” use of the FITNET FFS Procedure. This is particularly important for the new users of the procedure in industry and academia.

To this Tutorials part, a special section was added which deals with the general guidelines of the assessment procedure of the damage tolerance behaviour of aerospace structures. This part provides prospects on the application of FITNET FFS philosophy to the aerospace structures. This part is in development and hence it is placed in Tutorials section to present the basic principles of the analysis.

14.2 Fracture Tutorial: Failure Analysis of a Broken Forklift

14.2.1 Introduction

This tutorial analyses the failure of a fork of a forklift. It broke in a brittle manner during transportation of an aluminium block of a weight of less than 3.5 tonnes per fork, while the load carrying capacity the fork was designed for is 3.5 tonnes. The failure happened at a temperature of about +10 °C. The geometry of the broken fork is shown in Figure 14.1. Originally two forks were fixed to the truck by screws.

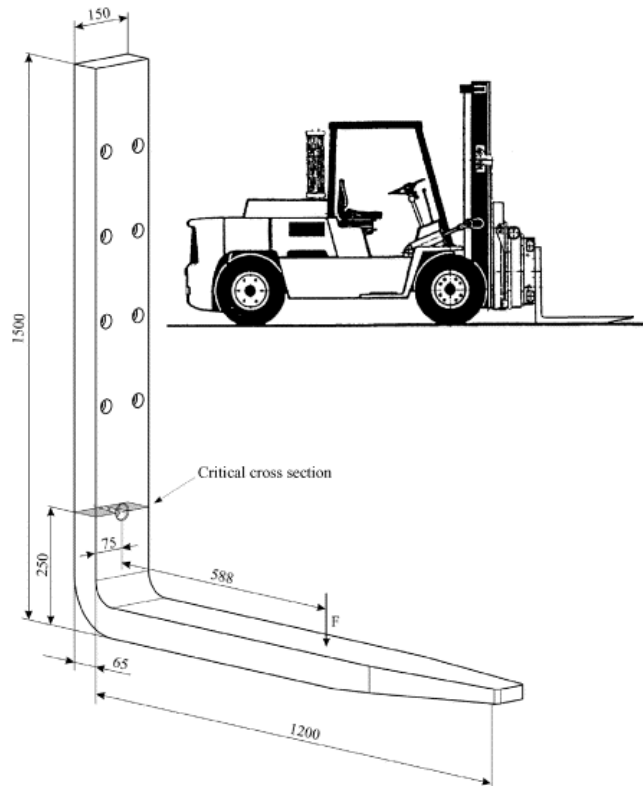


Figure 14.1 – Geometry and dimensions of the broken fork lift (all measures in mm).

The fracture surface is shown in Figure 14.2.

The aim of the present investigation is to figure out whether failure had to be expected for nominal loading and material conditions or if any other reason such as overloading or deficient material properties were the reason of failure.

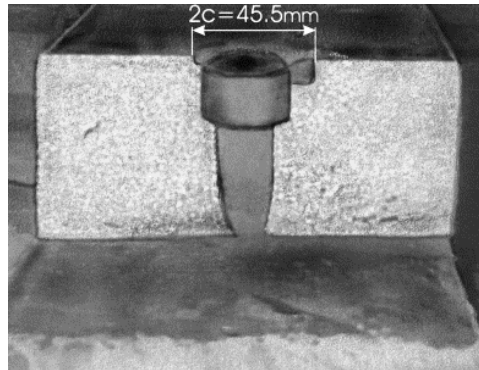


Figure 14.2 – Fracture surface of the broken fork. The failure originated at two edge cracks left and right from the hole at the top side.

14.2.2. Inputs

14.2.2.1 Flaw information

The geometry of the fork as given in Figure 14.1 is essentially a thick plate. The dimensions of the relevant cross section where fracture occurred are shown in Figure 14.3.

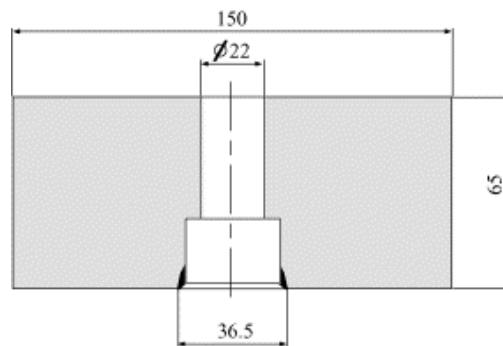


Figure 14.3 – Geometry and dimensions of the cross section where fracture occurred (all measures in mm).

Fracture mechanics analysis distinguishes between through cracks, embedded cracks and surface cracks. Real crack shapes are idealised by substitute geometries such as rectangles, ellipses and semi-ellipses. The idealisation has to be done such that the crack tip loading will be overestimated. Sometimes a crack or conglomerations of cracks have to be re-characterised if they interfere with each other or with a free surface. In the present case the two edge cracks are substituted by one through crack the dimensions of which include the whole diameter as demonstrated in Figure 14.4. For simplicity the crack is assumed to be of constant length $2c$ over the wall thickness.

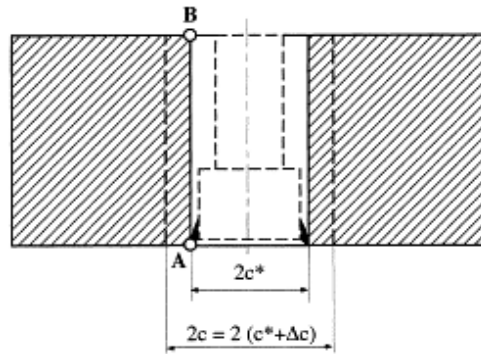


Figure 14.4 – Definition of the idealised crack dimension $2c$.

Usually the crack plane is assumed to be perpendicular to the larger of two principal stresses. There are, however cases, where a real crack will not grow within this plane because of mechanical reasons, i.e. both principal stresses are in the same magnitude, or because of heterogeneity of the material. In such cases a more complicated mixed-mode analysis has to be carried out. In the present case the situation is quite simple because the maximum principal stress direction is identical to the axis of the fork.

14.2.2.2 Stresses

In the FITNET procedure [14.2] the applied load can be introduced as a single load such as a tensile force, a bending moment or internal pressure. The consideration as a stress profile, which is, e.g., determined by a finite element analysis is, however, more common. Note that such a stress profile refers to the uncracked component. In the present case, the loading type is predominantly bending which would have allowed for the application of a simple analytical model for determining the bending stress. However, in order to consider also the membrane stress component, a finite element analysis was carried out, which yielded the stress profile shown in Figure 14.5 which was characterised by the stress values σ_1 and σ_2 at the front and back surfaces of the plate. Based on this information $\sigma_b=209$ MPa and $\sigma_m=2$ MPa were determined. These values refer to one half of the nominal applied force of 35 kN, which the fork lift was designed for.

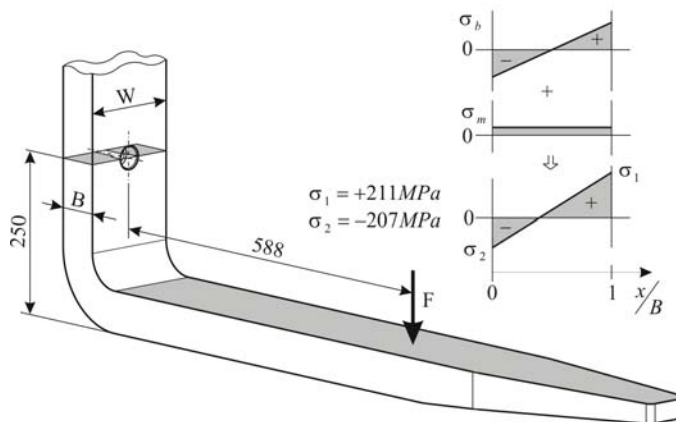


Figure 14.5 – Stress profile across the fork section containing the crack (all measures in mm).

In the present case only primary stresses have to be considered. In practice there are, however, many cases—for particular welds—where these have to be complemented by secondary stresses. In general primary stresses arise from mechanical applied loads including the weight of the structure whereas secondary stresses are due to suspended stresses. Typical examples of secondary stresses are welding residual stresses. Secondary stresses are of minor significance for common strength analyses because they are self equilibrating across the section. This is, however, no longer true when the same cross section contains a crack. In such a case secondary stresses can be a

major loading component, which has to be considered in any analysis. Because secondary stresses are of no relevance in the context of this paper they shall only be mentioned without going into detail. Note, that the FITNET procedure gives elaborate guidance on the treatment of secondary stresses.

14.2.2.3 Material Properties

The engineering stress-strain curve of the material is shown in Figure 14.6. Five tests were carried out but only the lowest curve is used for the FITNET analysis.

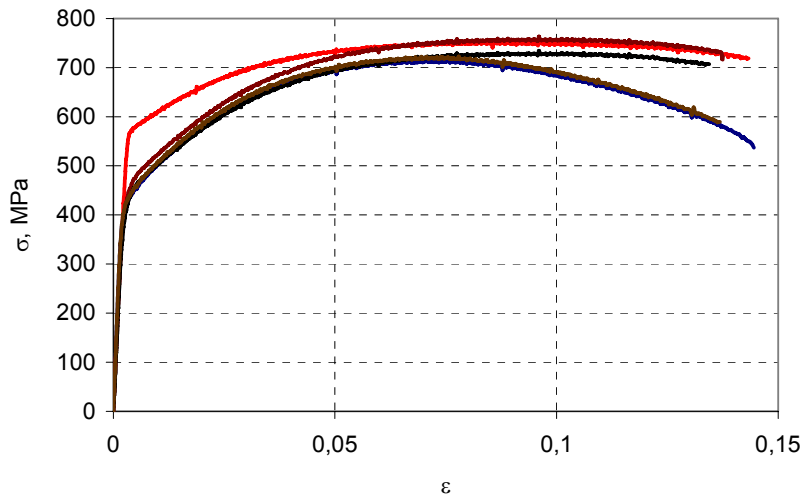


Figure 14.6 – Engineering stress-strain curves of the fork material.

The mechanical properties derived from this curve are summarised in Table 14.1. The true stress and strain values are determined by

$$\begin{aligned}\varepsilon_{true} &= \ln(1 + \varepsilon) \\ \sigma_{true} &= \sigma(1 + \varepsilon)\end{aligned}\quad (14.1)$$

Table 14.1. Tensile properties of the fork material

| E(GPa) | ν | $R_{p0.2}$ (MPa) | R_m (MPa) | A_g (%) | A_t (%) | Z(%) | N |
|--------|-------|------------------|-------------|-----------|-----------|-------|-------|
| 2.1 | 0.3 | 466 | 720 | 6.8 | 14.95 | 53.60 | 0.176 |
| | | 448 | 735 | 8.89 | 18.19 | 53.77 | 0.192 |
| | | 578 | 754 | 7.52 | 20.95 | 59.05 | 0.125 |
| | | 474 | 764 | 9.72 | 19.48 | 55.81 | 0.187 |
| | | 440 | 716 | 6.74 | 14.45 | 52.59 | 0.195 |

The fracture toughness was determined in terms of the crack tip opening displacement according to the British standard BS 7448, Part 1 [14.3]. Four tests were carried out using three-point bend specimens at room temperature. The test setup and a test record are given in Figure 14.7. The test record shows typical pop-in behaviour, i.e., cleavage fracture events disrupting the ductile tearing process. The crack is arrested subsequent to each pop-in. Note, however, that the specimen is subjected to displacement control in the test machine

whereas in reality load control might occur. Usually the crack would not be arrested in such a case but cause failure. Therefore, no benefit can be taken from the crack arrest following a pop-in which was specified as such by the test standard.

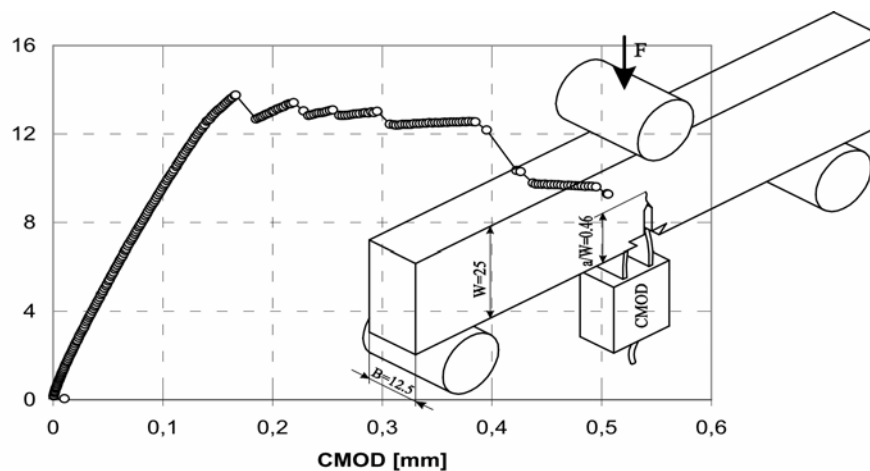


Figure 14.7 – Test setup for the determination of the critical CTOD and a typical test record.

For the FITNET analyses the lowest of the pop-in fracture toughness values is chosen. This was $\delta_c=0.02$ mm corresponding to $K_{mat}=49.7$ MPa \sqrt{m} . Also, information on the Charpy energy is necessary for the FITNET Option 0 (Basic). Nine tests have been carried out at three temperatures. The result is summarised in Table 14.2. The FITNET analysis is based on the minimum room temperature Charpy energy of 6J.

Table 14.2. Charpy energy of the fork material at different temperatures

| Charpy impact toughness J/80 mm ² | | |
|--|-------|-------|
| +10°C | +20°C | +50°C |
| 6,6,6 | 7,6,7 | 9,8,9 |

14.2.3. Assessment

FITNET pursues two different assessment philosophies, which are designated as crack driving force and failure assessment diagram concepts (Figures 14.8 and 14.9). Both are complementary and give identical results. In the CDF route the determination of the crack tip loading in the component and its comparison with the fracture toughness of the material are two separate steps. The crack driving force curve, which relates the applied load with the crack tip loading in terms of J or CTOD is a geometry independent function, which depends only on the deformation behaviour of the material. Failure is predicted when the crack tip loading exceeds the fracture toughness.

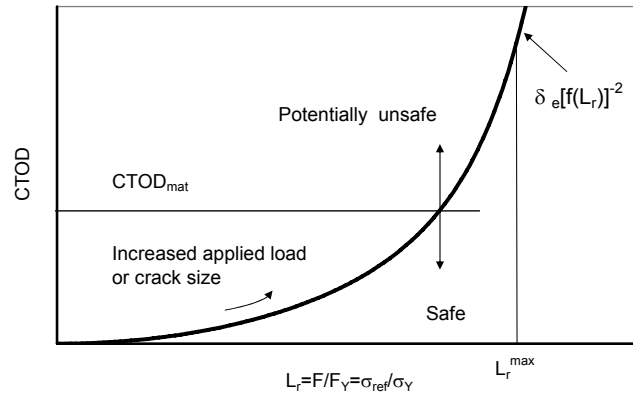


Figure 14.8 – FITNET assessment philosophies: CDF philosophy.

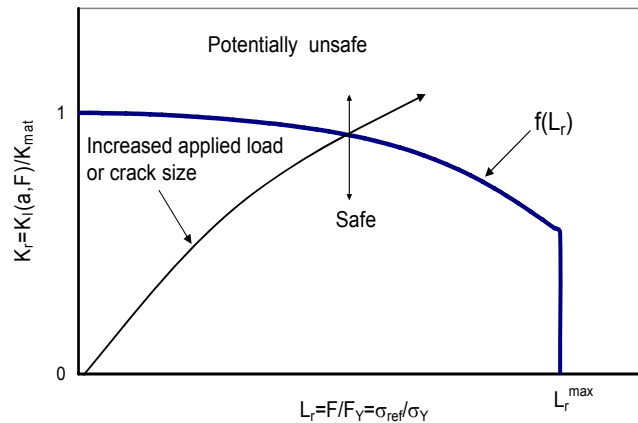


Figure 14.9 – FITNET assessment philosophies: FAD philosophy.

In the FAD route, a geometry independent failure line is constructed by normalising the crack tip loading by the material fracture resistance. The assessment of the component is then based on the relative location of a geometry dependent assessment point with respect to this failure line. In the simplest application the component is regarded as safe as long as the assessment point lies within the area below the failure line. It is regarded as potentially unsafe if it is located on the line or outside the area below the failure line. An increased load or larger crack size will move the assessment point along the loading path towards the failure line. In Figures 14.8 and 14.9, the basic CDF and FAD applications are illustrated which consider the fracture toughness as a single value (K_{IC} or J or CTOD at stable crack initiation). Note, that CDF and FAD applications also exist for R curve behaviour of the fracture resistance, which, however, will not be described here.

The basic equations of the CDF approach are

$$J = J_e \cdot [f(L_r)]^{-2} \tag{14.2}$$

$$J_e = \frac{K^2}{E'} \tag{14.3}$$

for the J integral and

$$\delta = \delta_e \cdot [f(L_r)]^2 \tag{14.4}$$

$$\delta_e = \frac{K^2}{E' \sigma_y} \tag{14.5}$$

for CTOD as crack tip parameters. The basic equation of the FITNET-FAD route is

$$K_r = f(L_r) \tag{14.6}$$

In Figure 14.10 and Figure 14.11 the CDF and FAD analyses are demonstrated for a crack size of $2c=45.5$ mm. It is shown that the higher analysis levels yield less conservative results. The option 0, which uses fracture toughness values estimated from Charpy energy, gave much lower critical loads than the higher options.

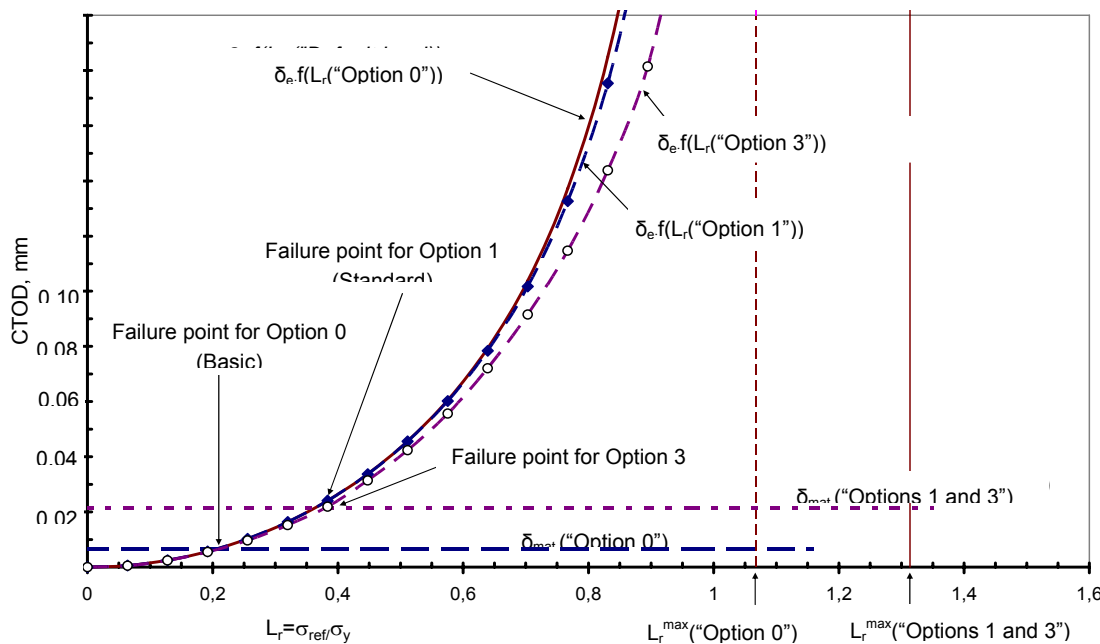


Figure 14.10 – CDF analysis of the fork assuming a crack width of $2c=45.5$ mm. [Failure is predicted for an applied load of 15 kN (Option 0), 27.38 kN (Option 1) and 29.9 kN (Option 3)].

The analysis is repeated for stepwise increased crack sizes $2c$. The critical crack size was then determined as that value of $2c$ that caused failure at the design load for one fork. As the final result the critical crack size was determined to be

- $2c=10.35$ mm (Option 0, Basic)
- $2c=33.2$ mm (Option 1, Standard)
- $2c=35.6$ mm (Option 3, Stress-strain defined),

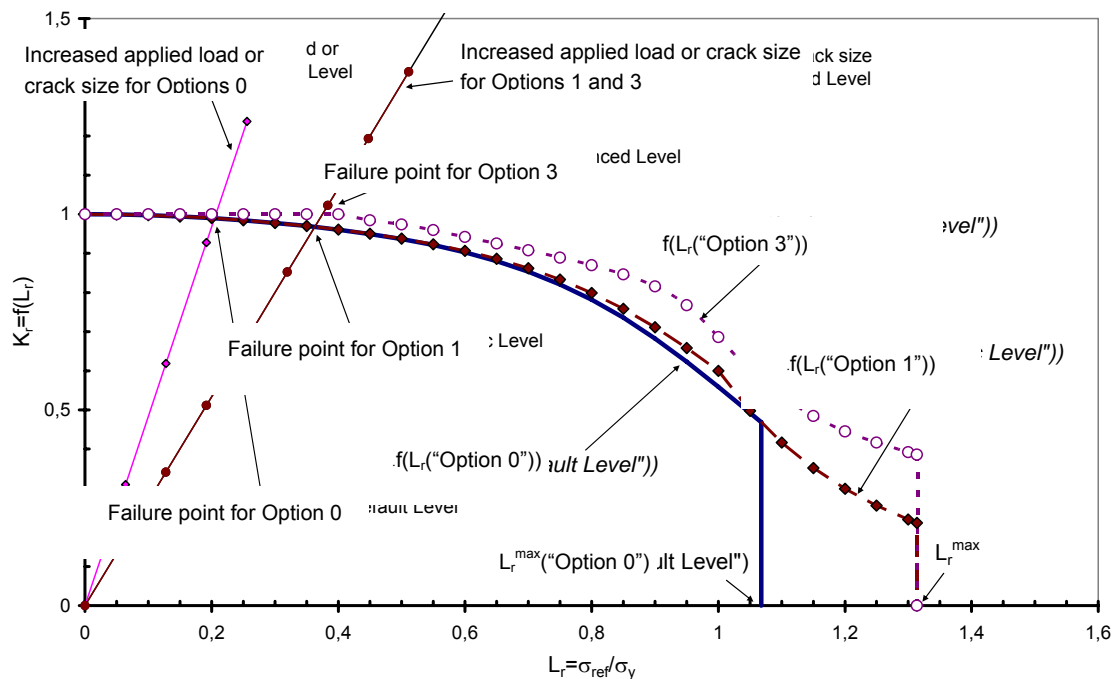


Figure 14.11 – FAD analysis of the fork assuming a crack width of $2c=45.5$ mm. The predicted failure loads are identical to those obtained by the CDF analysis in Figure 14.10.

Compared to the real overall surface dimension of the edge cracks at failure of 45.5 mm the predictions were conservative by 77.28% (Option 0, Basic); 27.03% (Option 1, Standard); 21.75% (Option 3, Stress-strain defined),

The discrepancy is small at the highest option because critical crack sizes are used to be very sensitive with respect to the input information. At the highest option the conservatism is mostly due to the simplified crack model used as the substitute geometry (Figure 14.4). In conclusion, it can be stated that the failure occurred as the consequence of inadequate design and not of inadmissible handling such as overloading. The failure could have been avoided by applying fracture mechanics in the design stage. The FITNET algorithm was shown to be an easy but suitable tool for this purpose.

14.2.4. References

[14.1] N. Gubeljak, U.Zerbst, J.Predan and M.Oblak, "Application of the european SINTAP procedure to the failure analysis of a broken forklift", Engineering Failure Analysis, Vol. 11, pp. 33-47, 2004

[14.2] "FITNET FFS Procedure", GIRT-CT-2001-05071

[14.3] BS 7448: Part 2: 1997: Fracture mechanics toughness tests, part 2. Method for determination of K_{Ic} , critical CTOD and critical J values of welds in metallic materials. London: British Standards Institution; 1997.

14.3 Fracture Tutorial: Fracture Analysis of Mismatched Components [14.4]

14.3.1. Introduction

This tutorial presents a fracture analysis of strength undermatched welds of thin-walled aluminium structures using FITNET procedure (Mismatch Option of the Fracture Module) [14.5]. The welds in the form of butt-joints were produced using the CO₂ laser beam (LBW) and friction stir welding (FSW) processes. Both LBW and FSW produce under-matched welds (i.e, weld having lower yield strength than base material). The optical macro-sections of both LBW and FSW butt-joints are shown in Figure 14.12.

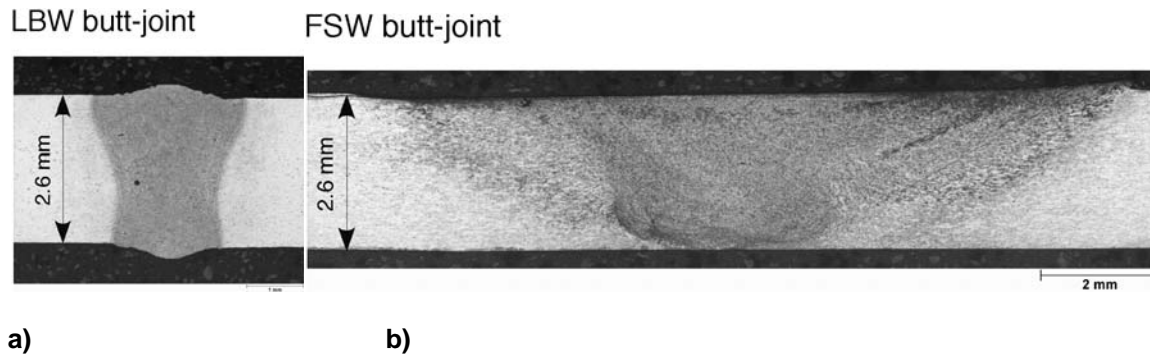


Figure 14.12 – Macro-sections of a) LBW and b) FSW butt-joints.

The material investigated within this tutorial is an age-hardening Al-alloy 6013 in T6 temper condition. Analytical results (obtained by using the CDF approach) are going to be compared to those obtained from laboratory tests.

14.3.2. Inputs

14.3.2.1 Flaw information

Central through thickness notch with fatigue crack located at the centre of the weld metals and HAZ (Heat Affected Zone) of LBW and TMHAZ (Thermo-mechanically Affected Zone) of FSW.

14.3.2.2 Stresses

All specimens are tested in tension.

14.3.2.3 Material Properties

It is known that the standard flat tensile specimens produce tensile properties of whole joint covering the interaction between base and weld areas. However, micro-flat tensile specimens enable the determination of local tensile properties. These 0.5 mm thick and 1.5 mm wide specimens were extracted using electrical discharge machining (EDM) from different locations of the LBW and FSW joints. Figure 14.13 shows the extraction technique. This technique yields full stress-strain curves obtained from the bulk material of the region of interest. The elongation was measured at a gauge length of $L_0 = 7$ mm. It should be noted that micro-flat tensile specimens are made of all-weld material and thus provide the intrinsic (local) material tensile properties. Table 1 gives the tensile strength and elongation values for all materials. For the LBW material, the standard specimens yielded much higher yield and ultimate tensile strengths than the micro-flat tensile specimens.

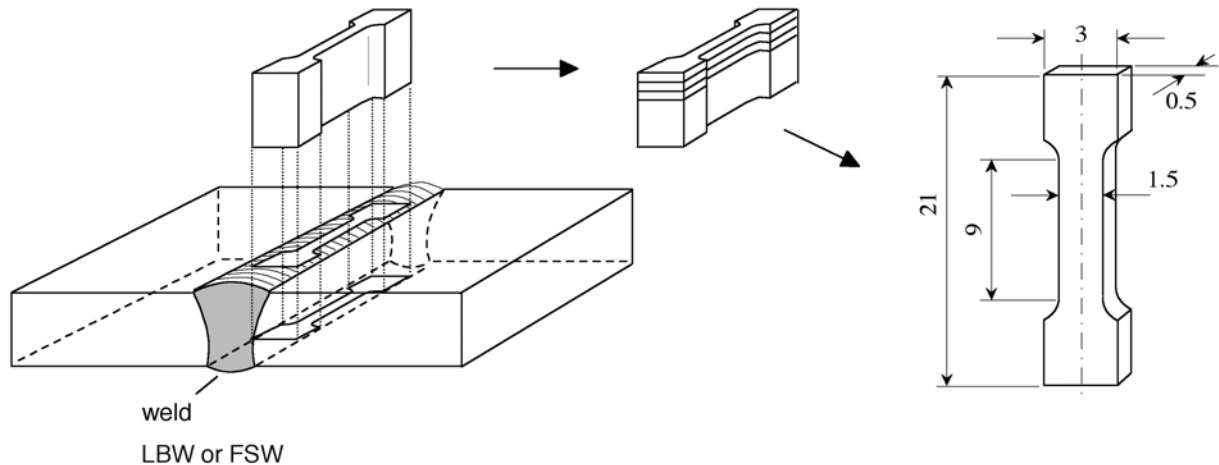


Figure 14.13 – Schematics of the micro-flat tensile specimen extraction from the LBW and FSW welds. All dimensions are given in mm.

Table 14.3. Tensile properties of the weld and base materials obtained from micro-flat and standard transverse flat tensile (gauge length 50 mm) specimens.

| Material | Yield strength $\sigma_Y = R_{p0.2}$ MPa | Tensile strength σ_{UTS} MPa | Elongation at fracture, <i>A</i> % | Mismatch factor, $M = \sigma_{YW} / \sigma_{YB}$ -- |
|--|--|---|---------------------------------------|---|
| Micro-flat tensile specimens | | | | |
| Base (LT) | 330 | 365 | 11.5 | |
| LBW (FZ) | 145 | 165 | 2.0 | 0.44 |
| FSW (nugget) | 185 | 295 | 28.5 | 0.56 |
| FSW (TMAZ) | 200 | 285 | 13.0 | 0.61 |
| Standard flat tensile specimens | | | | |
| Base (LT) | 360 | 395 | 12.6 | |
| LBW | 240 | 290 | 0.9 | |
| FSW | 210 | 285 | 2.6 | |

The CTOD δ_5 approach [14.6] offers a method for the determination of the fracture resistance curves, which is particularly suited for thin walled structures. Figure 14.14 shows the fracture resistance curves in terms of CTOD δ_5 obtained for the LBW and FSW joints from the respective C(T)50 specimens with $a/W=0.5$ using multiple specimen technique. The R-curve for the LBW weld exhibited the lowest, whereas for the FSW joint with a crack in the nugget area the highest R-curve.

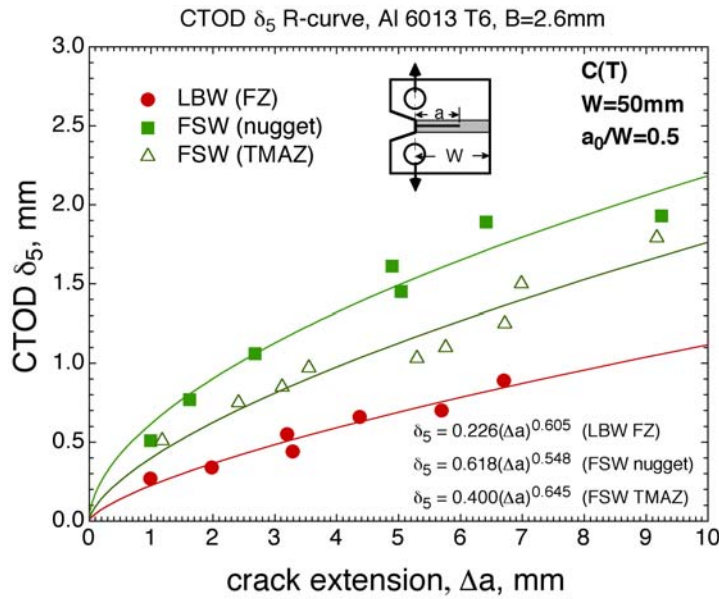


Figure 14.14 – R-curves of the materials.

14.3.3. Assessment

The FITNET Fracture Module provides two complementary analysis routes: Failure Assessment Diagram (FAD) and Crack Driving Force (CDF). Since both routes are based on the same set of equations, their predictions are also the same. Therefore, only the CDF route will be presented in this tutorial. The CDF expression in terms of the crack tip opening displacement (CTOD), δ , is given as:

$$\delta = \delta_e \cdot [f(L_r)]^{-2} \quad (14.7)$$

With the elastic part of CTOD, δ_e :

$$\delta_e = \frac{K^2}{m \cdot \sigma_Y \cdot E'} \quad (14.8)$$

K denotes the elastic stress intensity factor, the parameter m ($m=1$ for plane stress and $m=2$ for plane strain) is considered a constraint parameter, $E'=E$ for plane stress and $E'=E/(1-\nu^2)$ for plane strain (E =Young's modulus, ν =Poisson's ratio), and

$$L_r = \frac{F}{F_Y} \quad (14.9)$$

is the ratio of externally applied load, F , and the yield load, F_Y , of the cracked component which is a function of the material's yield strength, σ_Y , of the crack location and component/weld geometry. Regarding the selection of E' , the plane stress condition has been chosen due to the fact of the thin sheet material. The plasticity correction function, $f(L_r)$, is subdivided into different options within the FITNET FFS Procedure and is dependent on the extent of the material data input and on the case analysed (homogeneous or heterogeneous with strength mismatch). For a strength mismatched configuration (FITNET FFS Fracture Module Option 2), the plasticity correction function is defined as:

$$f(L_r) = \left[1 + \frac{1}{2} L_r \right]^{-1/2} \cdot \left[0.3 + 0.7 \exp(-\mu_M L_r^6) \right] \quad \text{for } 0 \leq L_r \leq 1 \quad (14.10)$$

$$f(Lr) = f(L_r = 1) \left(L_r^{(N_M - 1) / 2N_M} \right) \quad \text{for } 1 \leq L_r \leq L_r^{\max} \quad (14.11)$$

where

$$\mu_M = \frac{M - 1}{(F_{YM} / F_{YB} - 1) / \mu_W + (M - F_{YM} / F_{YB}) / \mu_B} < 0.6 \quad \text{else } \mu_M = 0.6 \quad (14.12)$$

$$\mu_B = 0.001 \frac{E}{\sigma_{YB}} < 0.6 \quad \text{else } \mu_B = 0.6 \quad (14.13)$$

$$\mu_W = 0.001 \frac{E}{\sigma_{YW}} < 0.6 \quad \text{else } \mu_W = 0.6 \quad (14.14)$$

$$L_r^{\max} = \frac{1}{2} \left(1 + \frac{0.3}{0.3 - N_M} \right) \quad (14.15)$$

Strain hardening exponents for mismatch, N_M , base, N_B , and weld materials, N_W , are defined as follows:

$$N_M = \frac{M - 1}{(F_{YM} / F_{YB} - 1) / N_W + (M - F_{YM} / F_{YB}) / N_B} \quad (14.16)$$

$$N_B = 0.3 \left(1 - \frac{\sigma_{YB}}{\sigma_{UTS,B}} \right) \quad (14.17)$$

$$N_W = 0.3 \left(1 - \frac{\sigma_{YW}}{\sigma_{UTS,W}} \right) \quad (14.18)$$

σ_{UTS} denotes the ultimate tensile strengths of base (subscript B) and weld (subscript W) materials. F_{YM} and F_{YB} are de yield load solutions for the mismatch and base material plates, respectively. F_{YM} , for a butt welded M(T) panel with strength undermatched weld, i.e. the plastic deformation at the crack tip is entirely confined to the weld material, is given by (see Figure 14.15):

$$\frac{F_{YM}}{F_{YB}} = M \quad \text{for } 0 \leq \psi \leq 1.43 \quad (14.19)$$

$$\frac{F_{YM}}{F_{YB}} = M \left[\frac{2}{\sqrt{3}} - \left(\frac{2 - \sqrt{3}}{\sqrt{3}} \right) \frac{1.43}{\psi} \right] \quad \text{for } \psi > 1.43 \quad (14.20)$$

$$M = \frac{\sigma_{YW}}{\sigma_{YB}} \quad (14.21)$$

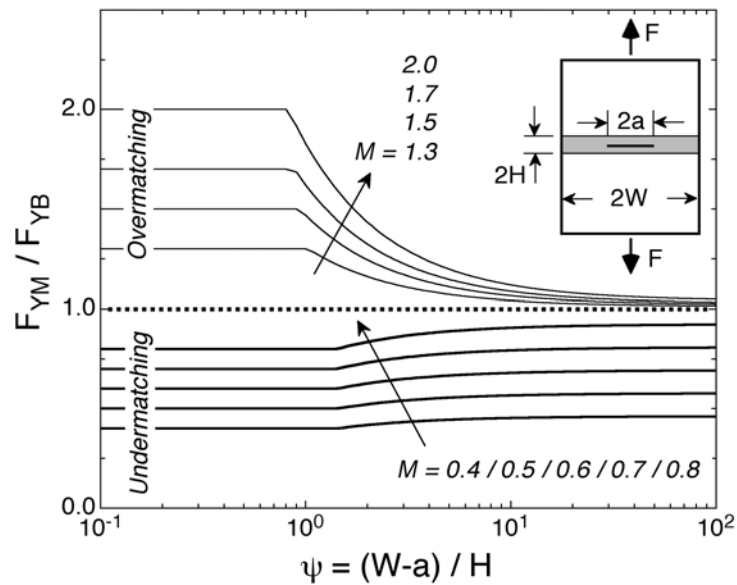


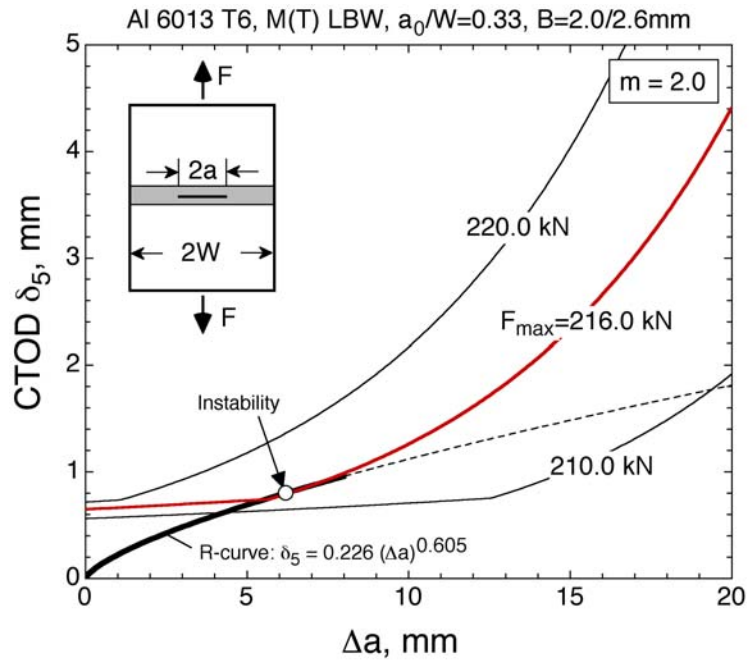
Figure 14.15 – Mismatch yield load solution of a M(T) panel with a crack in the weld centre.

By the use of equation (14.16), the FITNET FSS procedure takes account of the interaction between base and weld metals in terms of post-yield properties of the weld joint constituents. The described procedure aims at reducing the excessive conservatism (in case of overmatching) and non-conservatism (in case of undermatching) in prediction of critical conditions for weld flaws.

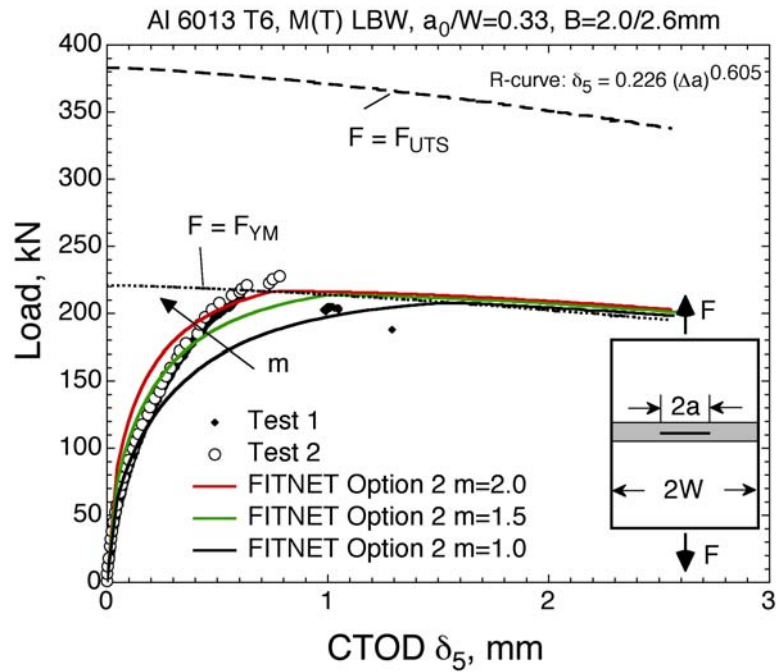
The K-factor for a middle cracked M(T) panel is available in a closed form solution [14.7]:

$$K = \frac{F}{2WB} \sqrt{\pi a} \sqrt{\frac{1}{\cos\left(\frac{\pi a}{2W}\right)}} \quad (14.22)$$

Where F is the applied load, 2W is the total panel width, a is the half crack length, and B is the panel thickness (B=2.6 mm for LBW and B=2.2 mm for FSW). Since K is a purely geometrical function, it is also valid for heterogeneous configurations like welded panels. All these expressions allow a CDF analysis to be performed. Figures 14.16 to 14.18 show the results obtained.

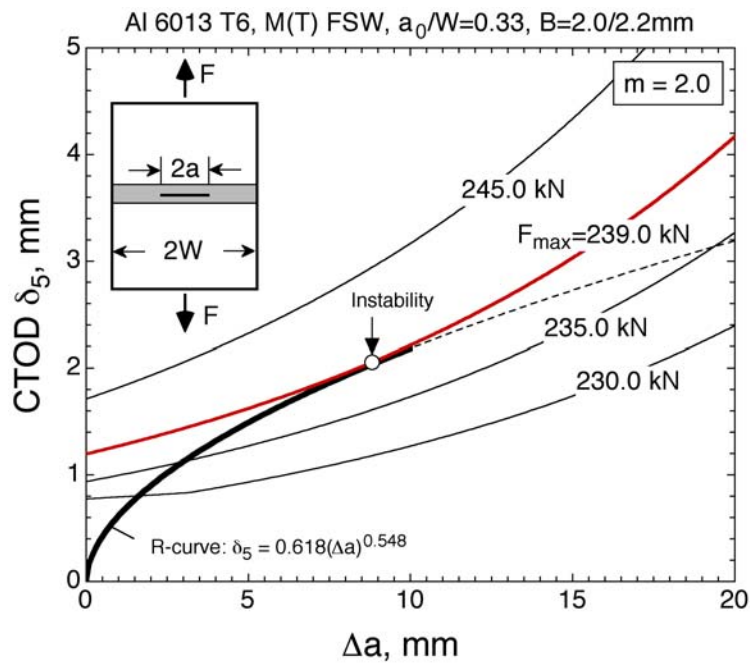


a)

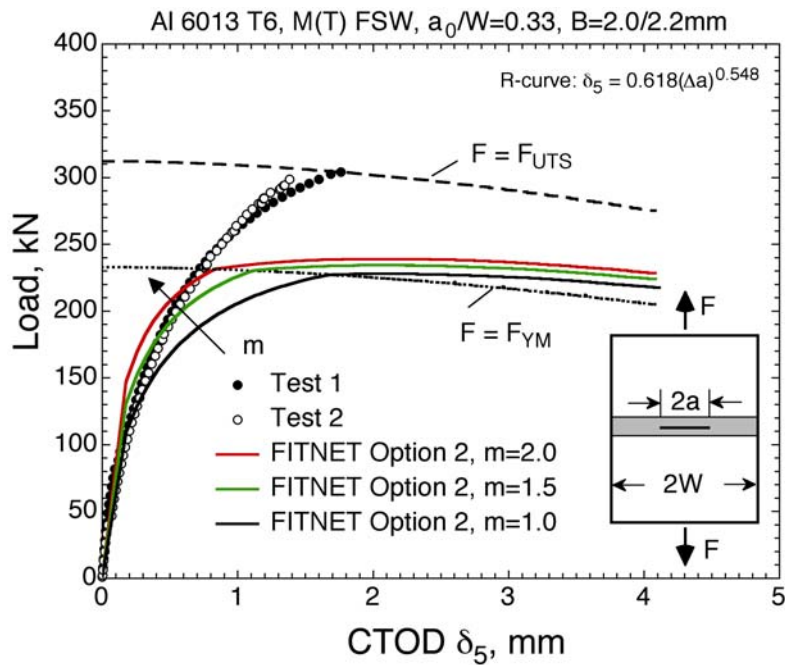


b)

Figure 14.16 – a) Prediction of the maximum load carrying capacity of the LBW M(T)760 panel. b) Comparison between the predicted and experimental results including the variation of the constraint parameter m .

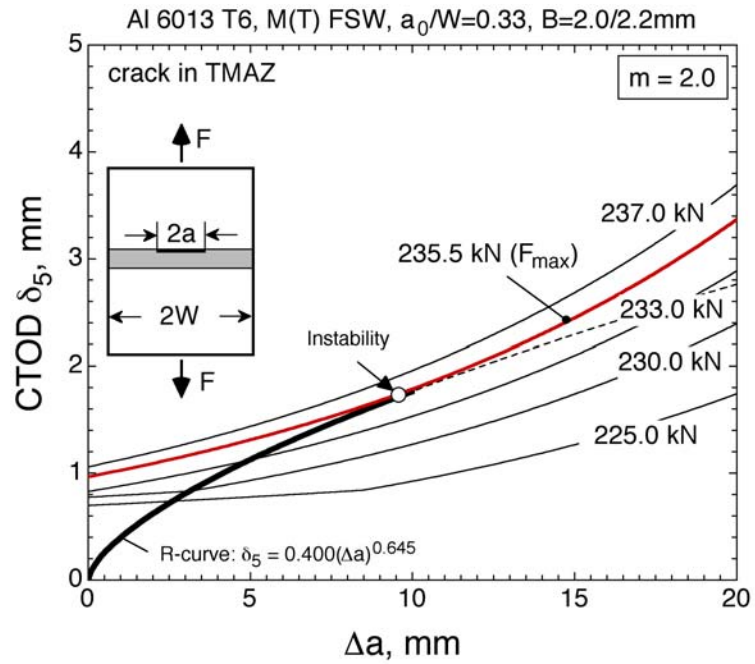


a)

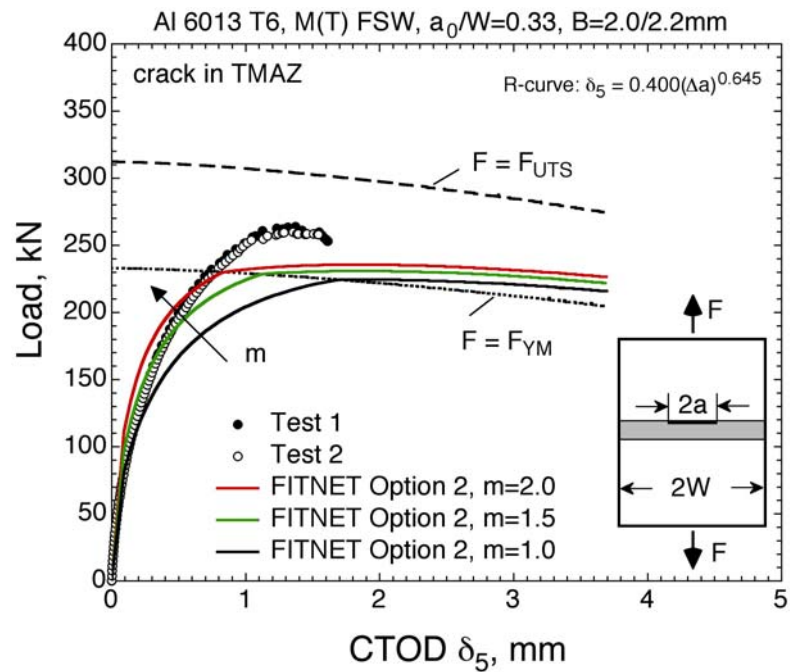


b)

Figure 14.17 – a) Prediction of the maximum load carrying capacity of the FSW M(T)750 panel with a crack in the nugget area. b) Comparison between the predicted and experimental results the variation of the constraint parameter m .



a)



b)

Figure 14.18 – a) Prediction of the maximum load carrying capacity of the FSW M(T)750 panel with a crack in TMAZ. b) Comparison between the predicted and experimental results the variation of the constraint parameter m .

The variation of the constraint parameter m shows that for higher m the predicted load-CTOD response becomes stiffer. The predicted maximum load, however, is affected marginally. For $m=2.0$, which represents the plane strain condition, the predicted curve describes the deformation behaviour more closely to the experimental load-CTOD curve. Indeed, due to the confined plastic deformation within the lower strength weld metal at the crack tip (the material is not free to flow) a higher constraint within the softer weld material should be expected. This is another important feature of the strength undermatched welds in thin-walled structures which needs to be taken into account during the assessment of weld flaws in such structures. Therefore, it is recommended to use $m=2.0$ for undermatched welds even if the plate thickness may suggest that the cracked component may be under the plane stress condition.

It can be seen that the application of the mismatch option of the Fracture Module of the FITNET FFS Procedure to LBW and FSW panes yields conservative estimations of the maximum load carrying capacity.

14.3.4. References

[14.4] E. Seib and M.Koçak, “Fracture Analysis of Strength Undermatched Welds of Thin-walled Aluminium Structures using FITNET Procedure”, IIW Doc.X-1577-2005, IIW Annual Assembly July 2005, Prague.

[14.5] “FITNET FFS Procedure”, GIRT-CT-2001-05071

[14.6] K.-H.Schwalbe, “Introduction of δ_5 as an operational definition of the CTOD and its practical use”, Fracture Mechanics, ASTM STP 1236, pp. 763-778, 1995

[14.7] H.Tada, P.C. Paris and G.R.Irwin, “The Stress Analysis of Cracks Handbook”, New York: ASME Press, 3rd edition, 2000.

14.4. Fracture Tutorial: Embrittlement Effect on Fracture Assessments [14.8]

14.4.1. Introduction

The structural integrity assessment of components has advanced greatly in recent years. New tools, such as the Failure Assessment Diagram used in the FITNET procedure, have provided a friendly, efficient methodology for assessing all kinds of components. This work applies the new approaches to assessing the structural integrity of pipelines subjected to high pressure hydrogen.

This analysis involves several specific factors. The first one is the material embrittlement due to the hydrogen whose main consequence is a decrease in fracture toughness. The last critical factor is the influence of crack geometry on the failure process because different geometries can lead to different failure mechanisms. This tutorial analyses fractures under different conditions.

14.4.2. Inputs

14.4.2.1 Flaw information

Burst tests were performed on real pipes to better understand the fracture behaviour of components and to analyse the critical parameters of the steel under pressure levels higher than those used in the environmental chamber for J- integral tests. Each pipe had a longitudinal internal artificial flaw, machined in the mid section as can be observed in the scheme proposed in Figure 14.19. The flaw had a triangular transverse section with a notch radius less than 0.075 mm and a longitudinal section nearly elliptical, with a small a/c axis ratio. This defect geometry ensured that plain-strain behaviour was obtained at the tip of the flaw. Table 14.4 summarizes geometric data.

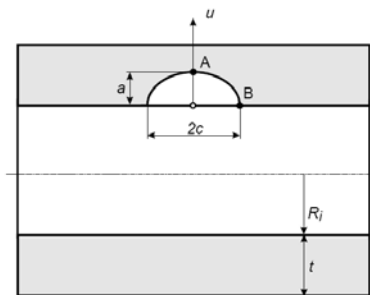


Figure 14.19 – Geometrical characteristics of flaw.

Table 14.4. Geometric data.

| Test | | TF.3 | TF.1 | TF.2 | TF.4 | TF.5 |
|----------------------------|-------|-------|-------|-------|-------|-------|
| Internal radius R_i (mm) | | 74.35 | 74.4 | 74.5 | 74.45 | 74.35 |
| Thickness t (mm) | | 5.65 | 5.6 | 5.5 | 5.55 | 5.65 |
| Defect | a/t | 0.64 | 0.64 | 0.65 | 0.72 | 0.69 |
| | a/c | 0.212 | 0.095 | 0.059 | 0.039 | 0.027 |

14.4.2.2 Stresses

The test method used [14.9] permitted a high pressure (P) of high purity hydrogen to be reached and sustained for enough time to achieve maximum embrittlement. This time was decided using previous results from J-integral tests. After arriving at this maximum embrittlement time, the pressure was sequentially increased until the pipe burst and

the pressure P_b measured. From this value, a fracture mechanic analysis was used to determine the stress intensity factor at bursting. In this step FITNET procedure was employed as a new approach [14.10]. Table 14.5 shows relevant data.

Table 14.5. Pressure data.

| Test | TF.3 | TF.1 | TF.2 | TF.4 | TF.5 |
|----------------------------|------|------|------|------|------|
| Hydrogen pressure P (MPa) | 16.2 | 12.4 | 10.1 | 8.1 | 7.1 |
| Burst pressure P_b (MPa) | 17.0 | 16.0 | 11.2 | 8.5 | 9.5 |

14.4.2.3 Material Properties

The use of hydrogen as a source of energy requires the development of transmission systems capable of withstanding higher pressures than normal [14.9, 14.11]. The structural components of such systems can thus be susceptible to fracture problems, particularly hydrogen embrittlement. These concerns led to a study of the behaviour, under high pressure hydrogen embrittlement of a steel normally employed in the past in the Spanish transmission pipeline system. This steel, similar to an X-42 type, was in the as-received condition showing an equiaxed ferrite-perlite microstructure with a grain size of ASTM 7; its chemical composition and mechanical properties are shown in Tables 14.6 and 14.7.

Table 14.6. Chemical composition

| C | Mn | Si | Cr | P | S | Co |
|------|------|------|------|-------|-------|------|
| 0.10 | 0.70 | 0.26 | 0.15 | 0.033 | 0.022 | 0.17 |

Table 14.7. Mechanical properties

| Yield Strength MPa | Tensile strength MPa | Reduction of area % | Elongation % |
|------------------------|-------------------------|------------------------|-----------------|
| Longitudinal direction | | | |
| 280 | 415 | 58 | 32 |
| Transversal direction | | | |
| 345 | 442 | 48 | 25 |

To determinate the fracture behaviour, J_{IC} tests were performed. The J integral tests were carried out using the method proposed in [14.12]. Half thickness Charpy specimens (5 mm thick) were used because of the limitation of pipe thickness. These were tested by three points bending and the compliance variation was used to determine the crack length evolution. Some of the tests were performed in air, and others were carried out inside a high-pressure chamber using high purity hydrogen, with a pressure up to 6.5 MPa. In these latter tests, the critical displacement rate was found by analysing the decrease in the J_{IC} parameter values with decreasing loading rate, in order to establish the rate below which there was no change in this parameter for maximum embrittlement. In Table 14.8 the variation in J_{IC} with displacement rate, for tests performed in 4MPa hydrogen pressure, is shown.

Table 14.8. Variation of J_{IC} with displacement rate in 4 MPa pressure hydrogen tests.

| Displacement rate (mm/min) | 0.2 | 0.02 | 0.002 |
|-------------------------------------|-----|------|-------|
| J_{IC} values(kJ/m ²) | 56 | 31 | 35 |

All the specimens tested in the gaseous hydrogen environment obeyed the minimum thickness criteria:

$$B \geq 25 \left(\frac{J_{IC}}{\sigma_Y} \right) \quad (14.23)$$

The results obtained in all the tests are given in Table 14.9, including the K_{JC} values, which were calculated from the J_{IC} values from the expression:

$$J_{IC} = \frac{(1-\nu^2)}{E} K_{JC}^2 \quad (14.24)$$

Table 14.9. Variation of K_{JC} with hydrogen pressure.

| Hydrogen pressure MPa | J_{IC} kJ/m ² | K_{JC} MPa m ^{1/2} |
|--------------------------|-------------------------------|----------------------------------|
| 0 | 99.8 | 147 |
| 2 | 48.0 | 101 |
| 4 | 33.3 | 85 |
| 6.5 | 22.3 | 69 |

The data confirms the high susceptibility of this steel to hydrogen embrittlement, as can be determined by the loss in toughness from 99.8 to 22.3 kJ/m² in air to 6.5 MPa respectively. The corresponding values for K_{JC} dropped from 147 to 69 MPa·m^{1/2}. An analysis of the decrease in toughness as a function of the hydrogen pressure shows an exponential dependence of K_{JC} on the pressure, equation (14.25), with a correlation coefficient of 0.93:

$$K_{JC} = 64.58 + 84.01 \exp(-0.366P) \quad (14.25)$$

Figure 14.20 shows this behaviour, as well as the asymptotic variation of fracture toughness with pressure level above 7 MPa. The resulting fracture surface of the specimen were examined by scanning electron microscopy, and showed gradual changing in the fracture mode with increasing hydrogen pressure from microvoid coalescence to quasi-cleavage.

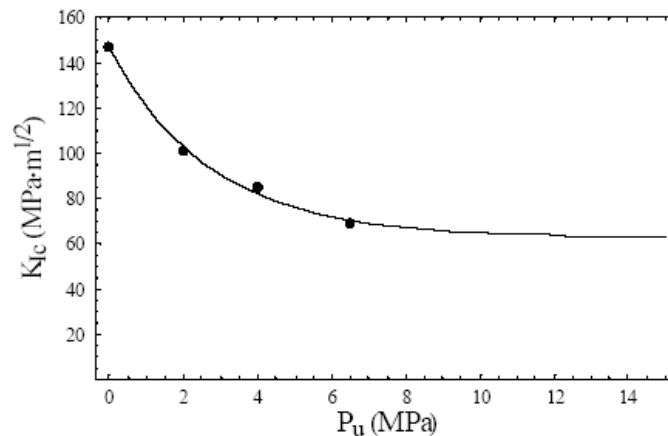


Figure 14.20 – Evolution of K_{JC} with the internal pressure.

14.4.3. Assessment

Table 14.10 shows a summary of the calculation of K_{Jc} as well as the $K_I(H)$ obtained for each pipe. Again, the high susceptibility of this steel to hydrogen is present; K_I drops from 61.8 MPa·m^{1/2} in 7.1 MPa pressure to 38.6 MPa·m^{1/2} in 16.2 MPa pressure.

Table 14.10. Calculation of K_I and K_{Jc} in pipe tested

| Test | TF.3 | TF.1 | TF.2 | TF.4 | TF.5 | |
|---|-------|-------|-------|-------|-------|-------|
| Internal radius R_i (mm) | 74.35 | 74.4 | 74.5 | 74.45 | 74.35 | |
| Thickness t (mm) | 5.65 | 5.6 | 5.5 | 5.55 | 5.65 | |
| Defect | a/t | 0.64 | 0.64 | 0.65 | 0.72 | 0.69 |
| | a/c | 0.212 | 0.095 | 0.059 | 0.039 | 0.027 |
| Hydrogen pressure P (MPa) | 16.2 | 12.4 | 10.1 | 8.1 | 7.1 | |
| Burst pressure P_b (MPa) | 17.0 | 16.0 | 11.2 | 8.5 | 9.5 | |
| K_{Jc} (MPa·m ^{1/2}) (equation 14.25) | 62.7 | 63.4 | 64.6 | 66.9 | 68.8 | |
| K_I (MPa·m ^{1/2}) | 38.6 | 49.8 | 43.7 | 48.5 | 61.8 | |

The use of Failure Assessment Diagrams in conditions that imply the continuous embrittlement of the material must be considered with extreme precaution, because, otherwise, the wrong safety conditions can be established. The philosophy of the FAD only has as its objective the representation of the safety state of the structure in real time, but it must be able to reproduce the evolution of the state of the material throughout all its service life. When representing in a FAD the evolution of the state of a component made up of materials which exhibit a variation in the critical failure conditions, either the fracture toughness or the limit load, this evolution must be taken into account by modifying the failure assessment line [14.13,14.14].

The structural integrity assessment of these pipes was carried out according to the methodology of the Failure Diagrams. Then, first of all, the definition of the Failure Assessment Line for Option 1, based on the knowledge of the yield stress and the ultimate tensile strength, is required. [14.10, 14.15]. The final failure can be produced either due to fracture or plastic collapse, and this can be, at the same time, local or global. The FITNET procedure provides the necessary tools in order to perform the calculations of the specific considered component [14.10]. It must be taken into account that the material of the pipes is under a state of embrittlement, and, as a consequence, its mechanical properties will change as a function of the pressure that the pipes are subjected to. Thus, the fracture toughness of the material can be estimated as

$$K_{mat} = K_{Ic} \cdot f(P) \quad (14.26)$$

where K_{Ic} is the fracture toughness of the material without considering any embrittlement effect, and $f(P)$ a function that gathers the influence of the pressure in the variation of K_{Ic} . Following this described line, the applied driving force values for each pipe were obtained, equations (14.27) and (14.28), and afterwards they were represented in the FAD.

$$K_r = \frac{K_I}{K_{mat}} \quad (14.27)$$

$$L_r = \frac{P}{P_y} \quad (14.28)$$

In each failure state represented in each FAD, two points appears, corresponding to the local and global plasticity failure analysis, although both of them share the same applied stress intensity factor. Next Figures show the load state of each pipe at the moment of failure.

- Pipe TF-1

Pipe TF1 was tested subjected to a uniform embrittlement pressure of 12.2 MPa for 5 hours; subsequently the pressure was increased to 16 MPa, the moment at which the fracture took place. The analysis of the fractograph showed a brittle dominant mechanism firstly with crack growth and with crack arrest after the decompression. The study of pipe TF1 by means of the Failure Assessment Diagram gathers two approaches: the global failure and the failure due to a local scale collapse. In Figure 14.21 both states can be observed.

The failure predicted values were 18% and 32% smaller for global and local collapse respectively than the real ones; the predictable failure can be found below the line $K_r = L_r$, thus the dominant mechanism has been the plasticity collapse (local or global).

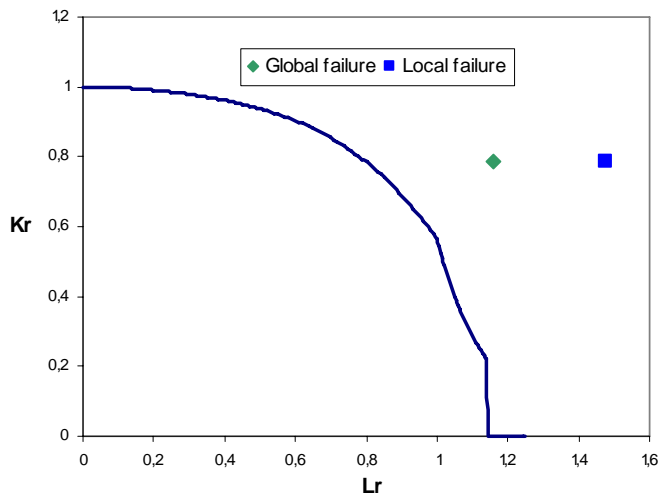


Figure 14.21 – FAD corresponding to TF-1 pipe.

- Pipe TF-2

Pipe TF2 which can be characterised as having a more open crack, was subjected to a uniform pressure of 10 MPa for 5 hours; after that, the pressure was increased to a value of 11.2 MPa, then taking place the failure. The fractographic analysis showed mechanisms related with high embrittlement processes. The load state at the moment of failure can be observed in the Figure 14.22. The expected values of failure using the FAD were 4% and 16% smaller for global and local approaches respectively than the actual ones. Both predictions are placed under the line $K_r = L_r$, the failure then has a plastic dominant component.

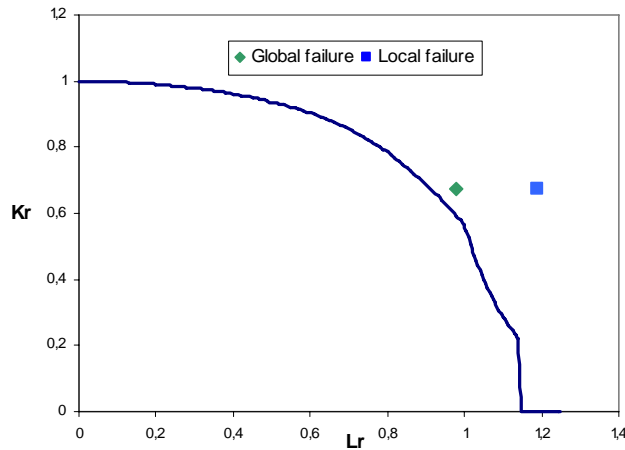


Figure 14.22 – FAD corresponding to TF-2 pipe.

- Pipe TF-3

Pipe TF3 was subjected to a pressure of 10 MPa for 5 hours; next it was conducted to failure which took place at a pressure of 17 MPa. The fractographic analysis exhibited a similar situation as in the above cases.

The failure analysis by means of the Failure Assessment Diagrams is shown in Figure 14.23, where it can be observed that only the local collapse conditions are fulfilled, not being expected the global plastic collapse. The real failure value was 17% higher that that estimated with FAD for local collapse.

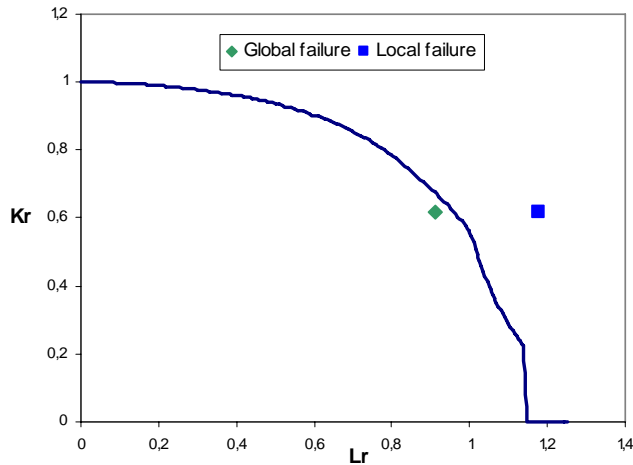


Figure 14.23 – FAD corresponding to TF-3 pipe.

- Pipe TF-4

Pipe TF4 was tested subjected to a uniform pressure of 8 MPa for 5 hours, increasing after this value to 8.5 MPa, when the pipe collapsed. The fractographic observations were very similar to the rest of the cases.

The study by means of the FAD reveals that the actual value of failure was 5% and 21% higher than the expected ones for local and global collapse, respectively. The situation of the points which represent the failure of the component below the line $K_r = L_r$, indicates that the dominant failure mechanism was the plasticity.

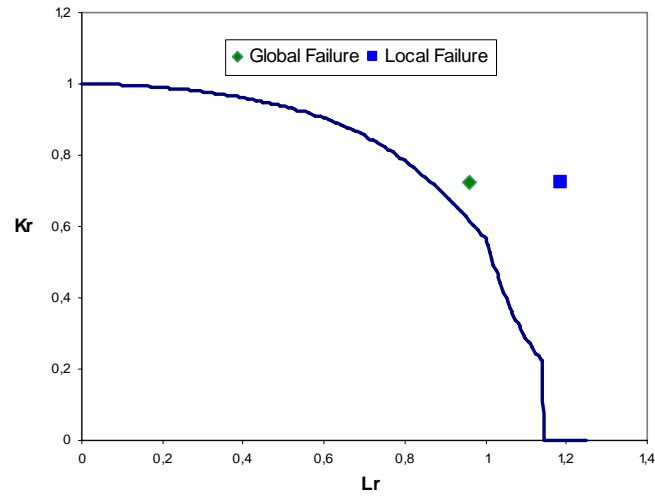


Figure 14.24 – FAD corresponding to TF-4 pipe.

- Pipe TF- 5

This last pipe was tested following the same considerations as in previous cases. First it was subjected to a uniform pressure of 7.1 MPa. After that, the pipe was taken to collapse by increasing the pressure to a value of 9.5 MPa. The fractographic study again showed the same conclusions.

The failure analysis, which is summarised in Figure 14.25, reveals that the expected values of collapse are about 12% and 19% smaller than the real one depending on the consideration of local or global failure.

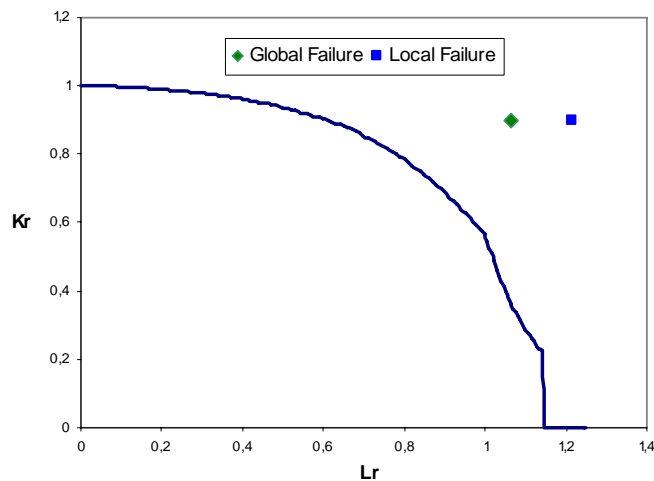


Figure 14.25 – FAD corresponding to TF-5 pipe.

In every previous case, it can be observed that the fracture takes place beyond the Failure Line, especially when a local plasticity approach is performed. This fact is usual in the studied cases in the bibliography [14.16] and can be justified by the presence of external determining factors of a geometric type, like the use of notched material instead of strictly cracked and others of a structural type like the degree of constraint at the crack tip.

In the previous analysis the Failure Assessment Diagrams have been used without any correction because of the damage in the material, applying the correction for the analysis of each particular situation. This approach,

nevertheless, can be applied, and offers interesting possibilities in materials subjected to damage during their operative life.

Remembering that, for the Failure Assessment Line (FAL) equation (14.29) is fulfilled,

$$K_r = \frac{K_I}{K_{Ic}} = f(L_r) \tag{14.29}$$

and according to equation (14.26), a modified Line of Failure which takes into account the embrittlement due to the hydrogen pressure can be obtained following equations (14.30) to (14.32).

$$f(L_r) = \frac{K_I}{K_{Ic} \cdot f(P)} \tag{14.30}$$

$$f(P) = \frac{62.59 + 84.01 \cdot \exp(-0.366P)}{147} \tag{14.31}$$

$$f(L_r)_{\text{mod}} = f(L_r) \cdot f(P) = f(L_r) \cdot [0.426 + 0.571 \cdot \exp(-0.366 \cdot L_r \cdot P_y)] \tag{14.32}$$

Figure 14.26 represents the failure analysis at the moment of fracture corresponding to pipe TF4. In this image, the Diagram modified according to the previous development can be observed. The safety conditions are exactly the same as those others derived from considering the evolution of the material in the definition of the points which represent the actual failure. That is:

$$\frac{0a}{0b} = \frac{0d}{0c} = 1.20 \tag{14.33}$$

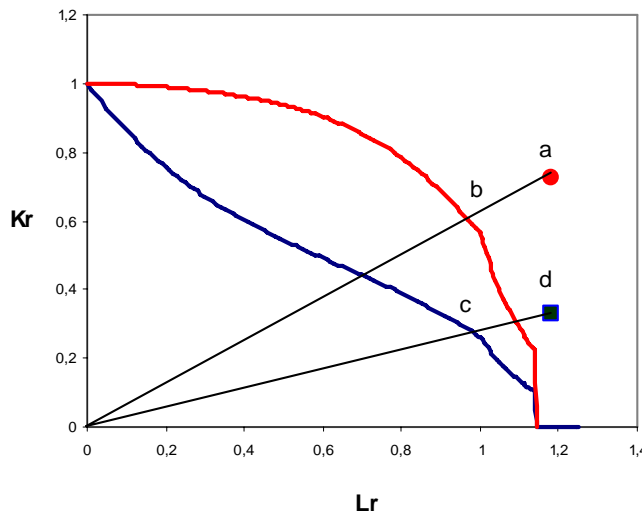


Figure 14.26 – FAD modified.

Summing up, a study of the fracture behaviour of pipes subjected to high pressure hydrogen was carried out using the concepts of structural integrity and applying the new FITNET approach based on the use of FADs. The selected material, used for decades in transmission lines, presents a high degree of susceptibility to hydrogen damage, especially when internal pressure is above 7 MPa. The evolution in material toughness can be included in the definition of the FAL. An alternative approach can be used considering the material approach in the calculation of the driving force. All the points which represents the failure of the tested pipes fall in the non-safe area of the FAD, except the one that analyses the possible global collapse for pipe TF-3. In all cases the predicted way of failure was local plastification which is confirmed by fractographic analysis. This behaviour,

which is well referenced in [14.13-14.16], has a justification in this case due to the use of components with flaws and the presence of constrain stresses in the crack tip.

14.4.4. References

[14.8] Álvarez, J.A., Gutiérrez-Solana, F., Lacalle, R. and Cicero, S., "Environmental Effects on Pipeline Steels: a Fitness for Service Perspective", In Proceedings of 16th European Conference of Fracture, ECF 16 (2006).

[14.9] Gutiérrez-Solana, F., "Fragilización por hidrógeno de tuberías de acero", PhD Thesis, Universidad de Cantabria, Santander, Spain, (1982).

[14.10] FITNET Consortium, FITNET: European Fitness for Service Network, EU's Framework 5, Proposal No. GTC-2001-43049, Contract No. G1RT-CT-2001-05071.

[14.11] Gutiérrez-Solana, F. and Elices, M., Proceedings of the first international conference on Hydrogen problems in steels. ASM Eds., PP.181-186, (1982).

[14.12] ASTM Standard E1820-99a Standard test method for measurement of fracture toughness. ASTM Eds. 1999.

[14.13] Koers, R., Turnbull, A., Gutierrez-Solana, F. and Alvarez, J.A. "Environment induced cracking-a fitness for service", In Proceedings of the OMAE2005-67567, edited by ASME, (2005).

[14.14] Alvarez, J.A. and Gutierrez-Solana, F., "An EPFM based methodology to characterize cracking behaviour and its application to environmental assisted processes", Nuclear Engineering Design, nº 17, pp.185-202, (2005).

[14.15] British Energy Generation Limited, R6: Assessment of the integrity of structures containing defects, Revision 4, 2001.

[14.16] Cicero, S., Ainsworth, R.A, "The Treatment of Constraint Effects in Integrity Evaluations", In Proceedings of the OMAE2005-67567, edited by ASME, (2005).

14.5 Fatigue tutorial: Fatigue Analysis of a Scallop by using FITNET Fatigue Routes 1 and 2 [14.17]

14.5.1. Introduction

Fatigue verifications of ship structures is compulsory since year 2000. The designer has to demonstrate that the ship hull details can resist without risk of fatigue cracks during the ship life time fixed in the specification, conventionally 20 to 25 years, i.e., some 10^8 cycles. Classification Societies provide rules to perform these verifications based on the Miner sum approach, i.e., FITNET routes 1 or 2. From ship on wave behaviour theory, and verified by the return experience, the critical zones are in the midship area (see Figure 14.27) and the details to be verified are those with hot spot, such as scallops and welded joints with brackets, etc.

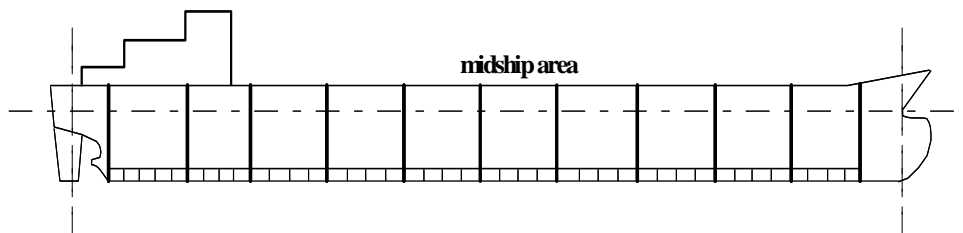


Figure 14.27 – Ship longitudinal section

To illustrate the routes 1 and 2 of FITNET FFS Procedure, we shall consider a scallop on a deck longitudinal stiffener. The two routes 1 (nominal stress) and 2 (notch stress) will be applied. The midship transverse section, the assessed detail location and the local geometry of the detail are given in Figure 14.28.

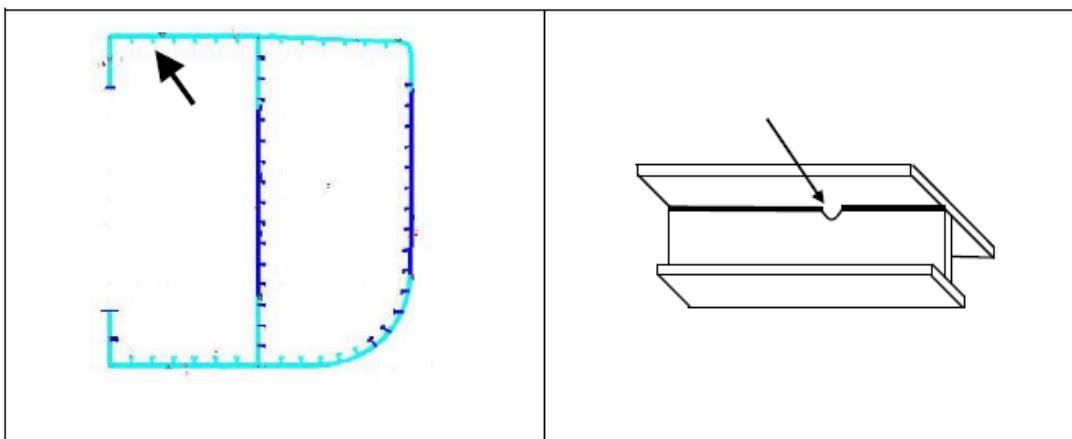


Figure 14.28 – Ship transverse section and assessed welded detail.

The ship has the following dimensions:

Length $L = 300$ m, Breadth $B = 57$ m, Depth $D = 30$ m, Draught $d = 21$ m, Block coefficient $C_b = 0.85$ (ratio of the loaded ship mass to 1.025 LBT). The plate thickness is 20 mm for the deck and 15 mm for the stiffener components.

14.5.2. Inputs

14.5.2.1 Flaw Information

The assessment concerns a new building, therefore the structure is assumed free of flaw.

14.5.2.2 Stresses

The structure scantling (dimensions) fulfils the classification rules which means that the midship vertical transverse modulus is equal to:

$$W_m = L^2 \cdot B \cdot (C_b + 0.7) \cdot 10^{-6} \text{ in m}^3 \quad (14.34)$$

The maximum midship vertical wave bending moments during the ship life are given by the classification rules as:

$$\text{hogging: } M_{wH} = 190 \cdot L^2 \cdot B \cdot C_b \cdot 10^{-3} \text{ in kN}\cdot\text{m} \quad (14.35)$$

$$\text{sagging: } M_{wS} = -110 \cdot L^2 \cdot B \cdot (C_b + 0.7) \cdot 10^{-3} \text{ in kN}\cdot\text{m} \quad (14.36)$$

The ship life is designed for 25 years. The classification society rules provide a long term cumulative distribution of the vertical wave bending moment range, therefore of stress range in deck. The distribution can be represented by a stair curve with 16 steps as given in the Table 14.11.

Table 14.11. Calculation of K_I and K_{Jc} in pipe tested

| $\Delta S/S_{\max}$ | n_i |
|---------------------|-------------|
| 1 | 5 |
| 0.88 | 68 |
| 0.74 | 342 |
| 0.63 | 1 895 |
| 0.51 | 8 160 |
| 0.44 | 13 160 |
| 0.40 | 47 370 |
| 0.35 | 47 370 |
| 0.32 | 92 105 |
| 0.30 | 131 580 |
| 0.28 | 265 260 |
| 0.22 | 568 420 |
| 0.16 | 1 684 210 |
| 0.13 | 2 736 840 |
| 0.09 | 26 315 790 |
| 0.05 | 68 421 055 |
| Σ | 100 333 630 |

14.5.2.3 Material Properties

The ship is built with normal steel of $\sigma_y = 235$ MPa.

14.5.3. Assessment

14.5.3.1 Route 1: Fatigue damage assessment using nominal stresses

- Step 1: Detected flaws

See 14.5.2.1.

- Step 2: Service condition, Nominal stress range

The nominal stress is the longitudinal stress range in deck induced by the wave vertical bending moment.

The bending moment range is given by:

$$\Delta M = M_{WH} - M_{WS} = L^2 B 10^{-3} [190C_b + 110(C_b + 0.7)] \quad (14.37)$$

The maximum stress range is:

$$\Delta S_{nom} = \frac{\Delta M}{W_m} = \frac{190 C_b + 110 (C_b + 0.7)}{C_b + 0.7} 10^3 = 214 \text{ MPa} \quad (14.38)$$

The stress range is lower than $2\sigma_y$ ($2\sigma_y = 470 \text{ MPa}$).

- Step 3: Environmental issues

The structure is protected against corrosion by an efficient coating.

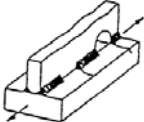
- Step 4: Threshold for fatigue assessment

The ship loads are induced by waves and so are random. In such conditions, there is no threshold below which no fatigue damage occurs.

- Step 5: Reference tables of classified components or structural details

The S-N curve can be found in the classification rule book catalogue. An extract is given in Table 14.12. This table shows that the S-N curve to be considered is the F curve.

Table 14.12 – Extract from the ship classification rules catalogue of details.

| Welded Joint Classification (cont'd) | | |
|---|-------------------------------------|---|
| Joint Classification | Description | Examples |
| Category 6 | | |
| E | 2) Intermittent fillet welds |  |
| F | 3) As (2) but adjacent to cut-outs. | |

The rule design curve is the 2 slopes curve without cut-off and the change of slope fixed at 10^7 cycles

$$m = 3 \text{ and } K_{D1} = 6.316 \cdot 10^{11}$$

The slope change stress range is:

$$\Delta S_I = (K_{D1}/10^7)^{1/3} = 39.8 \text{ MPa}$$

and the second part of the S-N curve is:

$$m = 5 \text{ and } K_{D2} = \Delta S_i^5 \cdot 10^7 = 9.987 \cdot 10^{14}$$

- *Step 6: Validity area of R ratios*

Ship structures are built as welded, so, due to welding residual stresses, no correction has to be done with respect to R ratio.

- *Step 7 Thickness reduction factor effects*

The thickness being less than 25 mm, no correction is required.

- *Step 8 Fatigue assessment using S-N Curves*

The Miner sum is given by:

$$D = \sum n_i / N_i \quad (14.39)$$

where $N_i = K_{D1} / \Delta S^3 \quad (14.40)$

or $N_i = K_{D2} / \Delta S^5 \quad (14.41)$

The Miner sum calculation details are given in Table 14.13. The value is:

$$D = 0.61$$

Table 14.13 – Miner sum calculation for nominal stress range.

| $\Delta S_i / S_{\max}$ | ΔS nom | n_i | n_i / N_i nom |
|-------------------------|----------------|-------------|-----------------|
| 1 | 214 | 5 | 0 |
| 0.88 | 188 | 68 | 0 |
| 0.74 | 158 | 342 | 0.002 |
| 0.63 | 135 | 1 895 | 0.007 |
| 0.51 | 109 | 8 160 | 0.017 |
| 0.44 | 94 | 13 160 | 0.017 |
| 0.40 | 86 | 47 370 | 0.048 |
| 0.35 | 75 | 47 370 | 0.032 |
| 0.32 | 69 | 92 105 | 0.048 |
| 0.30 | 64 | 131 580 | 0.054 |
| 0.28 | 60 | 265 260 | 0.091 |
| 0.22 | 47 | 568 420 | 0.093 |
| 0.16 | 34 | 1 684 210 | <i>0.077</i> |
| 0.13 | 28 | 2 736 840 | <i>0.047</i> |
| 0.09 | 19 | 26 315 790 | <i>0.063</i> |
| 0.05 | 11 | 68 421 055 | <i>0.011</i> |
| Σ | | 100 333 630 | 0.61 |

italic figure corresponds to the S-N curve part with $m = 5$

14.5.3.2 Route 2: Fatigue damage assessment using structural or notch stresses

A second possibility is to apply **Route 2**.

- *Step 1: Detected flaws*

The assessment concerns a new building, therefore the structure is assumed free of flaw.

- *Step 2: Service condition*

The notch stress approach requires two stress concentration factors: the structural hot spot stress SCF_{HS} and the notch effect SCF_{notch} .

The hot spot stress concentration factor has been determined by a finite element model of the detail submitted to tension. The found value is:

$SCF_{HS} = 1.1$ and the notch effect factor is given by:

$$SCF_{notch} = \lambda \cdot (\theta / 30)^{1/2} \quad (14.42)$$

with the following values:

Fillet weld $\theta = 45$ (see 7.3.2.1.2.3 in FITNET FFS Procedure)

well contoured end, perpendicular $\lambda = 2.15$ (see Table 7.4 in the Procedure) and so

$$SCF_{notch} = 2.15 \cdot (45 / 30)^{1/2} = 2.63$$

The notch stress range is: $\Delta S = SCF_{HS} \cdot SCF_{notch} \cdot \Delta S_{nom} = 619$ MPa

The hot spot stress range ($214 \cdot 1.1 = 235.4$ MPa) is lower than $2 \cdot \sigma_y$.

- *Step 3: Environmental issues*

The structure is protected against corrosion by an efficient coating.

- *Step 4: Threshold for fatigue assessment*

The ship loads are induced by waves and so are random. In such conditions, there is no threshold below which no fatigue damage occurs.

- *Step 5: Fatigue Data Specifications*

The rules book S-N curve to be associated to the notch stress is the following curve:

$$\text{mean curve } m = 3 \text{ and } K_{\text{mean}} = 3.913 \cdot 10^{13}$$

$$\text{standard deviation in } \log(C) = 0.1821$$

and the parameters of the design curve at minus 2 standard-deviations are:

$$m = 3 \quad K_{D1} = 1.692 \cdot 10^{13}$$

To take into account the non existence of threshold for fatigue, the rule design curve is a 2 slopes curve without cut-off. The change of slope, knee point, is fixed at 10^7 cycles (see 7.2.1.4 in the Procedure):

The stress range at the knee point is:

$$\Delta S_1 = (K_1 / 10^7)^{1/3} = 119.2 \text{ MPa}$$

and the second part of the S-N curve is:

$$m = 5 \quad K_{D2} = \Delta S_1^5 \times 10^7 = 2.406 \times 10^{17}$$

- *Step 6: Validity area of R ratios*

Ship structures are built as welded, so, due to welding residual stresses, no correction has to be done with respect to R ratio.

- *Step 7 Thickness reduction factor effects*

The thickness being less than 25 mm, no correction is required.

- *Step 8 Fatigue assessment using S-N Curves*

The Miner sum is given by equations (14.39) to (14.41).

The Miner sum calculation details are given in Table 14.14. The value is:

$$D = 0.54$$

Table 14.14 – Miner sum calculation for notch stress range.

| $\Delta S_i / S_{\max}$ | ΔS notch | n_i | n_i / N_i notch |
|-------------------------|------------------|------------|-------------------|
| 1 | 619 | 5 | 0.000 |
| 0.88 | 544 | 68 | 0.001 |
| 0.74 | 457 | 342 | 0.002 |
| 0.63 | 391 | 1 895 | 0.007 |
| 0.51 | 315 | 8 160 | 0.015 |
| 0.44 | 272 | 13 160 | 0.016 |
| 0.40 | 249 | 47 370 | 0.043 |
| 0.35 | 217 | 47 370 | 0.029 |
| 0.32 | 200 | 92 105 | 0.043 |
| 0.30 | 185 | 131 580 | 0.049 |
| 0.28 | 174 | 265 260 | 0.082 |
| 0.22 | 136 | 568 420 | 0.084 |
| 0.16 | 98 | 1 684 210 | <i>0.064</i> |
| 0.13 | 81 | 2 736 840 | <i>0.040</i> |
| 0.09 | 55 | 26 315 790 | <i>0.055</i> |
| 0.05 | 32 | 68 421 055 | <i>0.009</i> |
| Σ | | 9055 | 0.54 |

italic figure corresponds to the S-N curve part with $m = 5$

14.5.4. References

[14.17] Didactic material supplied by Michel Huther (Bureau Veritas)

14.6 Fatigue tutorial: Application of Structural Stress Method on Welded Components [14.18]

14.6.1. Introduction

This tutorial describes how the mesh-insensitive structural stress method (see Section 7.1 in FITNET FFS Procedure) can be applied for performing fatigue evaluation of welded components. For a given engineering component, the fatigue evaluation procedure can be divided into two steps:

- 1) Calculation of the structural stresses (σ_s) under a given unit load condition using a typical finite element model;
- 2) Obtainment of the fatigue life from the master S-N curve by converting the structural stress range to the corresponding equivalent structural stress range ΔS_s .

The details will be demonstrated by using an example called Yagi's component tests [14.19]. The component geometry and loading conditions are shown in Figure 14.29. Further details can be found in [14.19].

14.6.2. Inputs

To perform fatigue evaluation of a welded component using the mesh-insensitive structural stress method, the information required is essentially same as that in using other FEA based method, except that in performing FEA, balanced nodal forces are requested, instead of nodal stresses. Further details can be found in [14.20].

14.6.3. Assessment

In what follows, Yagi's component tests shown in Figure 14.29 will be used to demonstrate on how both the structural stress method and the master S-N curve can be used to evaluate fatigue lives:

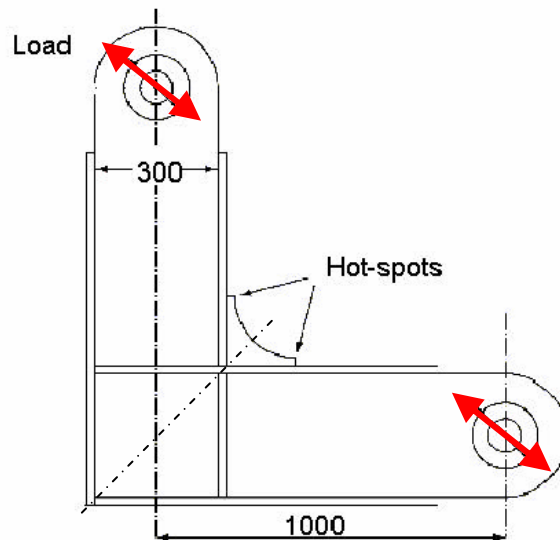


Figure 14.29 – Specimen geometry.

- 1) A plate finite element model is shown in Figure 14.30, where the fillet weld between the attachment and I beam flange is represented with a row of 45 degree angle inclined elements. Under the given loading conditions, the element nodal forces surrounding the entire weld toe line are extracted from a finite element analysis.

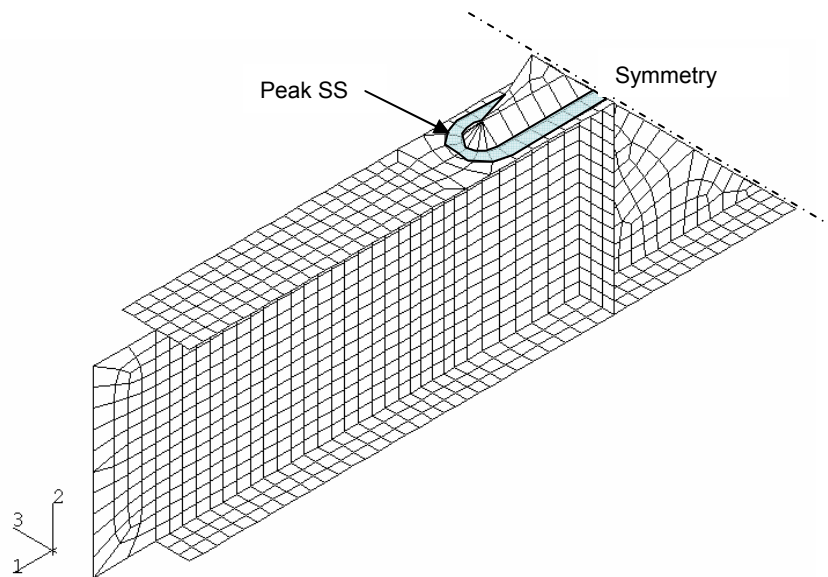


Figure 14.30 – Finite element model.

2) The structural stresses for all the nodes describing the curve formed by the weld toe are then calculated using a JIP structural stress post-processor. The definition of the structural stresses is shown in equation (14.43).

$$\sigma_s = \sigma_m + \sigma_b = \frac{f}{t} + \frac{6m}{t^2} \quad (14.43)$$

where t is the plate thickness, σ_m is the membrane stress and σ_b is the bending stress components being calculated from line force (f) and line moment (m).

In the post-processor, coordinate rotation, construction of the system of simultaneous equations relating nodal forces and moments to line force and moments are automatically carried out. Then, the structural stresses along the weld line are searched for the maximum value, as shown in Figure 14.31. (Note: for element sizes less than $1 \times 0.1t$, the effects of the discontinuity at the intersection between the I beam web plate and the weld line on the structural stress becomes noticeable. A weld line ending at the hot spot should be used, instead of the entire weld line as shown.)

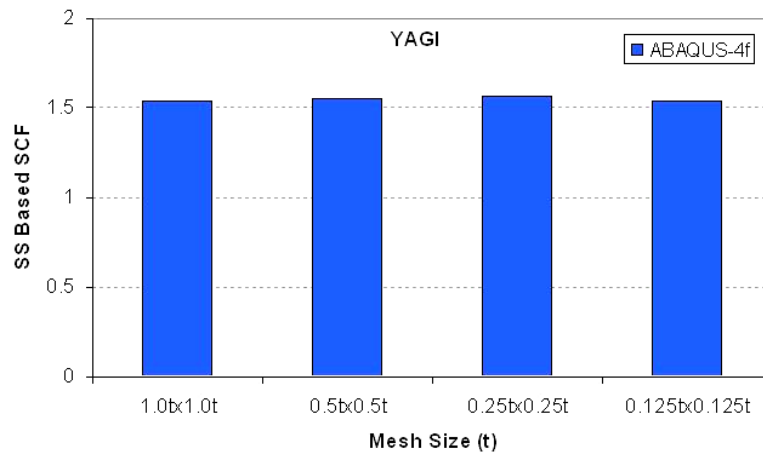


Figure 14.31 – Structural stress calculation example- Yagi’s tests [14.19].

3) With the structural stress calculated under the given constant amplitude loading conditions [14.19], the loading ratio is then used to obtain the structural stress range needed to enter equation (14.44). At the peak structural stress range location shown in Figure 14.30, the plate thickness t is the flange thickness. The bending ratio is determined as follows:

$$r = \frac{|\sigma_b|}{|\sigma_m| + |\sigma_b|} \tag{14.44}$$

At the given bending ratio r , $I(r)^{1/m}$ can be determined from Figure 14.32 (note that it is always recommended to use load-controlled conditions to be conservative). Then, the equivalent structural stress range ΔS_S is fully determined. Note that m takes the value of 3.6 [14.19-14.21].

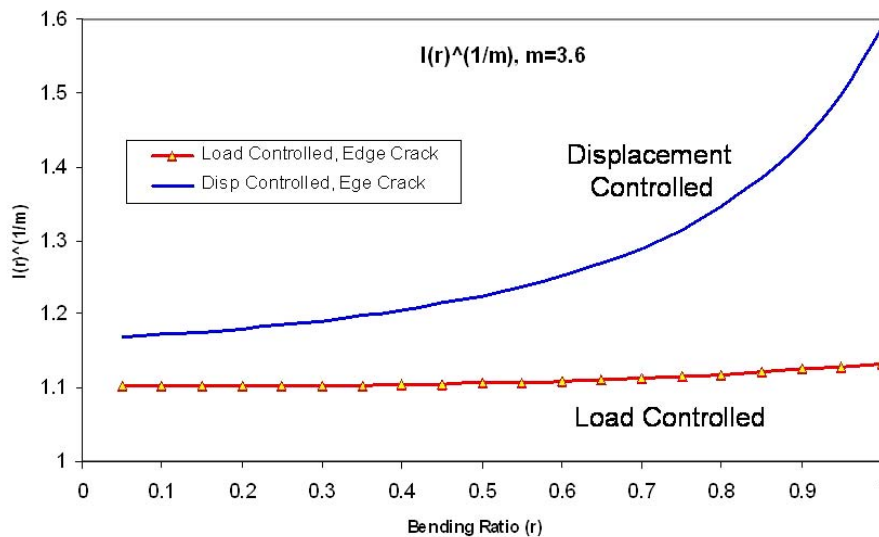


Figure 14.32 – $I(r)$ functions assumed an edge crack ($a/t = 0.7$, $m=3.6$).

The equivalent structural stress range is determined by:

$$\Delta S_s = \frac{\Delta \sigma_s}{t^{\frac{2-m}{2m}} \cdot I(r)^{\frac{1}{m}}} \quad (14.45)$$

4) With the given equivalent structural stress range ΔS_s , Figure 14.33 can be used to estimate the corresponding mean life by reading the cycles to failure from the mean line at ΔS_s from the ordinate.

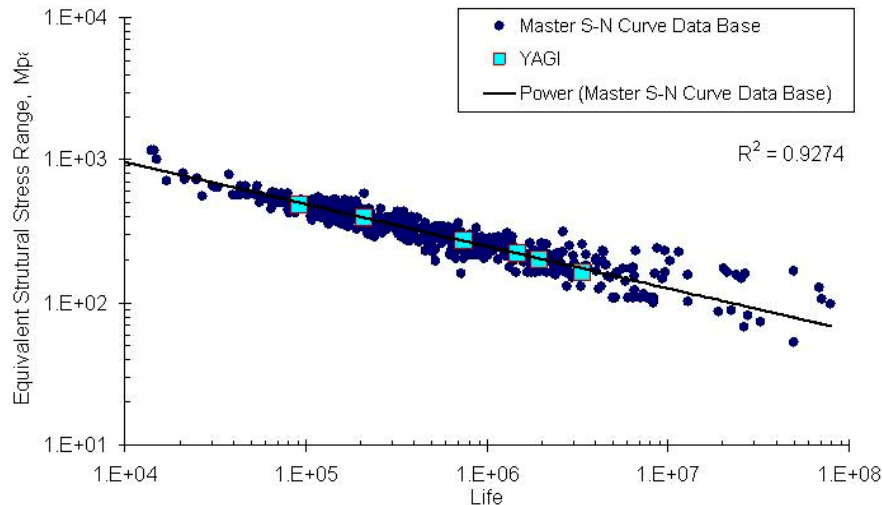


Figure 14.33 – Fatigue life evaluation of Yagi’s specimens [14.19] using the structural stress based master S-N curve approach (note that the equivalent structural stress range has a reference thickness of 1mm).

5) For known test results, such as the Yagi’s tests shown in Figure 14.33, the test results can be alternatively plotted against the master S-N curve for each pair of ΔS_s -N corresponding to each test condition. The actual test data for the component shown in Figure 14.29 reported in [14.19] are approximately located within the mean line of the master S-N curve, indicating that the life estimation using the mesh-insensitive structural stress method shows a good agreement with the actual test data. If the structural stress ranges versus tested lives are plotted and if the new structural stress approach is valid, the S-N data by Yagi [14.19] should be located within the scatter band in the S-N curves proposed in the FITNET Fatigue Module. Indeed, Figure 14.33 summarizes such a comparison. The five square symbols are the actual S-N data from Yagi’s tests and all small circle symbols are the S-N data same as those used to derive the mean master S-N proposed curves.

14.6.4. References

[14.18] Didactic material supplied by Pingsha Dong (Batelle)

[14.19] SR202 of Shipbuilding Research Association of Japan, Fatigue Design and Quality Control for Offshore Structures, 1991 (in Japanese), also published as International Institute of Welding (IIW) Document: IIW XIII-1414-91, 1991

[14.20] Dong, P., “A Robust Structural Stress Method for Fatigue Analysis of Ship Structures,” Proceedings of the 22nd International Conference on Offshore Mechanics and Arctic Engineering, June 8-13, 2003, Cancun, Mexico.

[14.21] Dong, P., “Mesh-Insensitive Structural Stress Method and Master S-N Curve Development for FPSOs,” Proceedings of this conference, OMAE-FPSO’04-0021, Houston, TX, Aug 30-Sept. 2, 2004.

14.7. Creep tutorial: Flat Plate under Constant Tensile Load [14.22]

14.7.1. Introduction

A Cn-Mn steel flat plate of width 100 mm is subjected to constant tensile load (Figure 14.34). The plate operates at 380°C and has a single edge notch of depth 20 mm. This tutorial will analyse the structural integrity of the plate and the evolution of the crack under these working conditions.

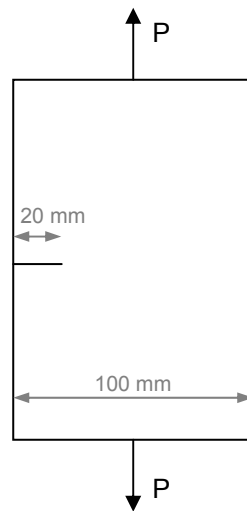


Figure 14.34 – Scheme of the plate and the working conditions.

14.7.2. Inputs

14.7.2.1 Flaw information

The plate has a single edge notch of depth 20mm. The defect is assumed to have been present from the start of high temperature operation.

14.7.2.2 Stresses

The plate operates at 380°C under a constant tension, P, corresponding to a nominal stress $P/Bw=100$ MPa.

14.7.2.3 Material Properties

Creep strain and creep rupture properties are related by equation (14.46) given by

$$\varepsilon_c(\sigma, t) = A' \left(\frac{\sigma}{\sigma_R + B'} \right)^{C'} \quad (14.46)$$

where A' , B' and C' are constants and σ_R is obtained from rupture data as the stress to give failure in time t . These data are fitted by a polynomial relationship between failure time, t_r , and $x = \log_{10}\sigma$:

$$\log_{10} t_r = 10.68 + 153.2(a + bx + cx^2 + dx^3 + ex^4) \quad (14.47)$$

where a , b , c , d and e are constants whose values are given in Table 14.15 along with all other material properties required.

Table 14.15. Material Properties

| | |
|---|---|
| Young's modulus (MPa) | 185 000 |
| Creep Strain (σ in MPa) | equation (14.46) with $A' = 0.526$ $B' = 23.0$ $C' = 6.9$ |
| Creep Rupture (σ in MPa, t_r in hours) | equation (14.47) with $a = -1.26$ $b = 2.62$ $c = -2.06$ $d = 0.72$ $e = -0.094$ |
| Incubation COD (mm) | 0.06 |
| Crack Growth Rate $da/dt=A\cdot(C^*)^q$ (equation(14.48)) | |
| A | 0.006 |
| q | 0.85 |
| (da/dt in mh^{-1} , C^* in $MPa\ mh^{-1}$) | |

14.7.3. Assessment

The assessment of the plate will follow the scheme proposed in the FITNET FFS Procedure (Creep Module) [14.23]:

- *Step 1. Establish cause of cracking and characterise initial defect.*

The component is a C-Mn steel plate of width 100 mm with a single edge notch of depth 20mm. The defect is assumed to have been present from the start of high temperature operation.

- *Step 2. Define service conditions.*

The plate operates at 380°C under a constant tension, P, corresponding to a nominal stress of 100 MPa.

- *Step 3. Collect materials data.*

As seen in 14.7.2.3.

- *Step 4. Perform basic stress analysis.*

For steady creep loading, the following data are required:

- Categorized (primary or secondary) stresses
- Reference stresses for appropriate crack lengths
- Stress intensity factors for appropriate crack lengths

In this case, the load is a primary membrane stress of 100 MPa.

The reference stress is calculated according to the limit load for this geometry given by

$$P_L = 1.155\sigma_Y Bw \left[1 - \frac{a}{w} - 1.232 \left(\frac{a}{w} \right)^2 + \left(\frac{a}{w} \right)^3 \right] \quad (14.49)$$

where the plane strain Mises solution has been adopted. For component applications, the appropriate limit load (plane stress or strain, Tresca or Mises) must be chosen on the basis of geometrical constraint and the multiaxial creep rupture surface. From its definition in the FITNET FFS Creep Module, the reference stress is then

$$\sigma_{ref} = \frac{0.866 \left(\frac{P}{Bw} \right)}{\left[1 - \frac{a}{w} - 1.232 \left(\frac{a}{w} \right)^2 + \left(\frac{a}{w} \right)^3 \right]} \quad (14.50)$$

which has a value

$$\sigma_{ref} = 114 \text{ MPa}$$

for the applied loading $P/Bw = 100 \text{ MPa}$ and initial crack size $a_0 = 20 \text{ mm}$.

For the single edge notch plate the handbook of Tada, Paris and Irwin [14.24] gives a solution for K

$$K = \sigma \sqrt{\pi a} \cdot F \left(\frac{a}{w} \right) \quad (14.51)$$

where $\sigma = P/Bw$

$$F = \left\{ \frac{\tan \theta}{\theta} \right\}^{1/2} \frac{0.752 + 2.02 \left(\frac{a}{w} \right) + 0.37 (1 - \sin \theta)^3}{\cos \theta} \quad (14.52)$$

where $\theta = \pi a/2w$. For the nominal stress of 100 MPa and $a/w = 0.2$, this gives

$$K = 34.3 \text{ MPa} \cdot \text{m}^{1/2}$$

- *Step 5. Check stability under time-independent loads*

This step is not considered in detail for this example. The check on time-independent failure would normally be based on short-term fault loadings rather than on the steady operating loadings. Reference may be made to R6 [14.22] for examples of such calculations.

- *Step 6. Check significance of creep and fatigue*

In this case, the load is constant and so fatigue is not a consideration. For the purpose of this example, it is assumed that creep is significant.

- *Step 7. Calculate rupture life*

The rupture life for failure by continuum damage mechanisms, t_{CD} , is evaluated from

$$t_{CD} = t_r [\sigma_{ref}^p(a)] \quad (14.53)$$

Hence, the time for failure by continuum damage

$$t_{CD} = 2.17 \cdot 10^6 \text{ h}$$

as depicted in Figure 14.35.

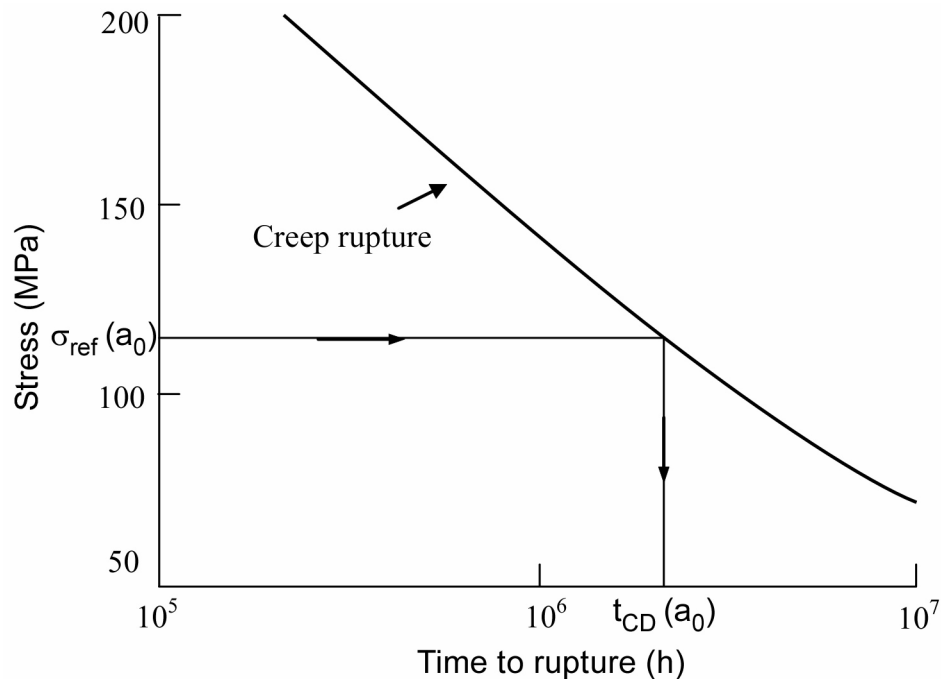


Figure 14.35 – Uniaxial stress/time-to-rupture data, illustrating calculation of t_{CD} .

- *Step 8. Calculate incubation time*

Creep crack incubation occurs when the creep strain accumulation, ϵ_c , at the reference stress of equation (14.50) after a time t_i produces a critical crack opening displacement [14.22,14.23]. Provided widespread creep conditions have been established, these terms are related by:

$$\varepsilon_c = 0.5 \left(\frac{\delta_i}{R'} \right)^{n/(n+1)} \quad (14.54)$$

The length parameter R' is defined by.

$$R' = \left(\frac{K^p}{\sigma_{ref}^p} \right)^2 \quad (14.55)$$

Thus

$$R' = (34.3/114)^2 \text{ m} = 90 \text{ mm}$$

which is comparable to the section width. This is generally the case, although for small cracks R' is comparable to crack size and for deep cracks R' is proportional to the remaining ligament. From equation (14.54), the creep strain for incubation is

$$\varepsilon_c = 0.5 \left(\frac{0.06}{90} \right)^{n/(n+1)} \quad (14.56)$$

using the data in Table 1. As the creep data for this material are not in the form of a power law, a value of n is not available and hence $n/(n+1)$ is set equal to the exponent q in the creep crack growth law ($q = 0.85$ in Table 14.15), as suggested in [14.22]. Whence

$$\varepsilon_c = 0.001$$

This may be substituted into equation (14.46) for $\sigma = 114$ MPa from equation (14.50) to give $\sigma_R = 260$ MPa. From equation (14.47), this corresponds to a rupture time of 20000 hours and hence the creep strain of 0.001 is accumulated in this time, i.e.

$$t_i = 20000 \text{ h}$$

as depicted in Figure 14.36.

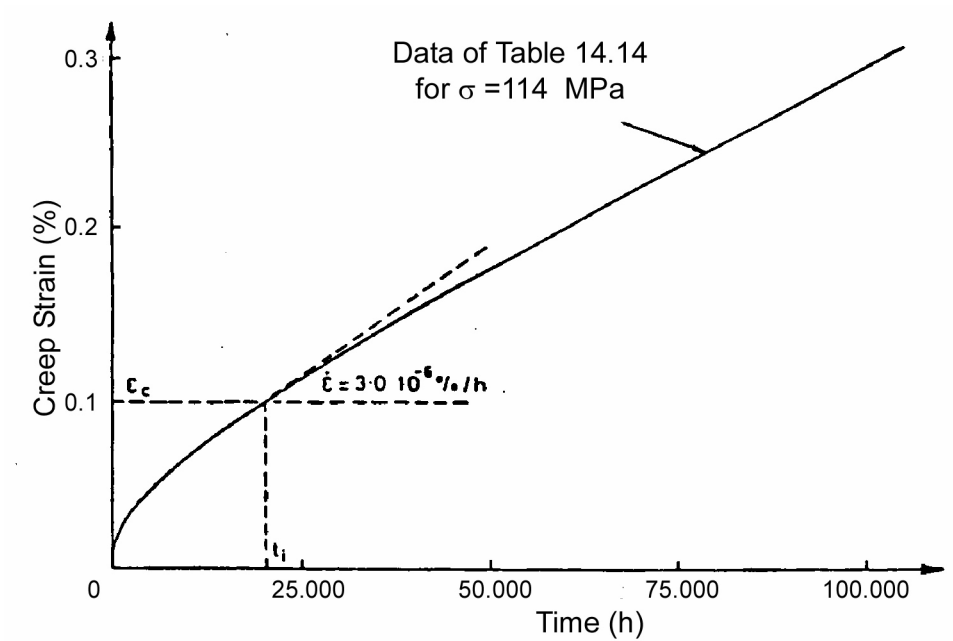


Figure 14.36 – Creep strain/time data, illustrating calculation of t_i

- Step 9. Calculate crack size after growth

The FITNET FFS Procedure specifies that the extent of crack growth occurring during the desired additional service life should be calculated at this stage. As an additional life has not been specified in the present example, the crack growth calculations are carried out until the calculated crack growth rate is high and failure is essentially reached. Crack growth is calculated according to the methods of the Creep Module using the C^* parameter:

$$C^* = \sigma_{ref} \dot{\epsilon}_c (\sigma_{ref}, \epsilon_c) R' \quad (14.57)$$

The reference stress and length parameter R' have already been calculated for the initial crack size. From Figure 14.36, the creep strain rate at the incubation time is:

$$\dot{\epsilon}_c = \frac{d\epsilon_c}{dt} = 3 \cdot 10^{-8} / h \quad (14.58)$$

Thus

$$C^* = 3 \cdot 10^{-7} \text{ MPa m h}^{-1}$$

at the incubation time. The corresponding crack growth rate using the crack growth law in Table 14.15 is:

$$\dot{a} = \frac{da}{dt} = 1.8 \cdot 10^{-5} \text{ mm h}^{-1} \quad (14.59)$$

By assuming that the crack growth and creep strain rates are constant for a short time, Δt , the crack size and accumulated creep strain can be updated, and new values for reference stress and creep strain rate can be obtained from equation (14.50) and equation (14.46) assuming a strain hardening rule. The value of C^* can then be obtained with R' evaluated for the new crack size, leading to a new value for da/dt . In practice it is more convenient to implement these calculations by incrementing crack size or creep strain using special purpose computer programs or spreadsheet calculations. A special purpose computer program was used here to predict the crack size as a function of time shown in Figure 14.37.

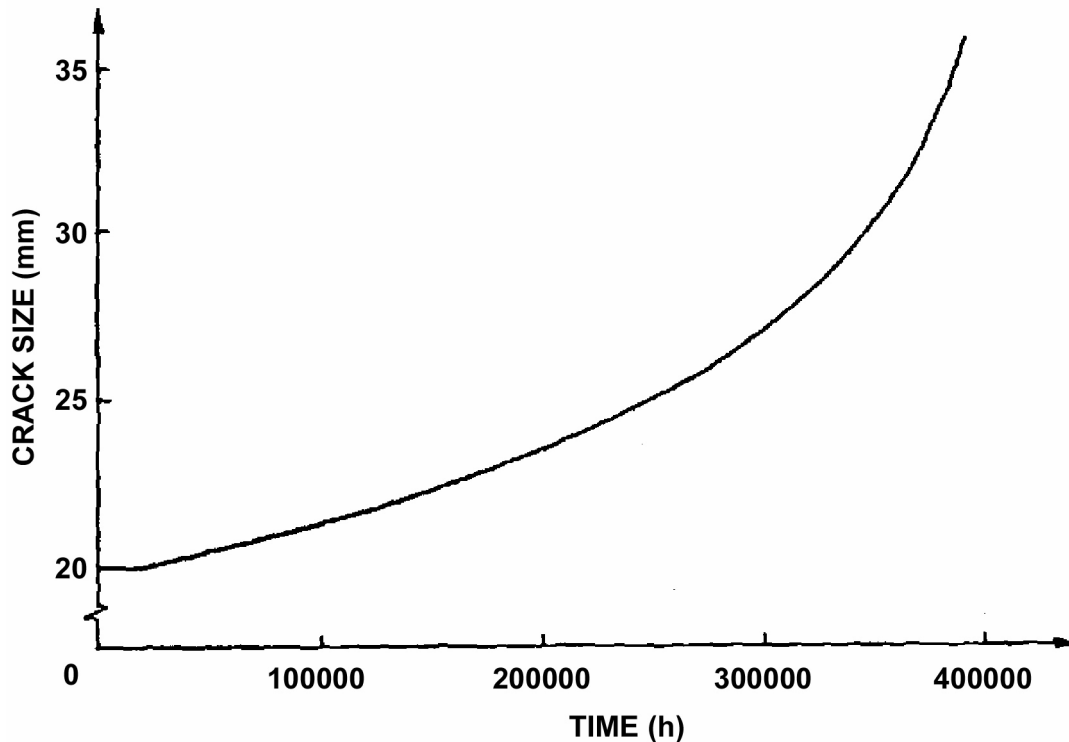


Figure 14.37 – Calculation of crack growth stage

- Step 10. Recalculate rupture life after growth

As the reference stress is calculated at each stage of the crack growth calculations of STEP 9, it is straightforward to recalculate t_{CD} . Even when the crack has grown to a depth of 35 mm, the reference stress of equation (14.50) is only 160 MPa and this corresponds to a remaining life of 650000 hours. It is then clear from the timescale in Figure 14.36 that in this example creep crack growth rather than creep rupture is the dominant failure mechanism.

- Step 11. Check stability of time-independent loads after growth

Again, these calculations are not considered in detail for this tutorial.

- Step 12. Assess significance of results

The following conclusions can be drawn for this example:

- The remaining creep rupture life was found to be high at all stages of the assessment, showing that creep crack growth, rather than creep rupture, is the dominant failure mechanism.
- Widespread creep conditions are achieved prior to the incubation time.
- An incubation time of $t_i = 20000$ hrs is predicted.

- The crack is predicted to grow by 15mm over 380000hrs.

The sensitivity of the calculated rupture life, t_{CD} , for the present example may be examined simply from equation (14.47). This shows that the rupture life is reduced by a factor of 2 for a 25 per cent increase in the reference stress.

14.7.4. References

[14.22] "R5: Assessment Procedure for the High Temperature Response of Structures", British Energy Generation, Issue 3, June 2003.

[14.23] "FITNET FFS Procedure", GIRT-CT-2001-05071

[14.24] H.Tada, P.C. Paris and G.R.Irwin, "The Stress Analysis of Cracks Handbook", New York: ASME Press, 3rd edition, 2000.

14.8. Creep tutorial: Cylindrical Pipe with an Internal Crack under Cyclic Loading [14.25]

14.8.1. Introduction

A $\frac{1}{2}\text{Cr}\frac{1}{2}\text{Mo}\frac{1}{4}\text{V}$ steel cylindrical pipe ($r_i=300$ mm and wall thickness, $w=100$ mm) is subjected to cyclic loading (Figure14.38). The pipe operates at 565°C and has a fully circumferential defect on the inside with the initial depth, a_0 , taken as 3mm. This tutorial will analyse the structural integrity of the pipe and the evolution of the crack under these working conditions.

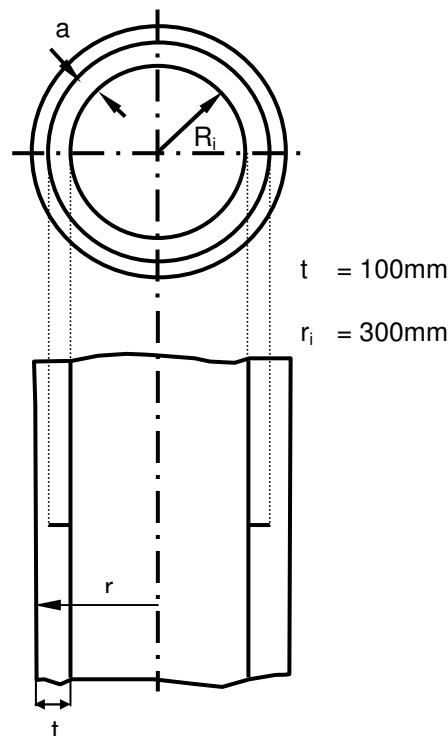


Figure 14.38 – Idealised structural geometry

14.8.2. Inputs

14.8.2.1 Flaw information

The defect is assumed to be a fully circumferential flaw on the inside of the pipe with the initial depth, a_0 , taken as 3 mm. The defect is assumed to have been present from the start of high temperature operation.

14.8.2.2 Stresses

The pipe operates at 565°C under a cyclic loading.

14.8.2.3 Material Properties

Creep strain data are described by the following parametric expression proposed by White [14.26].

$$\varepsilon = \varepsilon_p \left[1 - \exp(-rt^\mu) \right] + \dot{\varepsilon}_s t \quad (14.60)$$

with the maximum primary strain, ε_p , given by

$$\varepsilon_p = A' \sigma^{m(\theta)} \exp[-P/(\theta + 273)] \quad (14.61)$$

where $m(\theta) = \alpha - \gamma\theta$ and the secondary creep strain rate is given by

$$\dot{\varepsilon}_s = B \sigma^n \exp[-P/(\theta + 273)] \quad (14.62)$$

where θ is the temperature (in °C) and σ is the reference stress. The constants in equations (14.60) to (14.62) are given in Table 14.16 together with other required material properties. The creep strain rate may be obtained by differentiating equation (14.60) with respect to time as

$$\dot{\varepsilon} = \varepsilon_p r \mu t^{\mu-1} \exp(-rt^\mu) + \dot{\varepsilon}_s \quad (14.63)$$

However, as $\mu < 1$, the creep strain rate given by the above analytical expression becomes infinite at time zero. For short times and low strains ($< 10^{-4}$), the creep strain rate is approximated by dividing the strain of 10^{-4} by the time to reach this strain (obtained from equation (14.60)).

As the stresses acting during the dwell periods are treated as load controlled (as described in STEP 9), forward creep data are appropriate for calculating creep strains and strain rates.

Table 14.16. Material Properties

| | |
|---------------------------------------|---|
| Elastic Modulus (MPa) | 155 000 |
| Creep Strain | equations (14.60) to (14.63) with $r=2.42 \times 10^{-2}$ $\mu=0.64$ $A'=1.632 \times 10^{35}$ $P=9.292 \times 10^4$ $\alpha=16.32$ $\gamma=0.02044$ $B=1.065 \times 10^{-5}$ $Q=1.97 \times 10^4$ $n=4$ |
| Cyclic Crack Growth Rate (m/cycle) | $C=2.0 \times 10^{-9}$ $\ell=3$ |
| Creep Crack Growth Rate (m/h) | $A=0.0197$ $q=0.89$ |

14.8.3. Assessment

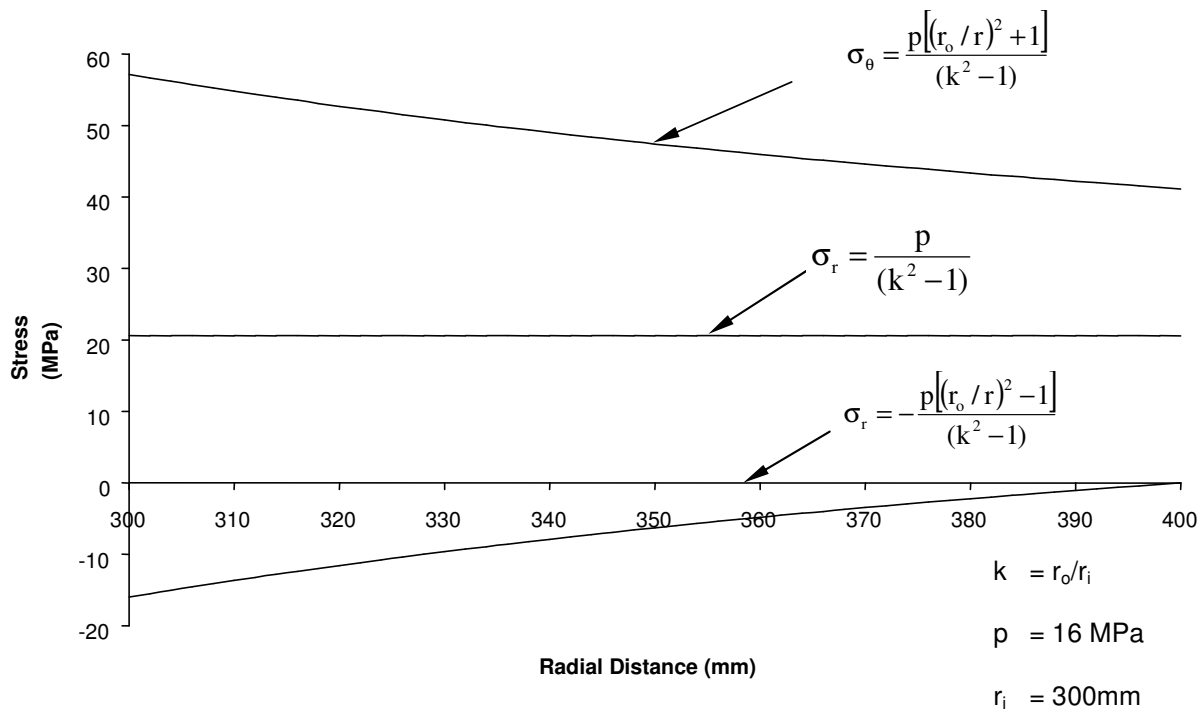
The assessment of the plate will follow the scheme proposed in the FITNET FFS Procedure (Creep Module) [14.27]:

- Step 1. Establish cause of cracking and characterise initial defect

The idealised structural geometry is shown in Figure 14.38. It comprises a homogeneous Type 316 Stainless Steel pipe of internal radius, $r_i=300$ mm and wall thickness, $w=100$ mm. A defect is assumed to be present at the start of high temperature operation so that the life to date is taken as zero. The defect is assumed to be fully circumferential on the inside of the pipe with the initial depth, a_0 , taken as 3mm.

- Step 2. Define service conditions

The pipe is subjected to repeated cyclic loading from an initially unstressed shutdown condition at ambient temperature (20°C) to an operating condition at 600°C, comprising an internal pressure of 16 MPa together with through wall axial and hoop thermal bending stresses of 200 MPa. The bending stresses are such that tensile stresses arise on the inside surface of the pipe (Figures 14.39 and 14.40). In the present examples 500 equal cycles, with 3000 hour dwells at operating conditions, are assumed to occur during the desired future service life of 1.5×10^6 hours.



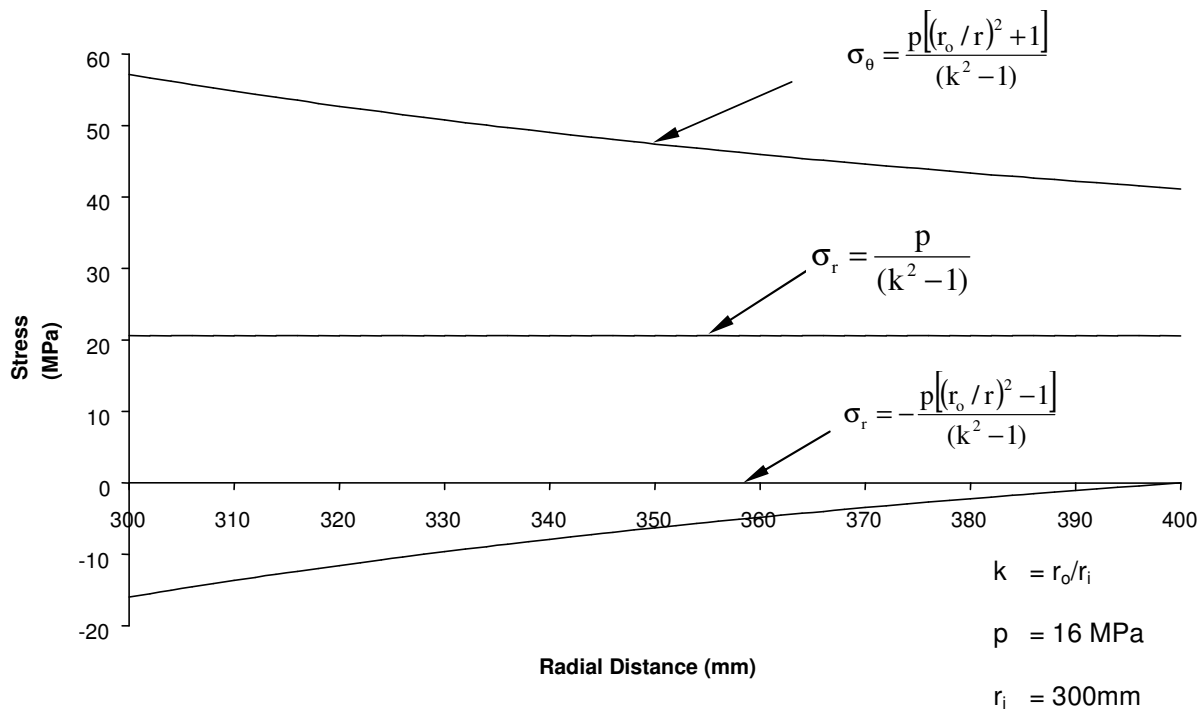
14.39 - Initial operating elastic stresses (Pressure Stresses)

Figure

The idealised structural geometry is shown in Figure 14.38. It comprises a homogeneous Type 316 Stainless Steel pipe of internal radius, $r_i=300$ mm and wall thickness, $w=100$ mm. A defect is assumed to be present at the start of high temperature operation so that the life to date is taken as zero. The defect is assumed to be fully circumferential on the inside of the pipe with the initial depth, a_0 , taken as 3mm.

- Step 2. Define service conditions

The pipe is subjected to repeated cyclic loading from an initially unstressed shutdown condition at ambient temperature (20°C) to an operating condition at 600°C, comprising an internal pressure of 16 MPa together with through wall axial and hoop thermal bending stresses of 200 MPa. The bending stresses are such that tensile stresses arise on the inside surface of the pipe (Figures 14.39 and 14.40). In the present examples 500 equal cycles, with 3000 hour dwells at operating conditions, are assumed to occur during the desired future service life of 1.5×10^6 hours.



14.39 - Initial operating elastic stresses (Pressure Stresses)

Figure

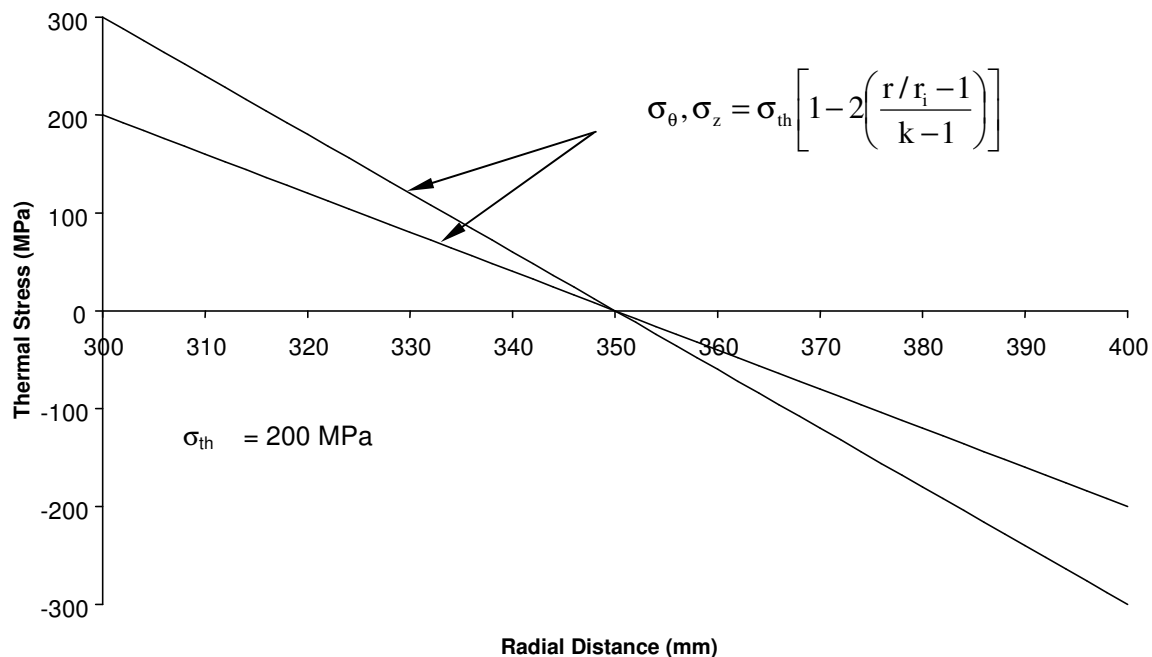


Figure 14.40 - Initial operating elastic stresses (Thermal Stresses)

- Step 3. Collect materials data

As seen in 14.8.2.3.

- Step 4. Perform basic stress analysis

For cyclic loading, the following are required:

- A shakedown analysis.
- The depth of the cyclic plastic zone on the surface of the defective section.
- The elastic follow-up factor.
- The stress intensity factors, K_{min} and K_{max} and the associated R ratio, which permit the effective stress intensity factor range, ΔK_{eff} to be calculated.
- The reference stress for the creep dwell.

Shakedown analysis

Details of shakedown analysis methods are given in [14.25-14.27]. Uncracked body elastic stresses are required as the starting point for the analyses. In this example, the pressure stresses are given by the Lamé thick cylinder equations with the thermal stresses taken as through wall bending stresses of equal magnitude in the hoop and axial directions (see Figures 14.39 and 14.40); k in these figures is the ratio of outer to inner radius, r_o/r_i . The initial total operating elastic stresses are then the sum of the pressure and thermal contributions.

In order to determine if the structure is operating within shakedown it is necessary to generate a residual stress field. For this example, it is convenient to select a residual stress field which is a factor, α , times the thermal stress field (i.e. axial and hoop bending stresses of 200α MPa). The shakedown stress field, $\tilde{\sigma}_s$, is then obtained by adding the residual stress field $\tilde{\rho}$ to the elastically calculated stress field, $\tilde{\sigma}_{el}$. Thus,

$$\tilde{\sigma}_s = \tilde{\sigma}_{el} + \tilde{\rho} \quad (14.64)$$

Shakedown stress fields are thereby determined for the cold (non-creep) and hot (creep) extremes of the loading cycle, denoted $(\tilde{\sigma}_s)_{nc}$ and $(\tilde{\sigma}_s)_c$ for shutdown and operating conditions, respectively. For the structure to attain strict shakedown, the shakedown stress fields at the cold and hot extremes of the loading cycle must satisfy the following criteria

$$(\bar{\sigma}_s)_{nc} \leq (K_s S_y)_{nc} \quad (14.65)$$

and

$$(\bar{\sigma}_s)_c \leq (K_s S_y)_c \quad (14.66)$$

where S_y is the minimum 0.2% proof stress, K_s is applied to S_y to obtain the material ratchet limit factor (see [14.25]) with the values $(K_s)_{nc}$ and $(K_s)_c$ at shutdown and operating conditions respectively, and $(\bar{\sigma}_s)_{nc}$ and $(\bar{\sigma}_s)_c$ are the shakedown equivalent stresses at shutdown and operating conditions respectively. [14.25] permits limited regions of a structure to be exempted from strict shakedown requirements. The structure is then deemed to be within global shakedown if at least 80% of every section consists of a ligament over which the shakedown criteria are satisfied at the two extremes of the loading cycle. For the current example which involve shutdown at 20°C, values of $(K_s)_{nc} = 0.752$ and $(S_y)_{nc} = 245$ MPa are assumed for the Type 316 Stainless Steel, leading to a shakedown criterion at shutdown of

$$(\bar{\sigma}_s)_{nc} \leq 184.2 \text{ MPa}$$

For operation at 600°C, assumed values of $(K_s)_c = 1.15$ and $(S_y)_c = 109.6$ MPa give a shakedown criterion at operation of

$$(\bar{\sigma}_s)_c \leq 126.0 \text{ MPa}$$

For this example, strict shakedown can be demonstrated for the pipe. Creep relaxation during early loading cycles reduces the stress at the hot extreme of the cycle until the cold extreme of the cycle reaches the limit of the shakedown criterion at shutdown (equation (14.65)). This situation is achieved using a residual stress field obtained by scaling the thermal stress field by $\alpha = -0.921$. Resulting steady cyclic stress profiles for the uncracked pipe are shown in Figures 14.41 and 14.42 for shutdown and operating conditions, respectively.

In order to take account of early cycles prior to attainment of the steady cyclic state, it is also necessary to determine the initial stress state. For this example, the initial stress state is obtained using a Neuber construction for the most highly stressed inside surface point as described in [14.25]. The initial elastic operating stress profiles shown in Figure 14.43 give an initial elastic equivalent stress at the inner surface of 256.8 MPa. This elastic equivalent stress has then been used, together with monotonic isochronous data for Type 316 Stainless Steel at 600°C, to estimate the initial equivalent stress at the inner surface as shown in Figure 14.44. This initial equivalent stress at the inner surface (141.8 MPa) has then been used to infer an initial residual stress field, which when combined with the initial elastic stresses, gives the correct value of inner surface equivalent stress. The required initial residual stress field is obtained by scaling the thermal stress field by $\alpha = -0.583$. Resulting initial stress profiles are shown in Figures 14.45 and 14.46 for shutdown and operating conditions, respectively.

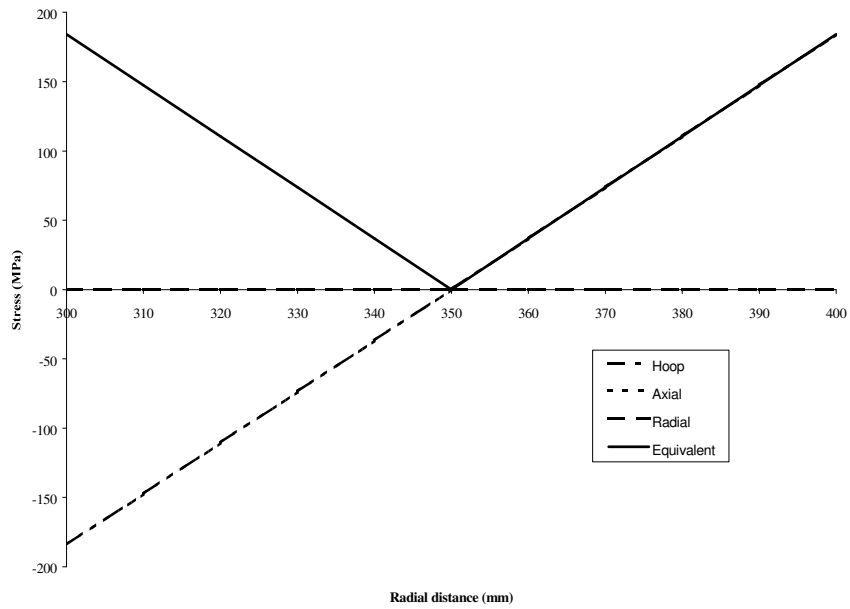


Figure 14.41 - Shutdown shakedown elastic stresses.

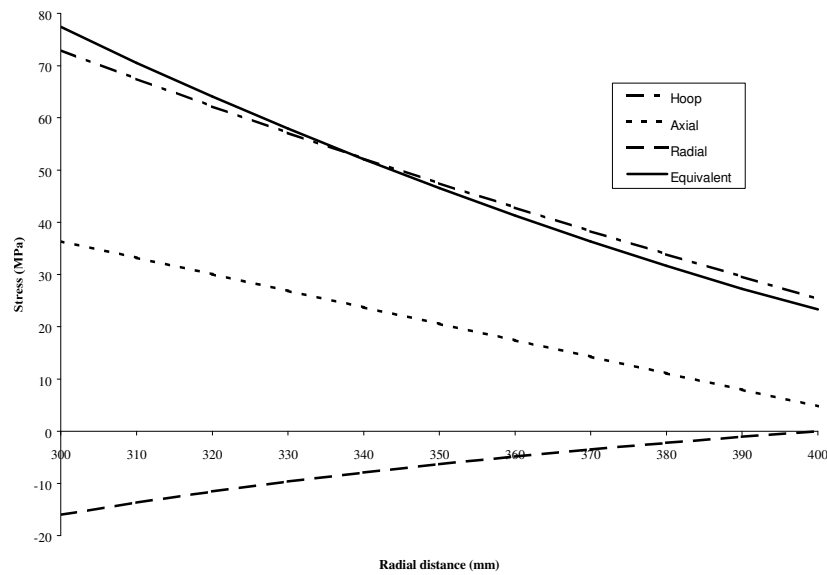


Figure 14.42- Operating shakedown elastic.

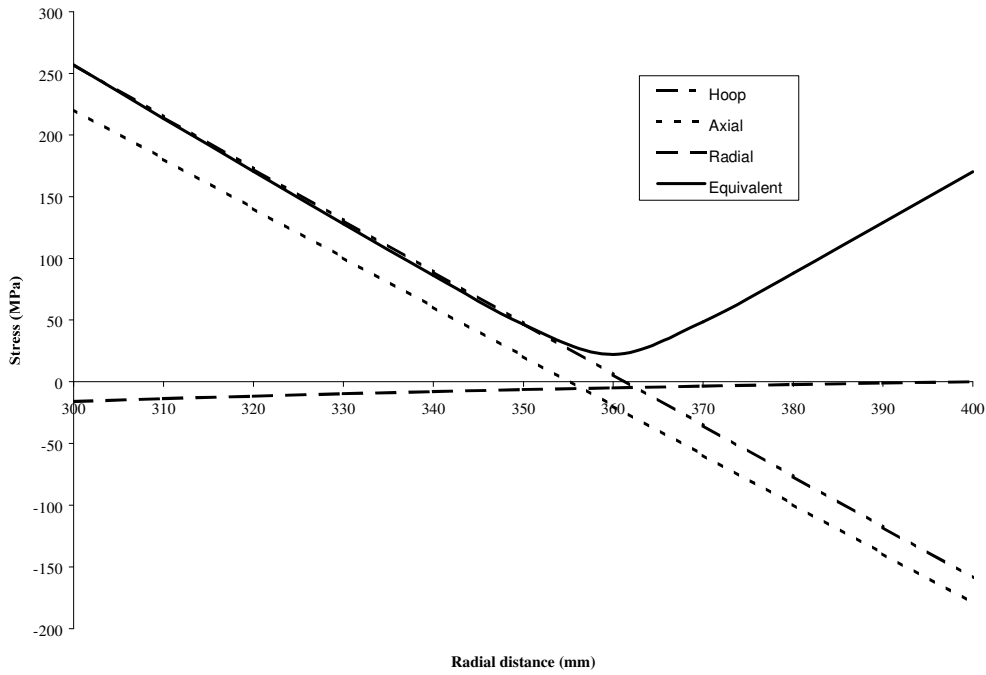


Figure 14.43 - Initial operating elastic.

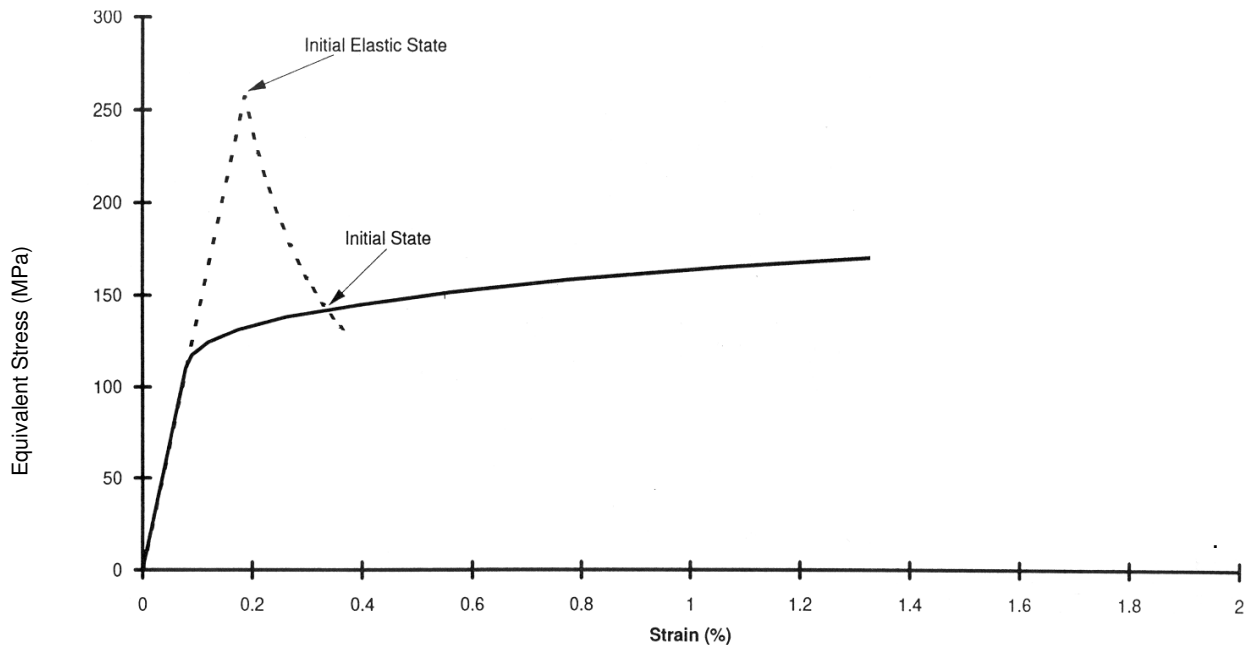


Figure 14.44 - Neuber construction for initial stresses at inner surface.

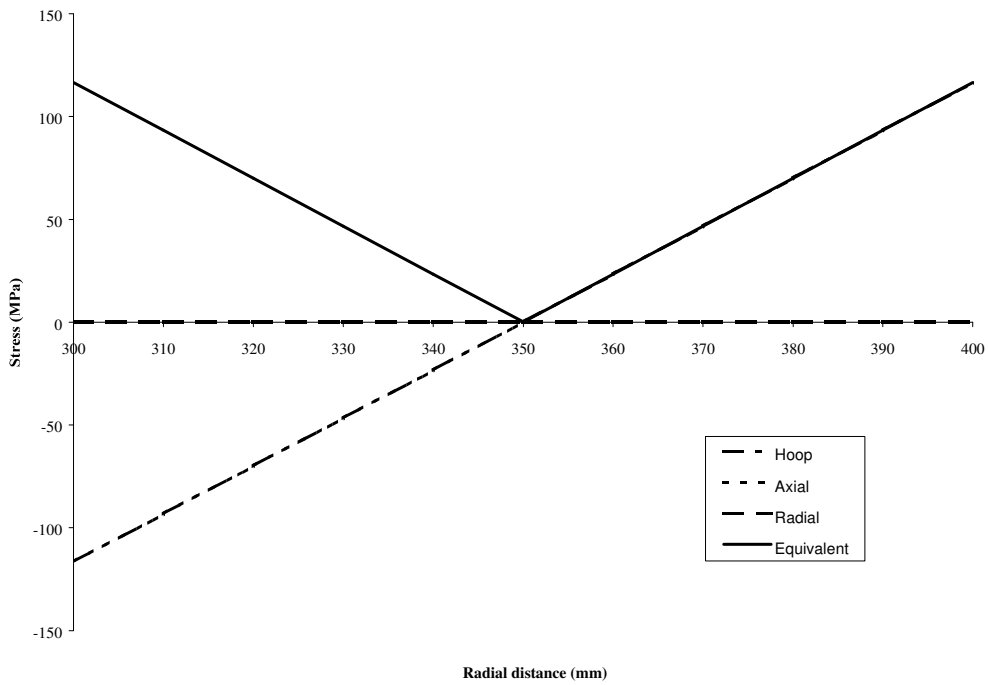


Figure 14.45 - Initial shutdown stresses (based on Neuber)

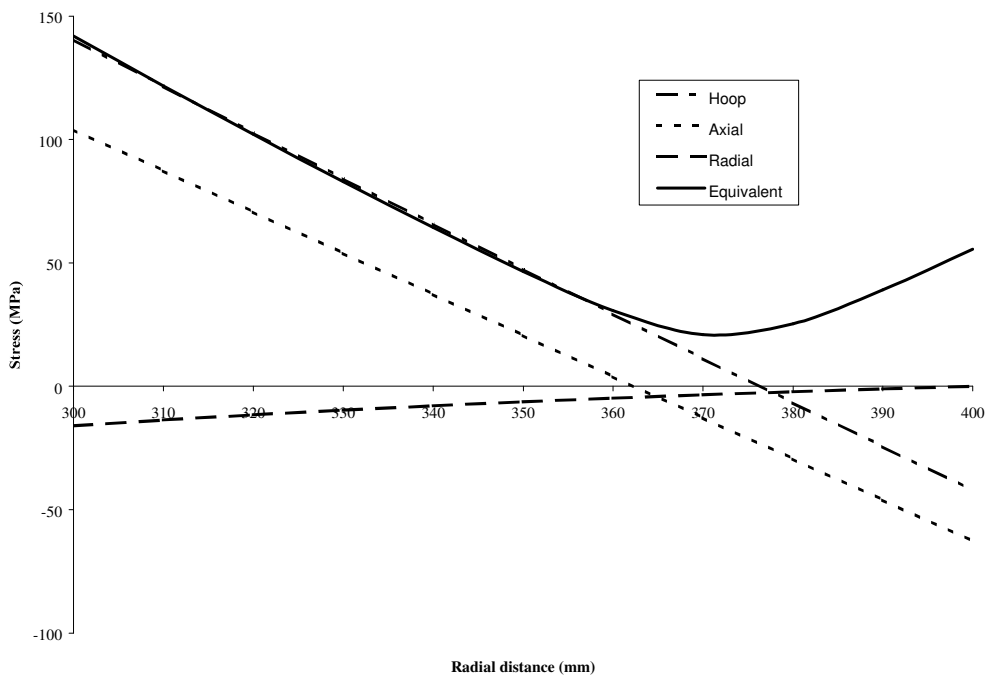


Figure 14.46 - Initial operating stresses (based on Neuber)

Surface cyclic plastic zone size

Strict shakedown has been demonstrated for this example. There is therefore no cyclic plastic deformation at the inner surface of the defective pipe section and the cyclic plastic zone size, r_p , is set equal to zero.

Stress intensity factors

The effective stress intensity factor range, ΔK_{eff} , is required as a function of crack depth. For this example, where the cyclic structural response is elastic, ΔK_{eff} is calculated using the stress intensity factors, K_{max} and K_{min} , corresponding to the maximum (i.e. operation) and minimum (i.e. shutdown) load conditions, respectively, of the cycle. As the axial stresses vary linearly through the pipe wall at both extremes of the cycle, the stresses can be represented by membrane and bending components, denoted σ_m and σ_b respectively. Membrane and bending stresses appropriate to both initial and shakedown conditions are given in Table 14.17.

Table 14.17. Axial Stresses (Used in Calculation of Stress Intensity Factors including Effective Stress Intensity Factor Range)

| Loading Conditions | Operation | | Shutdown | |
|---------------------------------|-----------------------|------------------------|-----------------------|------------------------|
| | Membrane Stress (MPa) | Bending Stress # (MPa) | Membrane Stress (MPa) | Bending Stress # (MPa) |
| Initial (Start of first cycle) | 20.6 | 83.4 | 0 | -116.6 |
| Shakedown (Steady cyclic state) | 20.6 | 15.8 | 0 | -184.2 |

Positive values indicate tensile stress on the inside surface of the pipe

Stress intensity factor solutions are therefore required for a cylinder with $R_i/w=3$ subjected to combined axial membrane and bending stresses, with the total stress intensity factor given by

$$K = (F_m \sigma_m + F_b \sigma_b) \sqrt{\pi a} \tag{14.67}$$

where the membrane and bending compliance functions, F_m and F_b respectively, are functions of R_i/w and a/w . The handbook of Tada, Paris and Irwin [14.28] gives graphical membrane compliance solutions for a range of R_i/w values, thereby permitting the solution for $R_i/w = 3$ to be approximated in polynomial form as

$$F_m = 1.123 - 0.103x + 2.030x^2 - 1.373x^3 + 0.790x^4 \tag{14.68}$$

for $0 < x < 0.6$ where $x = a/w$.

The corresponding bending compliance function has been derived using the computer program R-Code [14.29]), with the above membrane compliance function used as the Reference State Solution (RSS). The derived bending compliance function may be approximated in polynomial form as

$$F_b = 1.126 - 1.543x + 2.613x^2 - 3.986x^3 + 2.123x^4 \tag{14.69}$$

where the range of validity is the same as for the membrane compliance function. The effective stress intensity factor range, ΔK_{eff} has been evaluated as a function of crack depth from equations (14.70) to (14.73) for both initial and shakedown conditions using the compliance functions given in equations (14.68) and (14.69) together with the axial stresses given in Table 14.17. The effective stress intensity factor ranges (together with associated values of K_{max}) are shown as functions of crack depth in Figure 14.47 for both the initial and shakedown conditions. Note that for the current example $R < 0$ and hence $q_0 < 1$ for both initial and shakedown conditions (for all crack depths).

$$\Delta K_{eff} = q_0 \Delta K \tag{14.70}$$

$$\Delta K = K_{max} - K_{min} \quad (14.71)$$

$$q_0 = 1 \quad R \geq 0$$

$$q_0 = \frac{1-0.5R}{1-R} \quad R < 0 \quad (14.72)$$

$$R = \frac{K_{min}}{K_{max}} \quad (14.73)$$

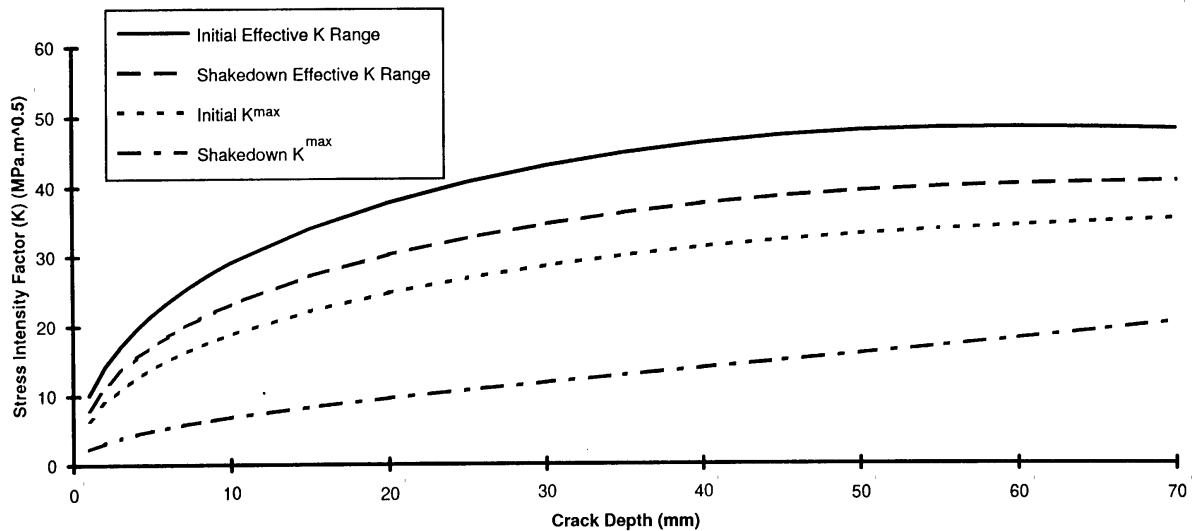


Figure 14.47 - Stress intensity factors.

For the period prior to the attainment of the steady cyclic state (i.e. $t < t_{cyc}$), the effective stress intensity factor range has been taken as the mean of the initial and shakedown values.

Reference stresses

The reference stress during the dwell periods has been calculated by determining the forces and moments acting across the section of interest. The forces and moments (per unit thickness), F and M respectively, acting across the section in the axial (superscript a) and hoop (superscript h) directions have been evaluated for both steady cyclic and initial conditions (based on Neuber) using the stress profiles shown in Figures 14.42 and 14.46, respectively. In both cases, the axial and hoop stresses may be well represented by membrane and bending stresses, σ_m and σ_b , respectively. Table 14.18 gives axial and hoop stresses appropriate to initial and shakedown conditions and associated forces and moments (per unit thickness) evaluated using

$$F = \sigma_m w \quad (14.74)$$

and

$$M = \frac{\sigma_b w^2}{6} \quad (14.75)$$

Equation (14.75) provides a conservative estimate of the moment by ignoring the effect of radius on the integration of the linear stress distribution. The reference stress has been determined using lower bound limit load theory treating the secondary (thermal) wall bending stress as primary, for a pipe containing an internal fully circumferential crack subjected to both axial and hoop forces and moments based on a Tresca yield criterion. The reference stress, σ_{ref} , may be calculated using

$$\sigma_{ref} = \frac{F}{F_L} \sigma_y \quad (14.76)$$

where σ_y is an arbitrary yield stress and F_L is the limit load. If proportional loading is assumed the limit loads can be determined from

$$\frac{F_L}{M_L} = \frac{F}{M} \quad (14.77)$$

where F and M are the forces and moments, respectively, from Table 14.18.

Table 14.18. Axial and Hoop Stresses, Forces and Moments (Used in the Calculation of Reference Stress)

| Loading Conditions | Axial | | | | Hoop | | | |
|----------------------------------|-------------------------------------|------------------------------------|--------------------------------------|--|-------------------------------------|------------------------------------|--------------------------------------|--|
| | Membrane Stress σ_{am} (MPa) | Bending Stress σ_{ab} (MPa) | Force per Unit Thickness F_a (N/m) | Moment per Unit Thickness M_a (Nm/m) | Membrane Stress σ_{hm} (MPa) | Bending Stress σ_{hb} (MPa) | Force Per Unit Thickness F_h (N/m) | Moment Per Unit Thickness M_h (Nm/m) |
| Initial (Start of First Cycle) | 20.6 | 83.4 | 2.06x10 ⁶ | 1.39x10 ⁵ | 49.1 | 91.4 | 4.91x10 ⁶ | 1.52x10 ⁵ |
| Shake down (Steady cyclic state) | 20.6 | 15.8 | 2.06x10 ⁶ | 2.63x10 ⁴ | 49.1 | 23.8 | 4.91x10 ⁶ | 3.97x10 ⁴ |

The limit loads for axially dominated collapse have the form

$$F_L^a = (2y - a)\sigma_y \quad (14.78)$$

and

$$M_L^a = \left[\frac{w^2}{4} + \frac{a^2}{2} - \frac{at}{2} - x^2 \right] \sigma_y \quad (14.79)$$

where w is the pipe wall thickness and y is the distance between the plastic neutral axis and the mid-wall thickness. The value of y is found from equation (14.77) based on values of F and M from Table 14.18, and the expressions involving y (equations (14.78) and (14.79)) for F_L^a and M_L^a . The resulting quadratic equation can then be easily solved.

For hoop dominated collapse the limit loads are

$$F_L^h = 2y\sigma_y \quad (14.80)$$

and

$$M_L^h = \left(\frac{w^2}{4} - y^2 \right) \sigma_y \quad (14.81)$$

The value of y is again calculated using these expressions in equation (14.77) together with values of F and M from Table 14.18. The maximum of the axial and hoop reference stress is then chosen. For both the initial and shakedown conditions the reference stress is hoop dominated, and is therefore independent of crack depth. For initial conditions the reference stress is

$$\sigma_{ref}^{cyc=1} = 88.1 \text{ MPa}$$

while for steady cyclic conditions

$$\sigma_{ref} = 57.6 \text{ MPa}$$

is obtained.

C* parameter

The parameter C^* is calculated according to

$$C^* = \sigma_{ref} \dot{\epsilon}_{ref} R' \quad (14.82)$$

where σ_{ref} is the reference stress. R' is defined by

$$R' = \left(\frac{K}{\sigma_{ref}} \right)^2 \quad (14.83)$$

- Step 5. Check stability under time-independent loads

This step is not considered in detail for this example. The check on time-independent failure would normally be based on short-term fault loadings rather than on the steady operating loadings. Reference may be made to [14.27,14.30] for examples of such calculations.

- Step 6. Check significance of creep and fatigue

For the purpose of this example, it is assumed that both creep and fatigue are significant.

- Step 7. Calculate rupture

Not considered in this example.

- Step 8. Calculate incubation time

Not considered in this example, although a conservative incubation time of zero is often assumed when creep and fatigue are significant.

- Step 9. Calculate crack size after growth

Strict shakedown of the uncracked structure has been demonstrated for this example and so a Method I crack growth calculation is appropriate. The creep and fatigue crack growth contributions are separately calculated and added for each cycle, with the creep crack growth rate, da/dt , given by

$$\frac{da}{dt} = A(C^*)^q \quad (14.84)$$

Values of the coefficients A and q used in the current example are given in Table 14.16. In general, the parameter C^* is calculated by the reference stress approach. It is also necessary to calculate a mean value of C^* for use in calculating creep crack growth occurring in the dwell periods prior to the attainment of the steady cyclic state (i.e. $t < t_{cyc}$). This is given in equation (14.85) as

$$\bar{C}^* = (\sigma_{ref}^{cyc=1} + \sigma_{ref}) \dot{\epsilon} R' / 2 \quad (14.85)$$

where $\dot{\epsilon}$ is evaluated as

$$\dot{\epsilon} \left[(\sigma_{ref}^{cyc=1} + \sigma_{ref}) / 2 \right] \quad (14.86)$$

For the current example, the stresses acting during the dwell periods after the steady cyclic state is reached are predominantly primary. Therefore, the small amount of stress relaxation that would occur during the dwell has been neglected and load-controlled loading has been assumed in calculating creep strain accumulation and crack growth during the dwell.

The stress intensity factor used in the calculation of R' in equation (14.83) is evaluated using the stresses at the beginning of the dwell and is therefore equal to K_{max} (see Figure 14.47). Prior to attainment of the steady cyclic state, a mean value of K_{max} has been used in the calculation of R' .

This is given by

$$\bar{K}_{max} = (K_{max}^{cyc=1} + K_{max}) / 2 \quad (14.87)$$

Where $K_{max}^{cyc=1}$ and K_{max} are the maximum stress intensity factors at the start of the first cycle (using a Neuber construction) and the cycle in the steady cyclic state, respectively. The cyclic crack growth rate law takes the form given in equation (14.88), with the cyclic crack growth rate, $(da/dN)_f$, given by

$$\left(\frac{da}{dN} \right)_f = C (\Delta K_{eff})^\ell \quad (14.88)$$

where the coefficients C and ℓ may be temperature dependent. Values of the coefficients C and ℓ used in the current example are given in Table 1. The calculation of ΔK_{eff} is described in [14.25,14.27]. The total crack growth per cycle is obtained by summing the cyclic and creep contributions. The crack extension over the desired future service life of 1.5×10^6 hours is then calculated iteratively using a computer program. The main features of the iterative procedure are as follows:

- (i) Calculate creep crack growth for the dwell period in the first cycle. It should be noted that this itself involves an iterative procedure in which the creep crack growth and strain rates are assumed constant for a short time, Δt . The crack depth and accumulated creep strain are then updated and new values of reference stress and creep strain rate obtained assuming a strain hardening rule. The value of C^* can then be obtained with R' evaluated for the new crack depth, leading to a new value of creep crack growth rate. For the current example,

these calculations have actually been implemented by incrementing crack depth, although details of the numerical procedures are not discussed here.

- (ii) Calculate cyclic crack growth for the first cycle and increment crack depth.
- (iii) Repeat calculations for subsequent cycles.

For the current example it is also necessary to determine t_{cyc} , the time to redistribute to the steady cyclic state. A value of elastic follow up factor $Z=3$ is arbitrarily assumed. With this assumption, the steady cyclic state is achieved after 1 cycle. Prior to attainment of the steady cyclic state, mean values of ΔK_{eff} and C^* are used to calculate cyclic and creep components of crack growth as described above. After the steady cyclic state has been established (i.e. $t > t_{cyc}$), values of ΔK_{eff} and C^* appropriate to steady state conditions are used in the crack growth calculations. The results of these iterative calculations lead to the crack depth as a function of time shown in Figure 14.48.

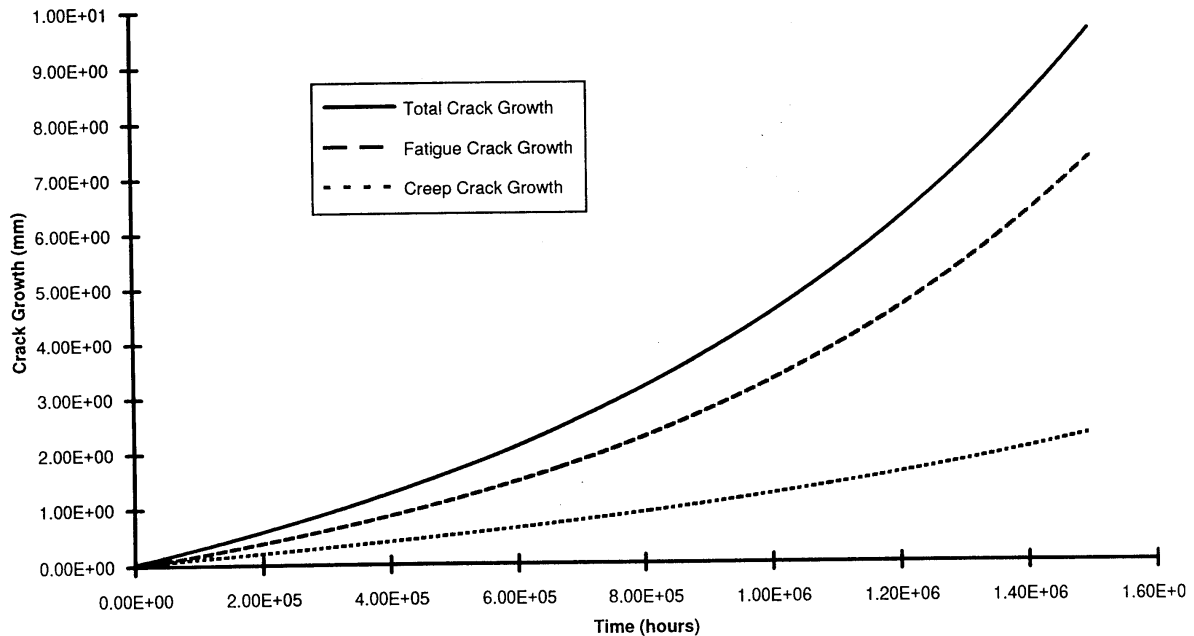


Figure 14.48 - Calculation of crack growth.

- Step 10. Recalculate rupture life after growth

Not considered in this example.

- Step 11. Check stability of time-independent loads after growth

Not considered in this example.

- Step 12. Assess significance of results

In practice, studies would be performed to examine the sensitivity of the results to the assumed input data. However, as the main purpose of this example is to illustrate the use of FITNET FFS Procedure for creep-fatigue crack growth, sensitivity studies have not been considered in this example.

14.8.4. References

[14.25] “R5: Assessment Procedure for the High Temperature Response of Structures”, British Energy Generation, Issue 3, June 2003.

[14.26] White, P.S., “SIWG recommendation on constitutive equations for Type 316 (CDFR) stainless steel”, GEC Report FDRC/SIWG/SASG/P(88)/183 (1988).

[14.27] “FITNET FFS Procedure”, GIRT-CT-2001-05071

[14.28] H.Tada, P.C. Paris and G.R.Irwin, “The Stress Analysis of Cracks Handbook”, New York: ASME Press, 3rd edition, 2000.

[14.29] R-Code Version 4.2, BEGL (2003).

[14.30] R6: Assessment of the integrity of structures containing defects, British Energy Generation Limited, Revision 4, 2001.

14.9. SCC tutorial: Failure Analysis of Different Pipes Containing an Internal Flaw

14.9.1 Introduction

This tutorial analyses the failure of some of the pipes employed in a power plant. These components are frequently subjected to environmental and mechanical strain involving subcritical crack growth. The evaluation of this type of crack is sometimes not feasible with a simple visual inspection or by means of other non-conventional techniques. In such cases, the loading test is a powerful tool for evaluating the safety conditions.

Among the most critical elements in a combined cycle thermal power plant are the heat exchanger pipes. One of these pipes, whose dimensions will be described below, is subjected during normal operating conditions to an internal pressure of 30 MPa. Once a year, there is a shutdown to review the installations during which the pipes are subjected to a loading test consisting in the application of an internal pressure which is double that of the working pressure.

It should be taken into account that, as shown in the figure, there may be semi-elliptical cross-section cracks, though these conserve the ratio $2c/a=2$ cte., and that these cracks may propagate due to stress corrosion cracking (SCC) processes whose characteristic velocity is 10^{-10} m/s.

It is known that before the start-up, all of the pipes are subjected to an inspection using non-destructive procedures with a sensitivity of 0.5 mm, and those which present any defect are withdrawn.

The aim of this study is to analyse the evolution over time of the safety conditions of the component and the effects on it of the loading test, as well as to examine the usefulness of these tests. Finally, the possible failure mechanism that leads to the elimination of the component will be estimated.

14.9.2 Inputs

14.9.2.1 Flaw information

Considering that there may be semi-elliptical cross-section cracks in the pipes studied, the dimensions of the relevant cross section are shown in Figure 14.49. For the sake of simplicity, the crack is assumed to be of constant length/depth ratio, $2c/2a=2$ over the wall thickness.

It is known that before the start-up, all of the pipes are subjected to an inspection using non-destructive procedures with a sensitivity of 0.5 mm, and those which present any defect are withdrawn. Thus, the possible presence of initial flaws of a size of $a_0=0.5$ mm must be considered as a working hypothesis.

The geometry of the cracked section, as shown in the form of a schema in Figure 14.49, is essentially a thin

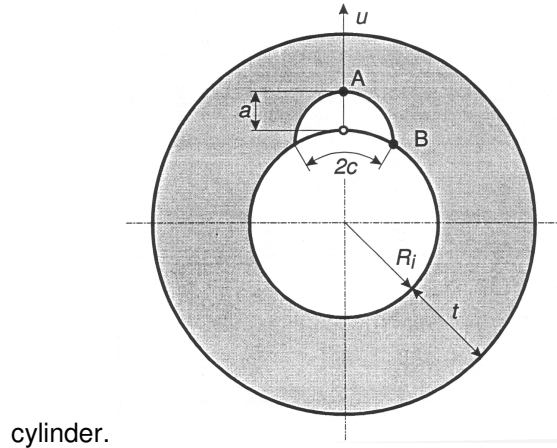


Figure 14.49 – Scheme of the cracked section including the most important parameters.

Since the example presented constitutes a SCC problem, the cracks can be predicted to grow with time at a constant speed of 10^{-10} m/s. Thus, their evolution over successive years must be considered. Table 14.19 shows this evolution.

Table 14.19. Crack growth evolution during service

| Time (years) | a (m) |
|--------------|-----------|
| 0 | 0.0005 |
| 1 | 0.0036536 |
| 2 | 0.0068072 |
| 3 | 0.0099608 |
| 4 | 0.0131144 |

14.9.2.2 Stresses

In the present case, the loading type is predominantly membrane stress component, characterised by the stress values σ_1 at the front surfaces of the plate. The applied stress in the longitudinal direction of the internal face of the pipe was obtained by means of the equation:

$$\sigma = \frac{pR_{med}}{2t} \quad (14.89)$$

To obtain this parameter, the dimensions of the pipe as described in Table 14.20 must be taken into account.

Table 14.20. Input parameters to obtain the stress value

| D _{ext} (m) | D _{int} (m) | t(m) | P _{service} (MPa) | P _{loading} (MPa) |
|----------------------|----------------------|--------|----------------------------|----------------------------|
| 0.3455 | 0.314 | 0.0157 | 30 | 60 |

In the determination of this stress value, it must be borne in mind that it is the uniform stress, without any crack presence and for an average thickness value of the pipe. Based on this information, a value of $\sigma_m=157.5$ MPa during the normal work, and $\sigma_m=315$ MPa during the loading test, were determined. These values refer to one half of the nominal diameter.

In the present case, only primary stresses have to be considered, as secondary stresses are of no relevance in the context of this tutorial. Note, that the FITNET procedure [14.31] gives extensive guidance on the treatment of secondary stresses.

14.9.2.3 Material Properties

The mechanical properties of the material have been obtained by means of conventional tensile test and Fracture Mechanic tests [14.32]. Table 14.21 summarises all the results obtained.

Table 14.21. Mechanical properties of the material

| | |
|-----------------------|-------------------------|
| σ_y | 650 MPa |
| σ_u | 750 MPa |
| E | 210000 MPa |
| K_{IC} | 100 MPam ^{1/2} |

14.9.3. Assessment

FITNET pursues two different assessment philosophies, which are designated as crack driving force and failure assessment diagram concepts. The two are complementary and give identical results. Failure is predicted when the crack tip loading exceeds the fracture toughness.

Figure 14.50 shows the basic FAD applications which consider the fracture toughness as a single value (K_{IC} or J or CTOD at stable crack initiation). Note that CDF and FAD applications also exist for R curve behaviour of the fracture resistance, which will not, however, be described here.

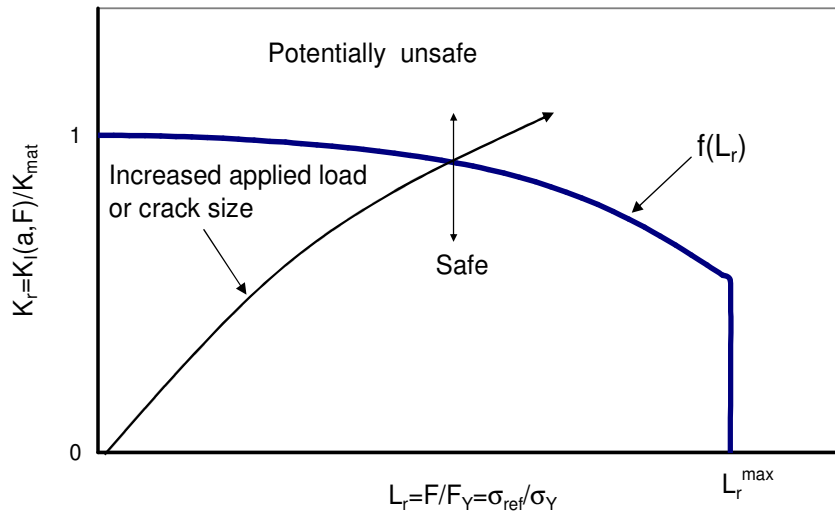


Figure 14.50 – FITNET assessment philosophies: FAD philosophy.

In the FAD route, a geometry independent failure line is constructed by normalising the crack tip loading by the material fracture resistance. The assessment of the component is then based on the relative location of a

geometry-dependent assessment point with respect to this failure line. In the simplest application, the component is regarded as safe as long as the assessment point lies within the area below the failure line. It is regarded as potentially unsafe if it is located on the line or outside the area below the failure line. An increased load or larger crack size will move the assessment point along the loading path towards the failure line.

The basic equations of the FAD philosophy are

$$L_r = \frac{\sigma_{ref}}{\sigma_Y} \quad (14.90)$$

$$K_r = \frac{K_I}{K_{mat}} \quad (14.91)$$

The basic equation of the FITNET-FAD route is

$$K_r = f(L_r) \quad (14.92)$$

In the case under study here, the first step to be taken to establish the safety conditions of the component is the selection of the characteristic equations of the geometry. To do this, the solutions presented in the FITNET procedure for the case of internal surface flaw in a cylinder oriented circumferentially are used. This procedure in Annex A provides suitable tools for obtaining the value of K_r .

The limit load value, considering that this is a component subjected only to internal pressure, is implemented in accordance with the specifications of the FITNET procedure (see Annex B).

Once the equations which allow the state of the component to be assessed for a stress and cracking state are defined, we must address its evolution. First, it should be pointed out that the initial state of service corresponding to a crack of 0.5 mm and a stress of 30 MPa presents the following values:

$$K_r = 0.409$$

$$L_r = 0.242$$

as can be observed in Table 14.22 and in Figure 14.51. The loading test carried out in these conditions which involves a pressure of 60 MPa raises these values until they are doubled, with

$$K_r = 0.81$$

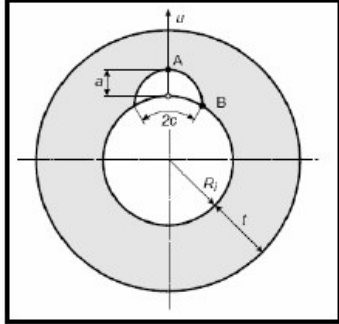
$$L_r = 0.48.$$

From the initial conditions exposed, the component is subjected to an SCC process involving crack growth since in this case, the threshold stress intensity factor K_{ISCC} is close to zero.

Once the law which defines the crack variation through time is established, the evolution of the FAD parameters can be addressed using the implementation of this law to the characteristic equations of the K_r and L_r parameters. Table 14.22 and Figure 14.51 show this process for the example studied. The latter shows the evolution of the safety conditions throughout the years of service, and during the loading test. This test is, as expected, the test which highlights the general state of the component, as it comes closer to failure conditions. However, in the case studied, the performance of the loading test does not provide any additional information on the cracking of the element. The eventual failure of the pipe studied is produced by a leaking process which took place four years after its installation.

Table 14.22 – Essential parameters in the assessment of the example proposed.

| Material | |
|---------------------------------|--------|
| σ_y (MPa) | 650 |
| σ_u (MPa) | 750 |
| E (MPa) | 210000 |
| K_{Ic} (MPam ^{1/2}) | 100 |
| Geometry | |
| R_i (m) | 0,157 |
| T (m) | 0,0157 |
| Loading test | |
| P (MPa) | 60 |



| a | P | K_I | K_R | L_r | |
|--------|----|--------|---------|---------|--------------------|
| 0,0005 | 30 | 4,097 | 0,04097 | 0,24231 | LOADING |
| 0,0005 | 60 | 8,195 | 0,08195 | 0,48463 | |
| 0,0036 | 30 | 11,230 | 0,11230 | 0,24291 | LOADING |
| 0,0036 | 60 | 22,460 | 0,22460 | 0,48583 | |
| 0,0067 | 30 | 15,641 | 0,15641 | 0,24443 | LOADING LEAKAGE |
| 0,0067 | 60 | 31,282 | 0,31282 | 0,48886 | |
| 0,0157 | 30 | 25,366 | 0,25366 | 0,25445 | LEAKAGE |
| 0,0157 | 60 | 50,73 | 0,50733 | 0,50890 | |

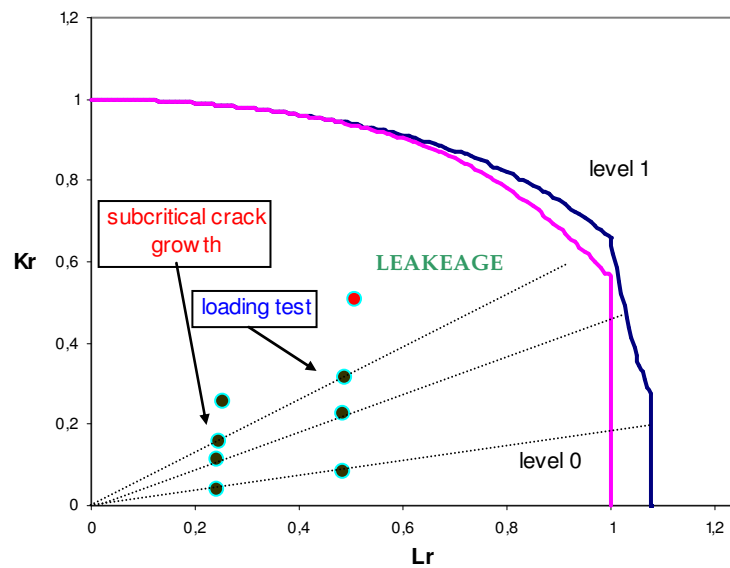


Figure 14.51 – FITNET assessment diagram applied to the worked example.

14.9.4. References

[14.31] “FITNET FFS Procedure”, GIRT-CT-2001-05071

[14.32] BS 7448: Part 2: 1997: Fracture mechanics toughness tests, part 2. Method for determination of K_{Ic} , critical CTOD and critical J values of welds in metallic materials. London: British Standards Institution; 1997.

14.10. LTA tutorial: Pipeline Local Thinned Area Assessment

14.10.1. Introduction

This tutorial shows the assessment of a pipeline containing an isolated local thinned area (LTA) due to corrosion. The local thinned areas were found during an internal inspection of the pipeline using a magnetic flux intelligent pig.

The dimensions are summarised as follows:

- Outside diameter (D_0) = 812.8 mm
- Wall thickness (t) = 19.1 mm

14.10.2. Inputs

14.10.2.1 Flaw Information

The largest reported LTA has a length (L) equal to 220 mm and a depth equal to 30% of the wall thickness.

14.10.2.2 Stresses

The maximum allowable operating pressure of the line is 14 MPa.

14.10.2.3 Material Properties

The specified minimum tensile strength is 530.9 MPa and the yield stress is 405 MPa.

14.10.3. Assessment

14.10.3.1 Safe Working Pressure Estimate

The safe working pressure of a single longitudinal flaw can be estimated by the following procedure:

a) Calculate the failure pressure of the unflawed pipe or vessel cylinder (P_0) using the design code allowable pressure equation by replacing the code allowable stress by the failure stress (σ_{cyl}). This can be:

$$P_0 = \frac{2t\sigma_{cyl}}{(D_0 - t)} \quad (14.93)$$

where

$$\sigma_{cyl} = (1/2)^n \cdot \sigma_{uts} \quad (14.94)$$

$$n = 65/\sigma_y \quad (14.95)$$

then

$$P_0 = 22.86 \text{ MPa}$$

b) Calculate the length correction factor (Q_C):

$$Q_c = \sqrt{1 + 0.8 \frac{L^2}{D_0 t}} = 1.869 \quad (14.96)$$

c) Calculate the remaining strength factor for longitudinal failure (rsf_c):

$$rsf_c = [t_{mm} / t] / [1 - (t_{mm} / t) \cdot Q_c^{-1}] = 0.8338 \quad (14.97)$$

where t_{mm} is the minimum wall thickness at the wall loss location.

d) Calculate the failure pressure of the corroded pipe or vessel (P_f):

$$P_f = P_0 \cdot rsf_c = 19.06 \text{ MPa} \quad (14.98)$$

e) Calculate the usage factor (f_c) to ensure a safe margin between the operating pressure and the failure pressure of the LTA flaw and to avoid general yielding:

$$f_c = \min[1/X_h; \sigma_y/\sigma_{cyc}] = 0.833 \quad (14.99)$$

X_h is the maximum of the code required hydrotest margin and the minimum required margin of safety. Here X_h has been considered 1.2

f) Calculate the safe working pressure of the corroded pipe or vessel (P_{sw}):

$$P_{sw} = P_f \cdot f_c = 15.87 \text{ MPa} \quad (14.100)$$

P_{sw} is bigger than the maximum allowable operating pressure. Therefore the pipeline is working under safe conditions.

14.10.3.2 Allowable Remaining Wall Thickness for Internal Pressure

The minimum allowable remaining wall thickness can be determined by the following procedure:

a) Calculate the code allowable stress (σ_A):

$$\sigma_A = \min[\sigma_y/Z_y; \sigma_{uts}/Z_u] \quad (14.101)$$

Z_y and Z_u are reserve factors provided by the different design codes. Typical values could be:

$$Z_y = 1.5$$

$$Z_u = 3$$

Then:

$$\sigma_A = 177 \text{ MPa}$$

b) Calculate the nominal failure stress of the unflawed pipe or vessel cylinder (σ_{cyl}) using equations (14.94) and (14.95):

$$\sigma_{cyl} = 475 \text{ MPa}$$

c) Calculate the minimum required remaining strength factor (rsf_{min}):

$$rsf_{min} = \max[X_h \sigma_A / \sigma_{cyl}; \sigma_A / \sigma_y] = 0.447 \quad (14.102)$$

d) Calculate the length correction factor (Q_c):

$$Q_c = \sqrt{1 + 0.8 \frac{L^2}{D_0 t}} = 1.869$$

e) Calculate the minimum allowable remaining wall thickness for internal pressure (t_{mP}):

$$t_{mP} = t \frac{rsf_{min} \left(1 - \frac{1}{Q_c}\right)}{\left(1 - \frac{rsf_{min}}{Q_c}\right)} = 5.21 \text{ mm} \quad (14.103)$$

t_{mP} is smaller than the pipe minimum wall thickness, ($t_{mm} = 13.3 \text{ mm}$). Therefore, the pipeline is working under safe conditions.

14.11. Crossed tutorial: Failure Analysis of a Hip Implant [14.33]

14.11.1. Introduction

This tutorial analyses the failure of a hip implant, which occurred nine months after the surgery operation. The base material of the implant is a metal matrix piece of alloy Ti-6Al-4V, coated by two surface layers; the first one is a 50 μm thick layer of pure porous titanium, and the other one is a hydroxiapatite layer of 150 μm .



Figure 14.52 – Aspect of the implant on reception

14.11.2. Inputs

14.11.2.1 Flaw information

From microscopy analysis it was determined that a crack grew from an initial defect originated in the irregular coating, as shown in Figure 14.53. The defect was 0.1 mm deep at the initial stage and 6.5 mm deep at failure, as shown in Figure 14.54. The crack front during the propagation process is not a straight crack front neither a semicircular crack front, but its geometry is between those ones during the process.

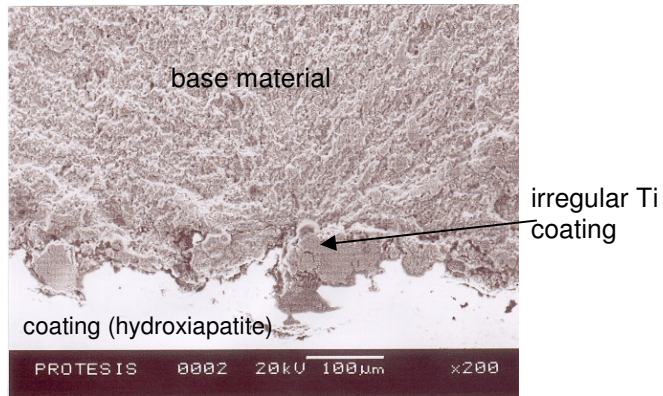


Figure 14.53 – Fatigue initiation at the Ti coating where some defects were observed

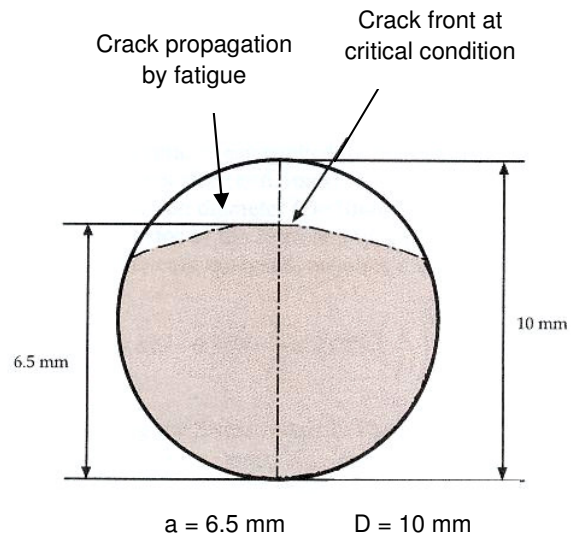


Figure 14.54 – Scheme of the crack geometry at failure

14.11.2.2 Stresses

Figure 14.55 presents a schema of the working conditions of the implant at failure.

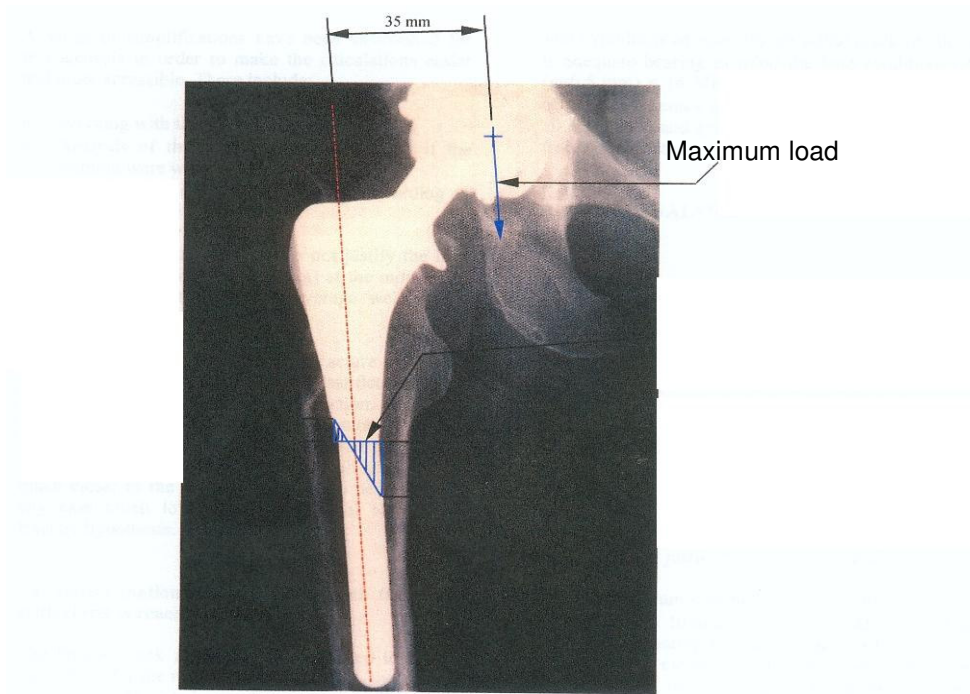


Figure 14.55 – Scheme of the working conditions

The implant worked as a cantilever beam, with a non centred load applied, transmitted at the contact implant-hip bone, due to the body weight of the patient. The assumption of cantilever beam fixed up to the fracture surface is supported by the absence of adhered bone to the upper part of the piece. Therefore, a mixed stress state at the ligament is achieved due to bending and compression. At the crack front, the obtained tension stresses are responsible of the final fracture.

$$\sigma_{T,máx} = \sigma_B - \sigma_C \quad (14.104)$$

where

$$\sigma_B = \frac{32 \cdot M}{\pi \cdot D^3} \quad (14.105)$$

$$\sigma_C = \frac{4 \cdot P^*}{\pi \cdot D^2} \quad (14.106)$$

Many studies have been performed [i.e, 14.34-14.39] in order to know the peak forces that appear in hip implants when the patient is walking. A value of 2.5 BW (Body Weight) seems to be reasonable.

During the whole process which starts with the surgery implant and finishes with the failure of the prosthesis, three stages can be distinguished:

- 1) *Crack nucleation*

2) *Quick crack propagation*: On this stage, the patient is considered to carry out a “normal” activity. It is supposed that he/she walks two hours per day with a pace of one step per second (0.5 cycles/second). Peak forces (P^*) are considered to be equal to 2.5 BW.

3) *Slow crack propagation*: The crack has growth in the previous stage and the patient has started to feel some pain, so he/she reduces his/her activity (1 hour/day) and uses crutches, so it is considered that peak forces are equal to 1.0 BW.

Failure occurs on this stage, so, when calculating the supported load at failure, peak forces are 1.0 BW.

14.11.2.3 Material Properties

These are the data available for the base material.

$$K_{IC} = 110 \text{ MPa}\cdot\text{m}^{1/2}$$

$$\sigma_Y = 895 \text{ MPa}$$

$$\sigma_u = 1000 \text{ MPa}$$

$$E = 114 \text{ GPa}$$

$$da/dN = 3.54 \cdot 10^{-14} \cdot (\Delta K)^{4.19} \quad (14.107)$$

when ΔK is given in $\text{MPa}\cdot\text{m}^{0.5}$ and da/dN in m/cycles

Continuous yielding is assumed.

14.11.3. Assessment

The assessment of the fracture conditions has been performed following the FITNET procedure [14.40]. Options 0 (Basic) and 1 (Standard) have been chosen for the assessment as a consequence of the existing information about material properties:

- Toughness K_{IC}
- Yield Stress σ_Y
- Ultimate Tensile Stress σ_u

These parameters define the FAL (Failure Assessment Line) as:

- *Option 0*:

$$K_r = [1 + 0.5 \cdot (L_r)^2]^{-1/2} \cdot [0.3 + 0.7 \exp(-0.6 \cdot L_r^6)] \quad \text{for } L_r \leq L_r^{\max} \quad (14.108)$$

$$K_r = 0 \quad \text{for } L_r \geq L_r^{\max} \quad (14.109)$$

$$L_{r\max} = 1 + (150/\sigma_Y)^{2.5} \quad (14.110)$$

- *Option 1*:

$$K_r = [1 + 0.5 \cdot (L_r)^2]^{-1/2} \cdot [0.3 + 0.7 \exp(-\mu L_r^6)] \quad \text{for } L_r \leq 1 \quad (14.111)$$

$$\mu = \min[0.001(E/\sigma_Y); 0.6] \quad (14.112)$$

$$K_r = K_r(1) \cdot L_r^{(N-1)/2N} \quad \text{for } 1 < L_r \leq L_r^{\max} \quad (14.113)$$

$$N = 0.3 \cdot (1 - \sigma_Y/\sigma_u) \quad (14.114)$$

$$L_r^{\max} = 0.5 \cdot (\sigma_Y + \sigma_u) / \sigma_Y \quad (14.115)$$

At failure conditions, the limit load solution has been taken considering the complete plastification of the residual ligament and establishing the equilibrium of loads and moments. The results have been these:

- *Straight crack front*

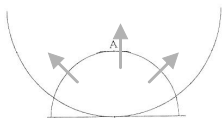
$$P_{LL} = 0.566 \text{ kN}$$

- *Semicircular crack*

$$P_{LL} = 0.895 \text{ kN}$$

The stress intensity factor can be established as a function of the applied load from the equations given below:

- *Semicircular crack front*



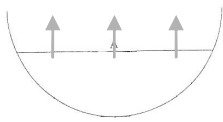
$$K_I = \sigma \cdot Y_F(a/D) \cdot (\pi \cdot a)^{1/2} \quad (14.116)$$

$$Y_F(a/D) = g \cdot (0.923 + 0.199 \cdot (1 - \sin(\psi))^4) \quad (14.117)$$

$$g = 0.5857 \cdot ((\tan \psi) / \psi)^{0.5} / \cos \psi \quad (14.118)$$

$$\psi = \pi \cdot a / 4 \cdot R \quad (14.119)$$

- *Straight crack front*



$$K_I = \sigma \cdot Y_F(a/D) \cdot (\pi \cdot a)^{1/2}$$

$$Y_F(a/D) = 1.04 - 3.64 \cdot (a/D) + 16.86 \cdot (a/D)^2 - 32.59 \cdot (a/D)^3 + 28.41 \cdot (a/D)^4 \quad (14.120)$$

Considering this solution, Figure 14.56 shows the evolution of the loading conditions following the $K_r(L_r)$, being $K_r = K_I/K_{IC}$ and $L_r = P/P_{LL}$. The intersection of the loading line $K_r(L_r)$ with the FALine defines the failure conditions, which corresponds to plastic collapse ($L_r > 1$).

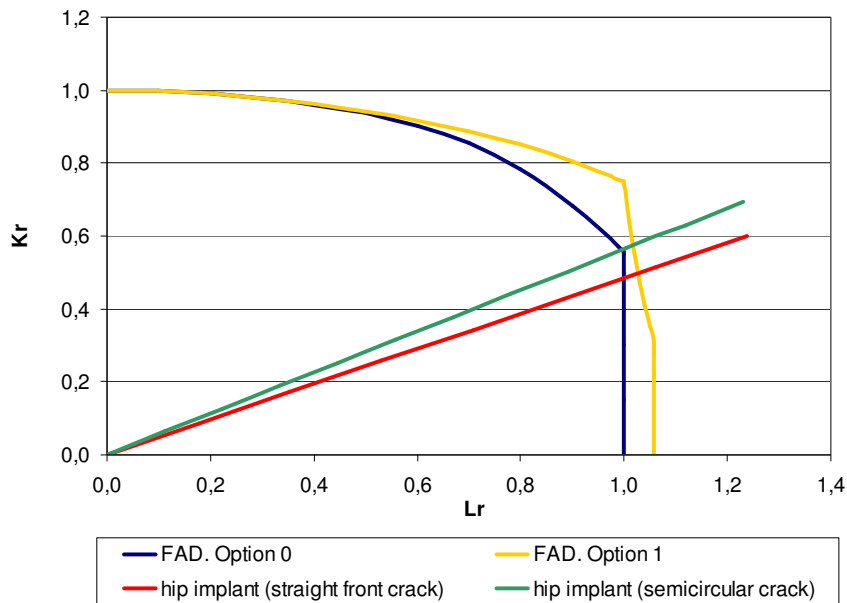


Figure 14.56 – Assessment of critical conditions by using FAD analysis.

The results are:

- *Straight crack front*

Default level: P = 0.566 kN

Level 1: P = 0.582 kN

- *Semicircular crack front*

Default level: P = 0.895 kN

Level 1: P = 0.915 kN

Therefore, the supported load is between 0.582 kN and 0.915 kN. The actual supported load is 0.735 kN so it can be said that the hypothesis of a crack front between straight and semicircular and peak loads of 1.0 BW are quite reasonable.

Some conclusions can be already obtained:

- Critical loading conditions corresponding to a normal weight
- Final failure due to plastic collapse of residual ligament.
- Good agreement with fractographic analysis and common sense.
- REAL SITUATION: the patient's weight is 0.735 kN, so it may be said that the crack front hypothesis in an intermediate situation between a straight crack front and a semi-circular crack front is very reasonable, as are also the peak forces equal to one at the moment of fracture.

On the other hand, it is possible to perform a fatigue crack growth assessment, because there is an initial defect and the Paris law is available (Route 4 in FITNET fatigue module) Therefore, the crack growth time until critical size is reached can also be obtained. The fatigue crack growth rate is adjusted by equation (14.107):

$$da/dN = 3.54 \cdot 10^{-14} \cdot (\Delta K)^{4.19} \quad \text{when } \Delta K \text{ is given in MPam}^{0.5} \text{ and } da/dN \text{ in m/cycles}$$

The load cycle to which the element is subjected varies from 0, support from the other leg or repose, up to 631.5 MPa, corresponding to the weight of 0.735 kN and peak forces of 2.5 BW. Thus the ΔK_I will have a value, depending on a , given by

$$\Delta K_I = Y_F(a/D) \cdot 631.5 \cdot (\pi \cdot a)^{1/2} \quad (14.121)$$

Taking $a_0 = 0.1$ mm as the initial crack length, introducing equation (14.121) in equation (14.107) and integrating this, the number of cycles required for the crack to reach the critical size of 6.5 mm is obtained. The number is between 145.738 cycles (straight front crack) and 539.088 (semicircular crack). This process can be divided in small steps and results are given in Tables 14.23 and 14.24.

Table 14.23. Determination of the crack growth time until the critical size is reached (BW=2.5).

| a (mm) | a med (mm) | Y (straight) | Y (f.semic.) | ΔN (straight) | ΔN (semic.) | N (straight) | N (semic.) |
|-----------------|------------|--------------|--------------|-----------------------|---------------------|----------------|---------------|
| 0,1 - 0,5 | 0,30 | 0,945 | 0,660 | 108999 | 490750 | 108999 | 490750 |
| 0,5 - 1 | 0,75 | 0,849 | 0,644 | 18829 | 59855 | 127828 | 550605 |
| 1 - 1,5 | 1,25 | 0,792 | 0,635 | 7961 | 20040 | 135789 | 570645 |
| 1,5 - 2 | 1,75 | 0,771 | 0,635 | 4294 | 9709 | 140083 | 580354 |
| 2 - 2,5 | 2,25 | 0,776 | 0,643 | 2449 | 5377 | 142533 | 585731 |
| 2,5 - 3 | 2,75 | 0,799 | 0,661 | 1420 | 3139 | 143953 | 588870 |
| 3 - 3,5 | 3,25 | 0,836 | 0,689 | 824 | 1857 | 144777 | 590727 |
| 3,5 - 4 | 3,75 | 0,889 | 0,728 | 471 | 1089 | 145248 | 591816 |
| 4 - 4,5 | 4,25 | 0,963 | 0,781 | 259 | 623 | 145507 | 592438 |
| 4,5 - 5 | 4,75 | 1,069 | 0,852 | 133 | 343 | 145640 | 592781 |
| 5 - 5,5 | 5,25 | 1,218 | 0,945 | 62 | 180 | 145702 | 592961 |
| 5,5 - 6 | 5,75 | 1,431 | 1,071 | 26 | 88 | 145728 | 593049 |
| 6 - 6,5 | 6,25 | 1,729 | 1,242 | 10 | 40 | 145738 | 593088 |
| BW = 2.5 | | | | | | N TOTAL | |

Table 14.24. Determination of the crack growth time until the critical size is reached (BW=1.0).

| a (mm) | a med (mm) | Y (straight) | Y (f.semic.) | ΔN (straight) | ΔN (semic.) | N (straight) | N (semic.) |
|-----------------|------------|--------------|--------------|-----------------------|---------------------|----------------|-----------------|
| 0,1 - 0,5 | 0,30 | 0,945 | 0,660 | 5067464 | 22815433 | 5067464 | 22815433 |
| 0,5 - 1 | 0,75 | 0,849 | 0,644 | 667745 | 2122708 | 5735208 | 24938140 |
| 1 - 1,5 | 1,25 | 0,792 | 0,635 | 291380 | 733428 | 6026589 | 25671568 |
| 1,5 - 2 | 1,75 | 0,771 | 0,635 | 158425 | 358205 | 6185014 | 26029773 |
| 2 - 2,5 | 2,25 | 0,776 | 0,643 | 90659 | 199035 | 6275672 | 26228808 |
| 2,5 - 3 | 2,75 | 0,799 | 0,661 | 52641 | 116360 | 6328313 | 26345168 |
| 3 - 3,5 | 3,25 | 0,836 | 0,689 | 30590 | 68903 | 6358903 | 26414071 |
| 3,5 - 4 | 3,75 | 0,889 | 0,728 | 17494 | 40417 | 6376397 | 26454488 |
| 4 - 4,5 | 4,25 | 0,963 | 0,781 | 9609 | 23124 | 6386006 | 26477612 |
| 4,5 - 5 | 4,75 | 1,069 | 0,852 | 4930 | 12740 | 6390936 | 26490352 |
| 5 - 5,5 | 5,25 | 1,218 | 0,945 | 2305 | 6673 | 6393241 | 26497025 |
| 5,5 - 6 | 5,75 | 1,431 | 1,071 | 970 | 3275 | 6394211 | 26500299 |
| 6 - 6,5 | 6,25 | 1,729 | 1,242 | 369 | 1478 | 6394580 | 26501777 |
| BW = 1.0 | | | | | | N TOTAL | |

Considering BW=2.5, the implant breaks after a number of cycles between 145.738 cycles (straight front) and 593.088 (semicircular front).

In fact, the second stage finishes a few thousands of cycles before, when the patient starts to feel pain and, then, the third stage starts. Considering that there is no nucleation time and adding a quick propagation step of 1.3 months for a straight front crack and 4.5 months for a semicircular

crack, the duration of the third stage can be obtained. This is 7.7 months for a straight front and 4.5 months for a semicircular front. This is equivalent to 415.800 and 243.000 cycles respectively. If we start to count the cycles from the end to the beginning of the process (on stage 3, BW=1.0), we obtain that such numbers are the amount of cycles that are necessary for a growth from 1.5 mm to 6.5 mm (straight) or from 2.0 mm to 6.5 mm (semicircular).

As a summary, three stages can be distinguished:

- STAGE 1: Nucleation, whose duration is considered 0.
- STAGE 2: Propagation with dynamic effects, from 0.1 mm to a value between 1.5 and 2.0 mm. Taking mean values, this would take about 3 months.
- STAGE 3: Propagation without dynamic effects. This takes 6 months

14.11.4. References

[14.33] S. Cicero, F. Gutiérrez-Solana, JA. Alvarez, L. Sánchez: "Failure Analysis of a Hip Implant by Using the FITNET FFS Procedure". Engineering Fracture Mechanics. Submitted.

[14.34] A.J Van der Bogert, L.Read, B.M.Nigg: "An analysis of hip joint loading during walking, running and skiing". Med. Sci. Sports Exerc. 1999. Jan; 31(1): 131-42

[14.35] S.J.Taylor, P.S.Walker: "Forces and moments telemetered from two distal femoral replacements during various activities". J.Biomech. 2001 Jul; 34 (7): 839-48

[14.36] S.J.Taylor, P.S.Walker, J.S.Perry, S.R.Cannon, R.Woledge: "The forces in the distal femur and the knee during walking and other activities measured by telemetry". J.Arthroplasty. 1998, Jun; 13(4): 428-37

[14.37] G.M.Kotzer, D.T.Davy, V.M.Goldberg, K.G.Heipke, J.Berilla, K.G.Heipke Jr, R.H.Brown, A.H.Burstein: "Telemeterized in vivo hip joint force data: a report on two patients after total hip surgery". J.Orthop.Res. 1991, Sep; 9(5): 621-33.

[14.38] R.A.Brand, D.R.Pedersen, D.T.Davy, G.M.Kotzar, K.G.Heipke, V.M.Goldberg: "Comparison of hip force calculations and measurements in the same patient". J.Arthroplasty. 1994, Feb; 9(1): 45-51

[14.39] B.W.Stansfield, A.C.Nicol: "Hip joint contact forces in normal subjects and subjects with total hip prostheses: walking and stair and ramp negotiation". Clin.Biomech. (Bristol, Avon) 2002, Feb; 17(2):130-39.

[14.40] "FITNET FFS Procedure", GIRT-CT-2001-05071

14.12. Crossed tutorial: Structural Integrity Assessment of Different Components of a Power Plant [14.41]

14.12.1. Introduction

All the components of a power plant were transported from the manufacturer facilities to the construction place. Two tubes failed in their connection to the lower header after their transport (firstly by ship and finally by road) to the place where the plant was being built and a brief storage (the whole process took between seven and eight weeks).

Hardness measurements in the Heat Affected Zone (HAZ) as well as in the welding gave very high hardness values (even greater than 500 HV), which justifies a martensitic microstructure and agrees with the intergranular propagation observed in the failure section. All these observations indicate that the heat treatment performed by the manufacturer was, at least, insufficient.

In both failures, the initiation of the cracks started on the outer surface and after that, cracks propagated to the inside of the tubes (Figures 14.57 and 14.58).

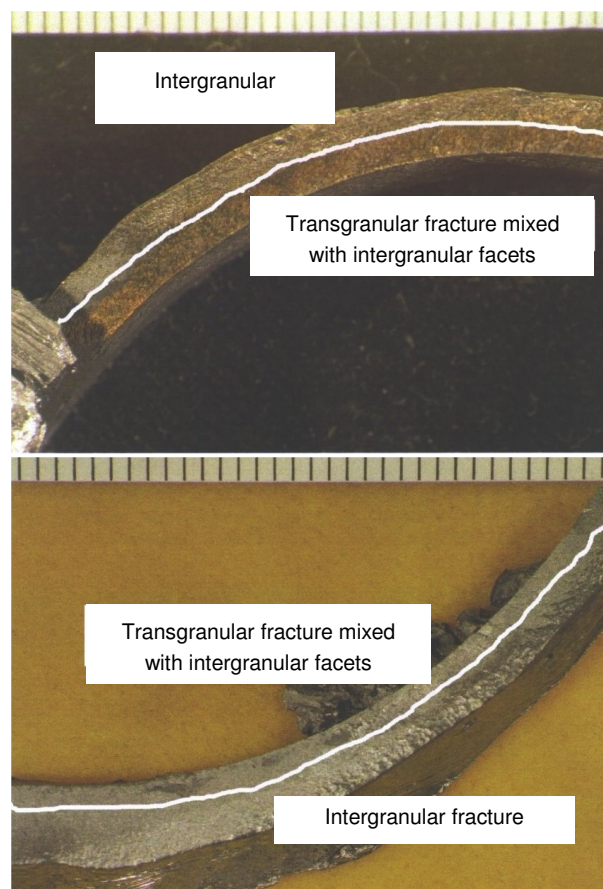


Figure 14.57 – Failure Sections.

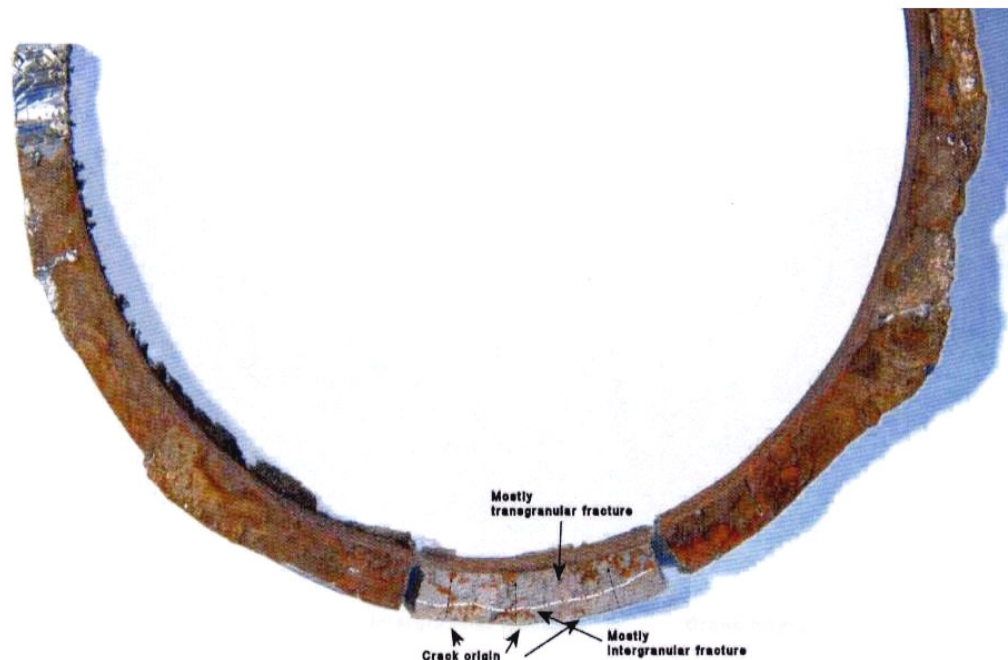


Figure 14.58 – Scheme of the failure micromechanisms.

14.12.2. Failure analysis

The detailed analysis of the events and the data mentioned above allows some hypotheses to be established. It seems clear that there is a HAC process which leads to the failure of the two first tubes and to the generation of a crack that causes the failure of the third tube during the heat treatment performed in plant.

A detailed explanation of the process is now performed: crack propagation occurs when the crack front is subjected to stresses (and environmental conditions) which are more severe than the material resistance. In order for a HAC process to occur, certain conditions are necessary. The first one is the presence of hydrogen (in this case, this is absolutely justified because of transport by sea) and a sensitive material (such as the martensitic structure in the welded joints, derived from the high hardness values). The second one is the existence of defects (very usual in welds) and local stresses (in this case, residual stresses caused by the welding process). The conditions to which the component is subjected are defined by K_I , and the resistance of the material to crack propagation in an aggressive environment is defined by K_{ISCC} , a material property for a given environment.

Once the material resistance is exceeded (for martensitic microstructures, $K_{ISCC} \sim 10\text{-}20 \text{ MPa}\cdot\text{m}^{1/2}$), cracks propagate at a constant rate whose value for martensitic microstructures is between 10^{-6} and 10^{-7} m/s. These rates justify the failure of the tubes in a few weeks. A crack would grow 2 mm (this is the growth of the cracks in the broken tubes) in a few hours. Actually, the process is slower and takes some weeks, because there is an initiation period and also, because when cracks propagate, they reach zones where conditions are less severe (i.e, starting from the outer surface, the residual stresses caused by the welding process, decrease in depth. Also, the material can be less sensitive to HAC due to different microstructures such as bainitic ...).

14.12.3. Proposed Solution, New Failures and Uncertainty

An additional heat treatment was performed in plant, as a consequence of the conclusions of the above report, in order to reduce the material hardness (and then the sensitivity to HAC as well as its brittleness). The treatment consisted in a stress relief annealing performed at 758 +/- 7°C (heating rate approx. 80 K/h, time on temperature 2h), followed by slow air cooling.

Hardness measurements performed after the process gave values between 200 and 280 HV. Another failure occurred during this treatment (Figure 14.59). This time, the failure was justified as a consequence of the existence of an initial internal crack (generated because of HAC) which propagated until fracture subjected to the thermal stresses of the heat treatment.

In order to detect possible cracks in the outer surface of the components, they were tested with penetrant liquids and magnetic techniques. No external crack was detected, but uncertainty concerning internal cracks was still present.

The analysis performed below aims to analyse the possibility of the existence of more internal cracks as well as the consequence of these hypothetical cracks to the Plant operating conditions.

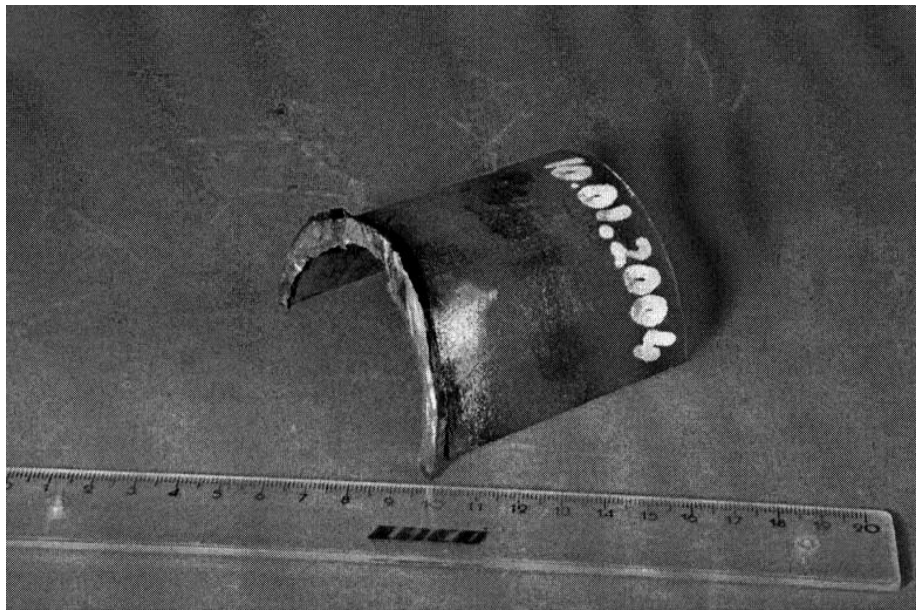


Figure 14.59 – Scheme of the failure micromechanisms.

14.12.4. Inputs

14.12.4.1 Flaw information

Because there were no more external cracks, it was statistically very unlikely that many internal cracks existed, and if they did, they would probably be very few. Also, if they did exist, it could be expected that their length should be limited and small. After the welding process, residual stresses in the order of the yield stress appear. This makes K_I achieve the value of K_{ISCC} with very small

cracks, in such a way that from a given crack size, cracks would propagate and produce failure. Summing up, making K_I (considering $\sigma = \sigma_y$ and the crack size being the unknown quantity) equal to K_{ISCC} , a maximum limit for the size of the cracks (if they exist) is obtained, if the possibility of bigger cracks that have arrested after a previous propagation is not considered because of the previously mentioned reasons (loss of necessary conditions: material sensitivity, high stresses,...). Only when the crack enters a zone unaffected by the welding (with a higher toughness) or local stresses decrease, the crack might grow initially and finally arrest with a bigger size than the one that is derived from the previous analysis.

This analysis has been performed for tubes RHTR2 ($t = 3.5$ mm, $R_i = 34.6$ mm) and HPSPHTR3 (with two different geometries, $t = 4.6$ mm and $R_i = 20.8$ mm, $t = 5.6$ mm and $R_i = 19.8$ mm) and for semicircular internal ($l=2a$) and circumferential internal cracks geometries (the latter gives similar but more conservative results than those obtained for semicircular internal cracks with the major axis equal to half of the internal circumference, which is the geometry observed in failures). Figure 14.60 shows these geometries.

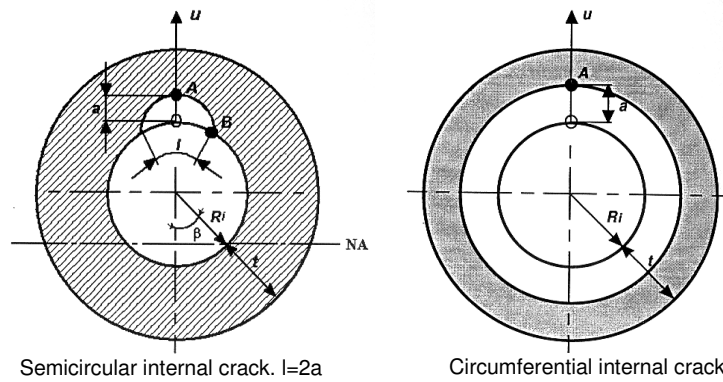


Figure 14.60 – Crack geometries considered.

Moreover, two values for K_{ISCC} have been considered: $10 \text{ MPa}\cdot\text{m}^{1/2}$ and $20 \text{ MPa}\cdot\text{m}^{1/2}$ (this gives conservative results for crack length), taken as extreme values for martensitic structures. The results of the calculations are shown in Table 14.25.

These crack sizes are the ones that will be used in the structural integrity calculations. Also, an additional conservative size of 2.0 mm will be considered (whose probability is very low) as the maximum limit for those cracks which could have initiated the propagation and stopped. This is approximately the length of the crack that appeared in the failure which occurred during the thermal treatment. No bigger cracks are expected because, if they had existed, they would have caused the failure of the section during that process.

Table 14.25. Maximum crack sizes at which no HAC would have occurred.

| | Semicircular crack | Circumferential crack |
|--|-------------------------|-------------------------|
| $K_{ISCC} = 10 \text{ MPa}\cdot\text{m}^{1/2}$ | $a_0 = 0.35 \text{ mm}$ | $a_0 = 0.12 \text{ mm}$ |
| $K_{ISCC} = 20 \text{ MPa}\cdot\text{m}^{1/2}$ | $a_0 = 1.40 \text{ mm}$ | $a_0 = 0.48 \text{ mm}$ |

14.12.4.2 Stresses and working conditions

A structural analysis of the components during the plant operation was performed. This analysis justified maximum stresses of 15 MPa in the reheater and 45.2 MPa in the superheaters (at lower header branches). All stresses are supposed to be membrane stresses.

Working temperatures are as follows:

| | |
|----------------------|--------|
| RHTR2 (t=3.5 mm): | 550 °C |
| HPSPHTR3 (t=4.6 mm): | 538 °C |
| HPSPHTR3 (t=5.6 mm): | 566 °C |

14.12.4.3 Material Properties

These are the data available for the base material.

$$K_{ISCC} = 10-20 \text{ MPa}\cdot\text{m}^{1/2}$$

$$K_{JC} = 168 \text{ MPa}\cdot\text{m}^{1/2}$$

$$da/dN = 2.0 \cdot 10^{-10} \cdot (\Delta K)^{3.85} \quad (14.122)$$

when ΔK is given in $\text{MPa}\cdot\text{m}^{0.5}$ and da/dN in mm/cycles

Table 14.26. Mechanical properties at different temperatures.

| | 500°C | 550°C | 600°C |
|------------------|--------|--------|--------|
| σ_y (MPa) | 300 | 270 | 215 |
| σ_u (MPa) | 380 | 330 | 255 |
| E (MPa) | 180000 | 174000 | 168000 |

Time to rupture at different temperatures:

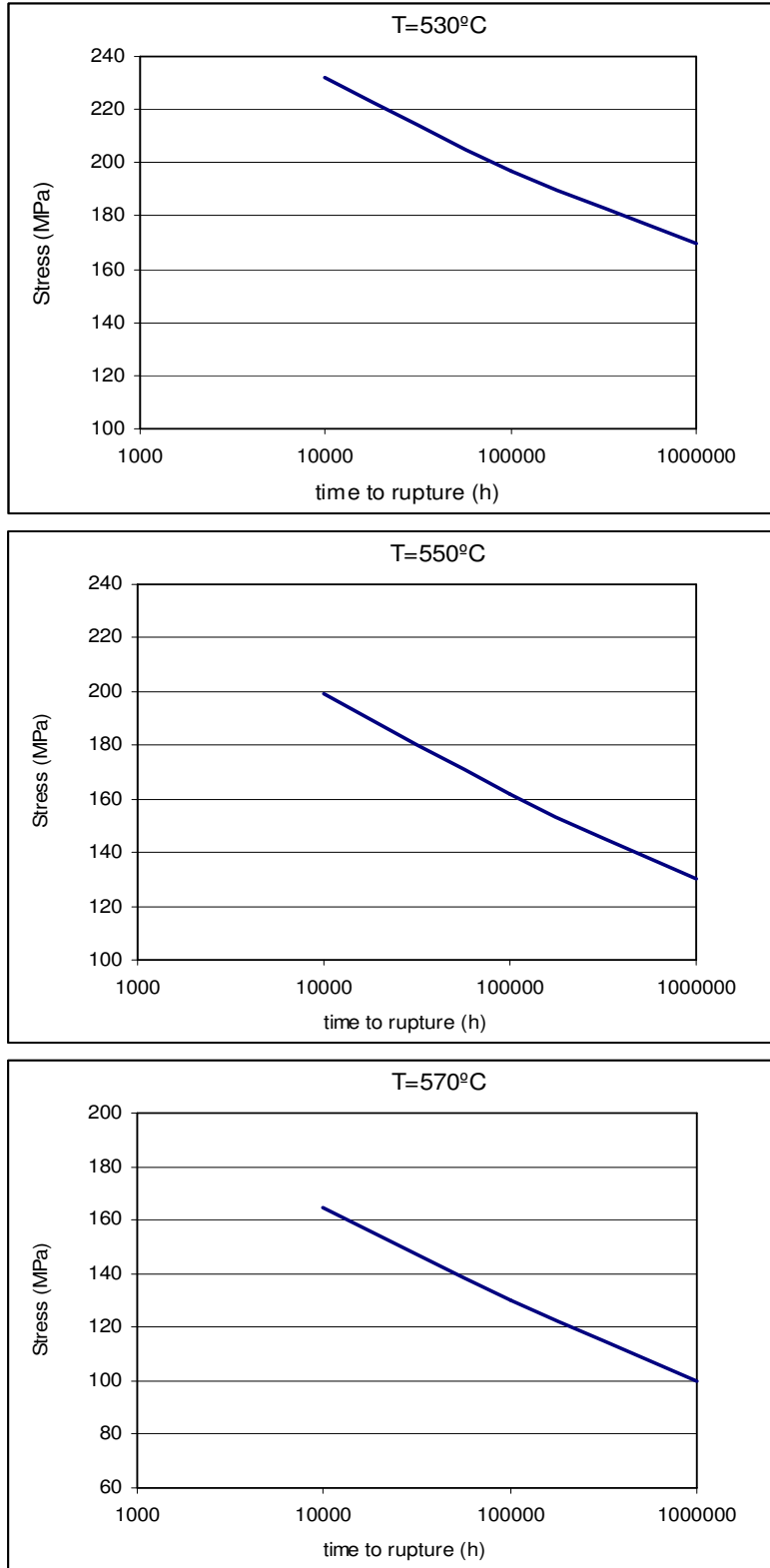


Figure 14.61 – Uniaxial stress-time to rupture data at different temperatures.

14.12.5. Assessment

It is necessary to distinguish which processes will determine the life of the components. There are two main processes:

-CREEP: tubes work at temperatures around 550°C, and because of that, cracks will propagate and lead to failure because of generalised creep damage or creep crack growth.

-FATIGUE: during the operation of the station, some transitory phenomena occur. These phenomena generate stress variations that cause crack propagation because of fatigue processes. Finally, cracks achieve a critical size that leads to failure because of FRACTURE-PLASTIC COLLAPSE. Based on the data supplied by the designer, we shall only consider the “hot start” transitory, which is responsible for nearly 100% of the fatigue damage assessed by the designer. 5000 cycles of this transitory will be considered in the 25 years of life considered for the plant. Stresses are considered to change from the operating values (given in 14.12.4.2) to zero.

The FITNET procedure will be used for the assessment. Chapter 8 (Creep Module) proposes a step by step procedure which will be followed here:

- *Step 1. Establish cause of cracking and characterise initial defect*

As seen above, creep and fatigue processes may affect the different tubes

- *Step 2. Define service conditions*

The tubes operate at temperatures and under stresses shown in 14.12.4.2.

- *Step 3. Collect material data*

As seen in 14.12.4.3

- *Step 4. Perform basic stress analysis*

Only primary membrane stresses are considered.

Reference stresses and stress intensity factor solutions are considered as follows:

Semicircular internal crack ($l=2a$):

$$\sigma_{\text{ref}} = \sigma \frac{\pi}{\pi - \frac{al}{2R_i t} - 2 \arcsin \left[\frac{a}{2t} \sin \left(\frac{l}{2R_i} \right) \right]} \quad (14.123)$$

$$K_I = f_0 \sigma \sqrt{\pi a} \quad (14.124)$$

Circumferential internal crack:

$$\sigma_{\text{ref}} = \sigma \frac{(R_i / t + 1)^2 - (R_i / t)^2}{(R_i / t + 1)^2 - (R_i / t + a / t)^2} \quad (14.125)$$

$$K_I = \frac{1}{\sqrt{2\pi a}} \int_0^a \sigma(u) \sum_{i=1}^{i=3} f_i(a/t, R_i/t) \left(1 - \frac{u}{a}\right)^{i-\frac{3}{2}} du \quad (14.126)$$

- *Step 5. Check stability under time-independent loads*

For the crack geometries considered, it can easily be verified that no failures occur due to fracture-plastic collapse.

- *Step 6. Check significance of creep and fatigue*

The cyclic plastic zone was calculated and compared to the different crack sizes that were considered. In all cases, the plastic zone was much smaller than the crack size or any other dimension characteristic of the structure, so fatigue is considered insignificant.

For the purpose of this example, it is assumed that creep is significant.

- *Step 7. Calculate rupture life*

The rupture life for failure by continuum damage mechanics, t_{CD} , can be obtained from the reference stress and the corresponding graph in Figure 14.61. In all cases t_{CD} is bigger than 10^6 hours years (and then, much more than 25 years).

- *Step 8. Calculate incubation time*

Initiation time is calculated in all cases according to (14.127):

$$t_i = 0.0025 \left[\sigma_{ref}^p(a_0) \cdot t_r(\sigma_{ref}^p(a_0)) / K^2 \right]^{0.85} \quad (14.127)$$

where a_0 is the initial crack length, t_r is the creep rupture time for uniaxial data (material property), K is the stress intensity factor and σ_{ref}^p is the primary load reference stress

The t_i values obtained are small enough in many cases in order to reject them. In other cases, incubation time was large but it was also neglected, which is a conservative hypothesis with no consequences in the final conclusions.

- *Step 9 (Calculate crack size after growth), Step 10 (Recalculate rupture life after growth) and Step 11. (Check stability under time-independent loads after crack growth).*

The extent of crack growth is calculated for all types of tubes and crack geometries (3 tubes·2 crack geometries·3 crack lengths =18 calculations). The creep crack growth law that was used in the calculations is given by (14.128):

$$\frac{da}{dt} = 0.005 \cdot \left(K^2 / (\sigma_{ref}^p \cdot t_r) \right)^{0.85} \quad (14.128)$$

As an example, Table 14.27 shows the calculations corresponding to HPSPHTR3 ($t=5.6$ mm), circumferential crack and $a_0=2.0$ mm. Steps are one year long.

Table 14.27. Creep calculations for HPSPHTR3.

| a0 | σref (MPa) | KI (MPam ^{1/2}) | tr (h) | (da/dt)creep (mm/h) | a increment (mm/year) | afinal |
|-------|------------|---------------------------|-----------|---------------------|-----------------------|--------|
| 2,000 | 67,332 | 5,831 | 1,089E+08 | 4,16E-07 | 3,65E-03 | 2,004 |
| 2,004 | 67,395 | 5,839 | 1,079E+08 | 4,20E-07 | 3,68E-03 | 2,007 |
| 2,007 | 67,459 | 5,847 | 1,069E+08 | 4,24E-07 | 3,72E-03 | 2,011 |
| 2,011 | 67,523 | 5,855 | 1,059E+08 | 4,28E-07 | 3,75E-03 | 2,015 |
| 2,015 | 67,589 | 5,864 | 1,049E+08 | 4,33E-07 | 3,79E-03 | 2,019 |
| 2,019 | 67,655 | 5,872 | 1,039E+08 | 4,37E-07 | 3,83E-03 | 2,022 |
| 2,022 | 67,722 | 5,880 | 1,029E+08 | 4,41E-07 | 3,86E-03 | 2,026 |
| 2,026 | 67,789 | 5,889 | 1,019E+08 | 4,46E-07 | 3,90E-03 | 2,030 |
| 2,030 | 67,858 | 5,897 | 1,008E+08 | 4,50E-07 | 3,94E-03 | 2,034 |
| 2,034 | 67,927 | 5,906 | 9,984E+07 | 4,55E-07 | 3,98E-03 | 2,038 |
| 2,038 | 67,997 | 5,915 | 9,883E+07 | 4,59E-07 | 4,02E-03 | 2,042 |
| 2,042 | 68,068 | 5,924 | 9,781E+07 | 4,64E-07 | 4,07E-03 | 2,046 |
| 2,046 | 68,140 | 5,933 | 9,680E+07 | 4,69E-07 | 4,11E-03 | 2,050 |
| 2,050 | 68,213 | 5,942 | 9,578E+07 | 4,74E-07 | 4,15E-03 | 2,054 |
| 2,054 | 68,287 | 5,951 | 9,477E+07 | 4,79E-07 | 4,20E-03 | 2,059 |
| 2,059 | 68,362 | 5,960 | 9,375E+07 | 4,84E-07 | 4,24E-03 | 2,063 |
| 2,063 | 68,438 | 5,969 | 9,273E+07 | 4,90E-07 | 4,29E-03 | 2,067 |
| 2,067 | 68,515 | 5,979 | 9,171E+07 | 4,95E-07 | 4,34E-03 | 2,072 |
| 2,072 | 68,593 | 5,988 | 9,068E+07 | 5,01E-07 | 4,39E-03 | 2,076 |
| 2,076 | 68,672 | 5,998 | 8,966E+07 | 5,06E-07 | 4,44E-03 | 2,080 |
| 2,080 | 68,752 | 6,008 | 8,863E+07 | 5,12E-07 | 4,49E-03 | 2,085 |
| 2,085 | 68,833 | 6,017 | 8,761E+07 | 5,18E-07 | 4,54E-03 | 2,089 |
| 2,089 | 68,916 | 6,027 | 8,658E+07 | 5,24E-07 | 4,59E-03 | 2,094 |
| 2,094 | 68,999 | 6,038 | 8,555E+07 | 5,31E-07 | 4,65E-03 | 2,099 |
| 2,099 | 69,084 | 6,048 | 8,452E+07 | 5,37E-07 | 4,71E-03 | 2,103 |

It can be seen that K_I values are low during the whole process (stability under time-independent loads). During the first 25 years of service the crack grows 0.103 mm.

For all the 18 cases, it is demonstrated that the life of components is longer than 25 years.

14.12.6. References

[14.41] S. Cicero, F. Gutiérrez-Solana, J.A. Alvarez: "Structural Integrity Assessment of Different Components of a Power Plant". Engineering Failure Analysis, 2006, To be published.

14.13. Qualitative tutorial: Application of FITNET Philosophy to the Aeronautical Industry [14.42]

14.13.1. List of abbreviations

The following abbreviations are used within this tutorial:

| | |
|------|--|
| AA | Airworthiness Authorities |
| AAS | Airworthiness Affected Structure |
| AC | Advisory Circular |
| ALS | Airworthiness Limitation Section |
| CS | Certification Specification (European regulations) |
| DET | DETAiled visual inspection DOCs Direct Operating Costs |
| DSG | Design Service Goal EC Eddy Current |
| ESG | Extended Service Goal |
| FAA | Federal Aviation Administration |
| FAR | Federal Aviation Regulation (US American regulations) |
| FC | Flight Cycles |
| F&DT | Fatigue and Damage Tolerance |
| FEM | Finite Element Method |
| FFS | Fitness-For-Service |
| FH | Flight Hours |
| FR | FRame |
| FSFT | Full Scale Fatigue Test |
| GVI | General Visual Inspection |
| I | Inspection Interval (in FC or FH) |
| ICA | Instructions for Continued Airworthiness |
| IFC | Initial Flaw Concept |
| ISB | Inspection Service Bulletin |

| | |
|-------|---|
| ISP | Inspection Starting Point |
| LH | Left Hand side of the aircraft |
| LOV | Limit Of Validity |
| MED | Multiple Element Damage |
| MPD | Maintenance Planning Document |
| MSB | Modification Service Bulletin |
| MSD | Multiple Site Damage |
| NDI | Non Destructive Inspection |
| NDT | Non Destructive Testing |
| PSE | Principal Structural Element |
| RH | Right Hand side of the aircraft |
| SB | Service Bulletin |
| SDC | Structural Damage Capability |
| SHM | Structural Health Monitoring |
| SIP | Structural Inspection Program |
| SMP | Structure Modification Point |
| SN | Stress vs. Number of cycles (presentation of material data for fatigue) |
| SRM | Structural Repair Manual |
| STR | STRinger |
| TH | Inspection THreshold (in FC or FH), time to first inspection |
| TOGAA | Technical Oversight Group Aging Aircraft |
| US | Ultra Sonic |
| WFD | Widespread Fatigue Damage |

14.13.2. List of symbols

| | |
|----------------|---|
| a | crack length |
| a _c | critical crack length, maximum tolerable crack length |

| | |
|----------------------------|--|
| $a_{crit\ WFD}$ | critical crack length in case of MSD/MED |
| a_{det} | detectable crack length |
| a_0, a_i | initial crack length |
| da/dn | crack growth rate |
| I_{MPD} | general interval of frame inspection program of MPD |
| I_{MSD} | inspection interval for structure susceptible to MSD |
| K | stress intensity factor |
| K_c | critical stress intensity factor |
| n | crack growth period between detectable and critical crack length |
| n_i | crack growth period between initial flaw and critical crack length |
| n_{MSD} | crack growth period between detectable and critical crack length for structure containing MSD cracks |
| N | fatigue life |
| N_{det} | fatigue life up to detectable crack length resulting from damage at in-service aircraft or FSFT specimen |
| N_E | safe fatigue life |
| N_F | calculated mean fatigue life based on SN data |
| N_{limit} | life limit for safe life structure NT justified fatigue life in full scale fatigue test with no detectable crack |
| N_{test} | fatigue life obtained in FSFT |
| R | ratio of minimum stress to maximum stress of a stress cycle |
| SF | scatter factor for safe life item according to AC 25.571-1C |
| T | time |
| TH_{IFC} | inspection threshold based on initial flaw concept |
| TH_{insp} | inspection threshold |
| TH_{mod} | limit for modification |
| TH_{MPD} | general inspection threshold of frame inspection program of MPD |
| $WFD_{average\ behaviour}$ | occurrence of widespread fatigue damage – mean value |
| α | correction factor on stress intensity factor for geometry |

ΔK stress intensity factor range

$\Delta\sigma$ stress range

σ stress

$\sigma_{c, \text{allow}}$ allowable static limit stress

$\sigma_{c,l}$ static limit stress

14.13.3. Introduction

This special tutorial describes the application of FITNET FFS procedure for the aeronautical structures. These structures involve predominantly thin-walled components and assessed for postulated and real damage conditions for fatigue and fracture. This procedure involves the subjects of fatigue, fracture and non-destructive testing / non-destructive inspection (NDT/NDI). The FFS procedure should be applied to metallic structures during development and design as well as during service. The aerospace industry is one of the industries, which makes significant effort to evaluate the effect of damages onto the safety and economy of the products. Although the procedure to be developed is intended to be generally applicable to metallic structural components, there are several specific aspects, which need to be considered in aeronautical applications. Therefore, this tutorial provides guidelines for the assessment of damage under static and cyclic loadings.

14.13.4. FFS procedure for aeronautical application – general

Damages due to fatigue, manufacturing defects and accidental damages play a significant role in the assessment of structural metallic aircraft components. Postulated damages are assessed during the pre-development, development and design of aircraft components as well as during certification and life extension activities. Furthermore, real damages occurring during major tests or in-service need to be analyzed.

The following chapters describe the relevant input parameters to these assessments, the procedure, the principle results and their repercussions to the aircraft operation.

The FFS procedure is applied in the aeronautical field in the following phases:

- Pre-development/development/design phase – postulated damage
- Certification phase – postulated damage
- In-service phase – real damage
- In-service – life extension phase – postulated damage

The applications of the FFS procedure in these phases differ slightly, mainly because of the objectives. During the pre-development/development/design phase the major goal is the determination of so-called allowable stresses, which must not be exceeded in order to fulfil the regulations and/or the requirements defined by the manufacturer as well as by the customer. During the certification phase an evaluation of the strength, detail design and fabrication must show that catastrophic failure due to fatigue, corrosion, manufacturing defects, or accidental damage, will be avoided throughout the operational life of the airplane. This is assured by defining adequate

maintenance actions, e.g. inspections, based on the structural behaviour of postulated damages. During the in-service the FFS procedure is used to investigate existing damages and to define the repercussions (structural modifications and/or inspections). The same applies to test findings during certification tests. During life extension activities the procedure is similar to that of the certification phase, since the objective is to extend the operation of the aircraft beyond the design service goal, while maintaining the reliability of the structure. These applications are explained in more detail by the following flow charts and the subsequent descriptions.

The FFS procedure in the aeronautical field comprises three stages, i.e. crack initiation (fatigue life), crack growth and fracture (residual strength).

14.13.5. FFS procedure for pre-development/development/design phase

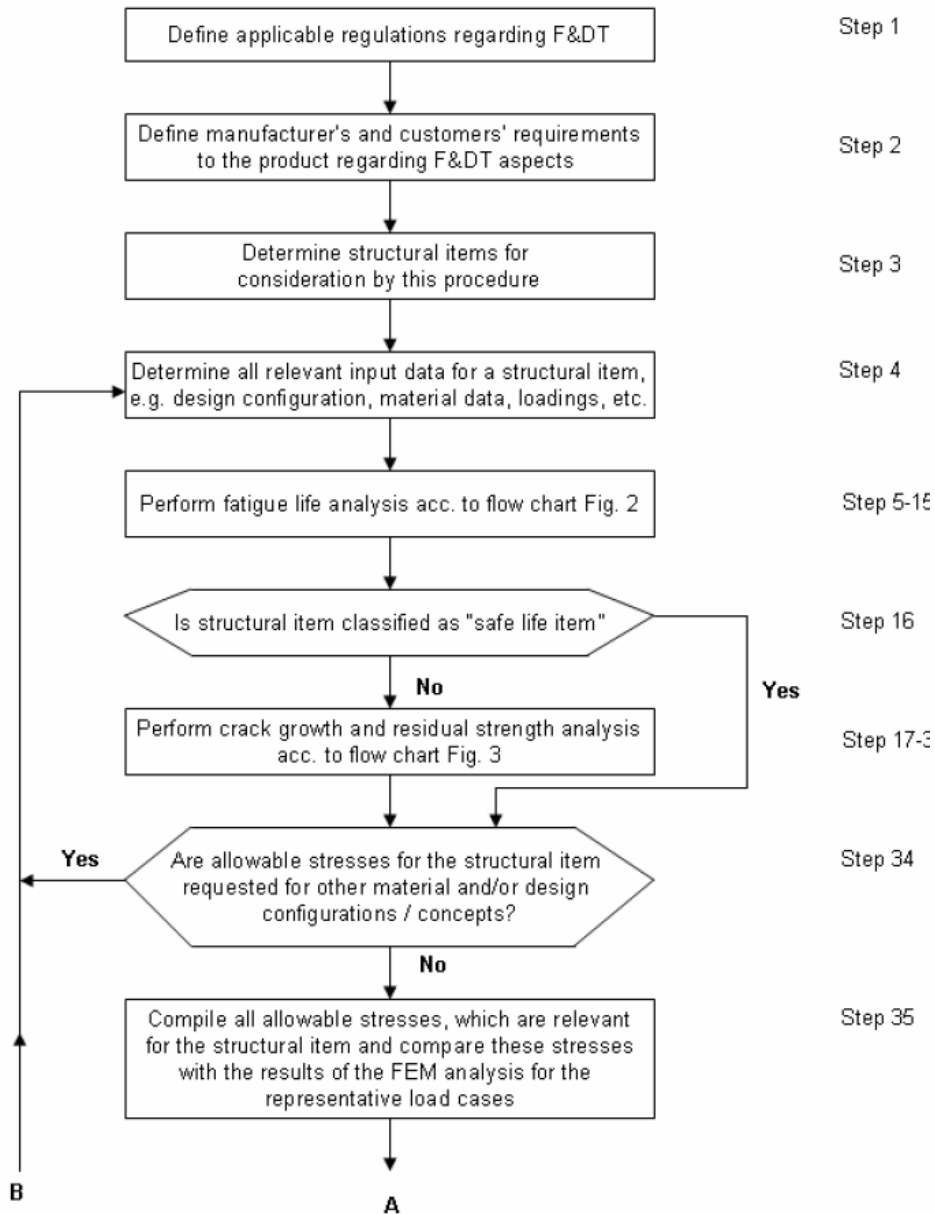


Figure 14.62 – Flow chart for overall F&DT procedure during pre-development/ development/ design phase - part 1

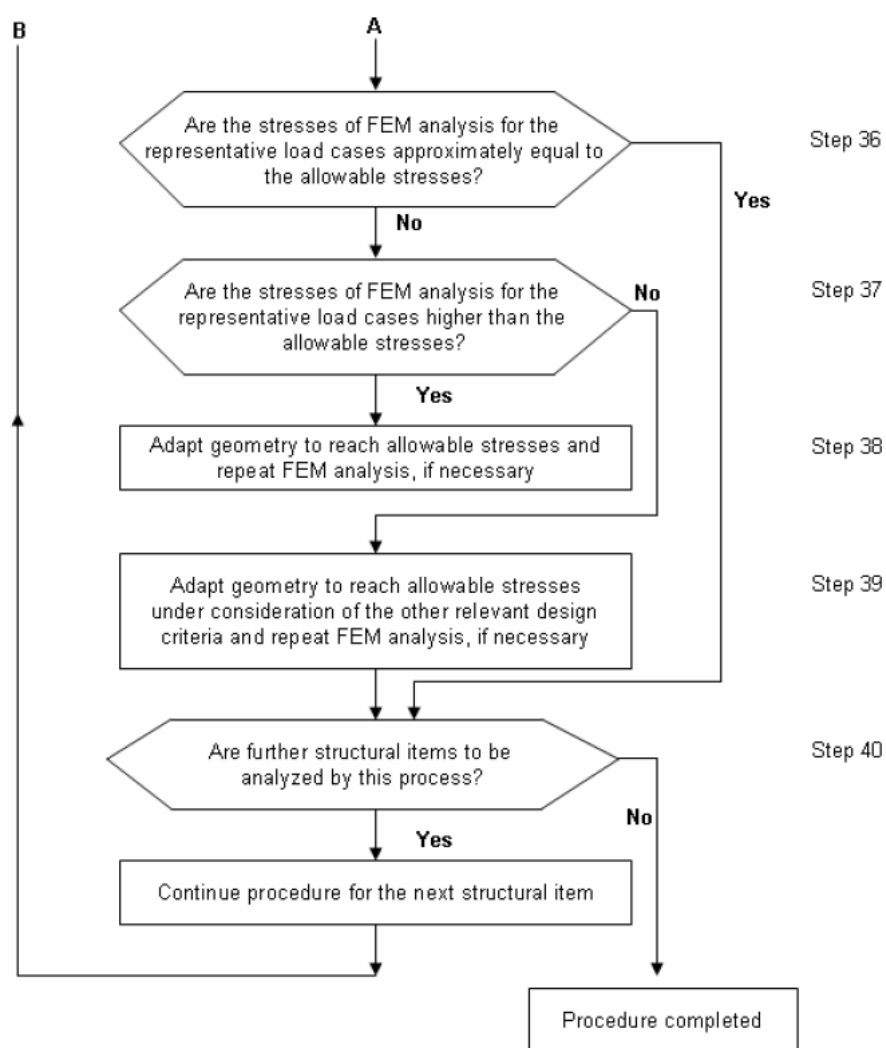


Figure 14.62 – Flow chart for overall F&DT procedure during pre- development/ development/ design phase - part 2 –

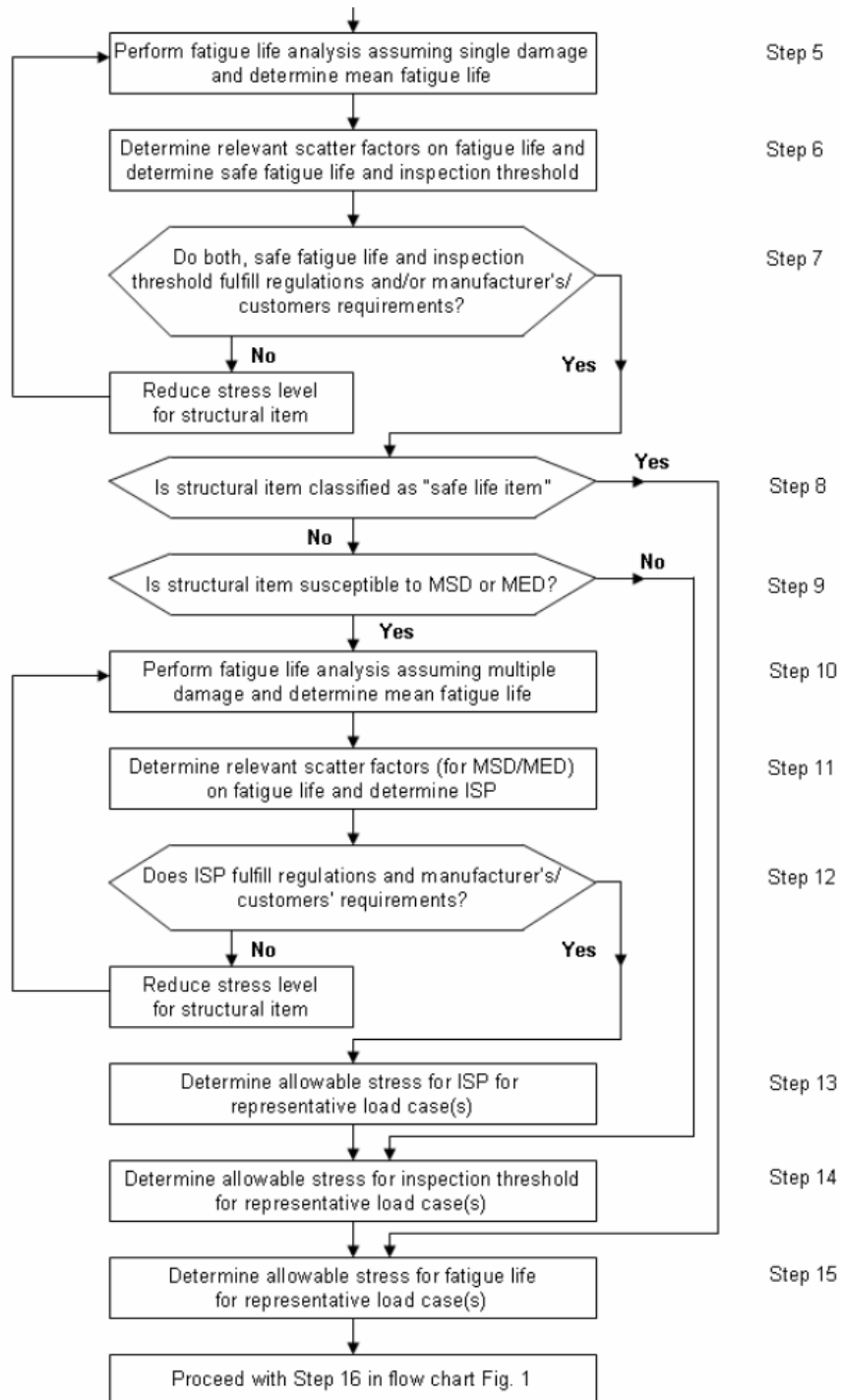


Figure 14.63 – Flow chart for fatigue life analysis during pre-development/development/design phase

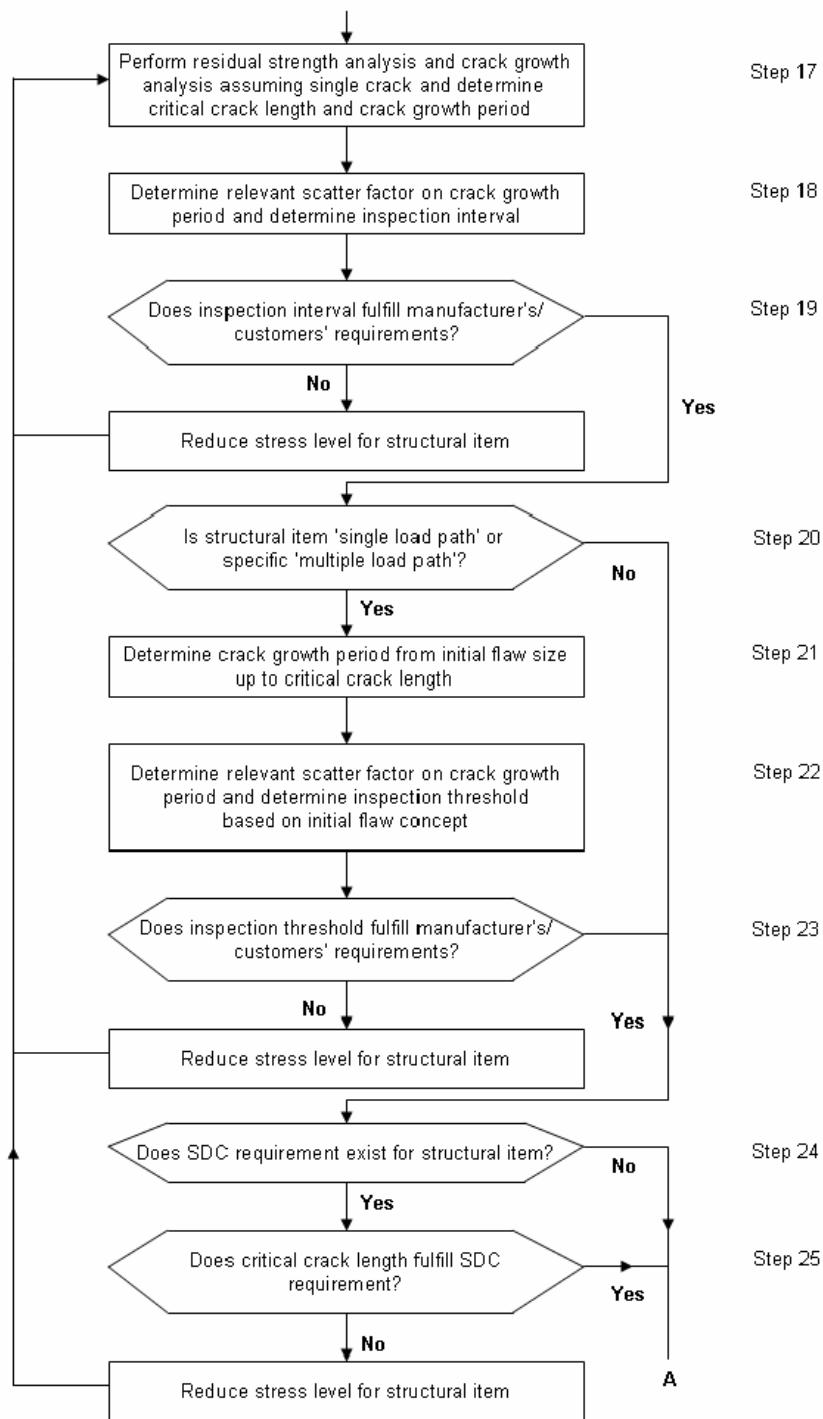


Figure 14.64 – Flow chart for residual strength and crack growth analysis during pre-development/development/design phase - part 1 –

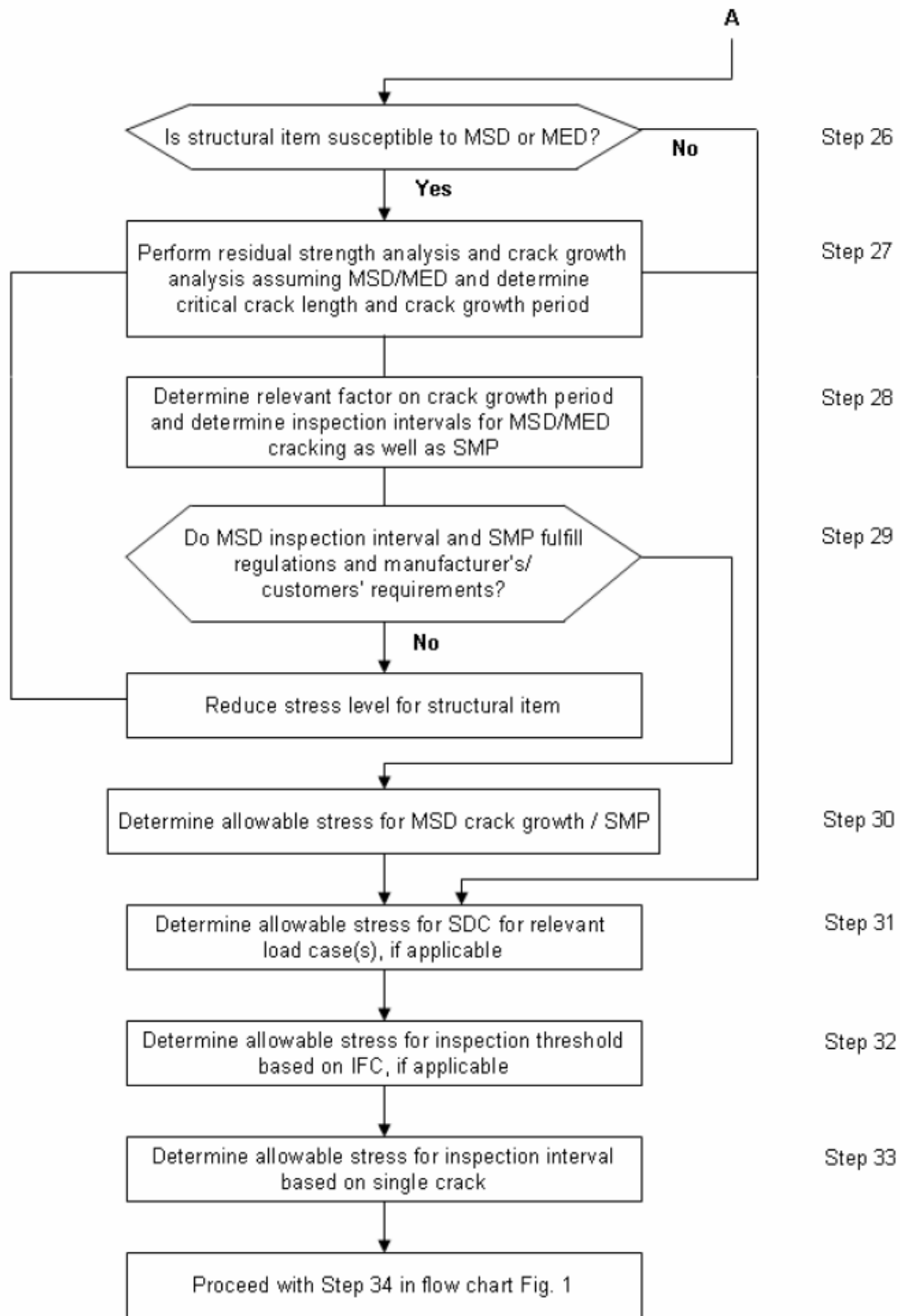


Figure 14.64 – Flow chart for residual strength and crack growth analysis during pre-development/ development/ design phase - part 2 –

The major objective of the F&DT analysis during the pre-development/development/design phase is to give an input to the design and dimensioning of the aircraft. This is done by the determination of the allowable stresses for all relevant criteria for the selected structural items. The allowable stresses are based on postulated damages.

-Step 1 – Applicable regulations

The relevant fatigue and damage tolerance (F&DT) regulation, which deals with damage tolerance, cracks and the applicable loads, is the FAR 25.571 and the corresponding Advisory Circular (AC) 25.571. The corresponding European regulations, CS 25.571, contain in principle the same requirements. Since all manufacturers strive for the US American certification of their products, the FAR regulations are considered by all major aircraft manufacturers in addition to their national or European regulations.

The current issue of the regulation is FAR 25.571 Amendment 96 “Damage tolerance and fatigue evaluation of structure”, which was published in 1998, see [14.43]. The corresponding AC is AC 25.571-1C, see [14.44].

The major requirements in paragraph 25.571 are:

- An evaluation of the structure has to show that a catastrophic failure due to fatigue, corrosion, or accidental damage, will be avoided throughout the operational life of the airplane.
- A structural inspection program has to be developed considering probable damage locations, crack initiation mechanisms, crack growth time histories and crack detectability. This applies to damage tolerant structure.
- The damage tolerance evaluation includes:
 - Identification of possible damage locations and extent of damage
 - Damage tolerance analysis and tests
 - Determination of inspection threshold and interval
 - Widespread fatigue damage assessment supported by sufficient full scale testing
 - Inspection threshold for certain type of structure based on crack growth instead of the fatigue life approach.

During the past few years the further development of the fatigue and damage tolerance regulation and the AC has been discussed between the Airworthiness Authorities of countries with significant aerospace industry and major airframe manufacturers. As the result, a draft regulation and a draft AC has been forwarded to the relevant FAA organizations for approval, see [14.45] and [14.46]. It may be assumed, that the modified regulation and AC will be published within the next few years. Therefore it is common practice of the major manufacturers to consider forthcoming regulations, which are still under discussion, as far as the economic implications to the product are acceptable for both, manufacturer and customers.

The major additional requirements in the forthcoming regulation and AC are:

- Structural damage capability (SDC) has to be demonstrated, i.e. the structure must be able to withstand the required residual strength load in the presence of damage equivalent to either the complete failure of any individual load path, or partial failure of a load path between damage containment features.
- A Limit of Validity (LOV) for the maintenance program must also be determined and included in the relevant documents. The LOV is the period of time, expressed in appropriate units (e.g. flight cycles), for which it has been shown that the established inspections and replacement times will be sufficient to preclude development of widespread fatigue damage.
- More stringent requirements for the determination of the inspection threshold for single load path structure, the threshold should not be greater than 50 percent of the design service goal (DSG) unless special analysis can prove higher values.

- Step 2 – Manufacturer's and customers' requirements

Besides the regulations, which must be fulfilled to obtain certification, several requirements and criteria are established by the manufacturer and the customers in order to achieve a product with aerodynamic and structural efficiency, i.e. with low production costs, low weight and low direct operating costs (DOCs).

The following requirements are relevant regarding F&DT:

- Design service goal which is defined as the period of time (in flight cycles/hours) established at design and/or certification during which the principal structure will be reasonably free from significant cracking.

For safe life structure (for definition see chapter 3.5) the DSG has to be demonstrated by analysis supported by test in order to ensure the safety of the aircraft, i.e. it has to be shown, that the fatigue life (crack initiation life) is greater or equal to the DSG under consideration of the relevant scatter factor.

For damage tolerant structure (for definition see chapter 3.5) the DSG is used to demonstrate the economic efficiency of the structure, i.e. the analysis should show, that the fatigue life is greater or equal to the DSG considering a less severe scatter factor compared to safe life structure.

- Structural inspection program: For damage tolerant structure the regulations require the establishment of a structural inspection program to ensure the airworthiness of the aircraft. The inspection program has to consider probable damage locations, crack initiation mechanisms, crack growth time histories and crack detectability. The following four topics have to be defined for all damage tolerant structural items:

- Inspection area
- Inspection threshold
- Inspection interval
- Inspection method

During the pre-development/development/design phase the so-called frame inspection program is defined, which includes a general inspection schedule for the overall maintenance program applicable to structure and systems. This frame inspection program is a baseline for dimensioning of the structure regarding F&DT. The inspection threshold (first inspection) and the interval (follow-

on inspections), generally defined in flight cycles (FC) or flight hours (FH), should be met by the fatigue life and the crack growth period, respectively, considering relevant scatter factors.

- Two-bay-crack criterion: Both, current regulation and AC do not require a minimum residual strength capability (minimum critical crack length), the two-bay-crack criterion or any other specified damage capability. However, the major airframe manufacturers interpret the forthcoming requirement of SDC as a two-bay-crack for the undisturbed skin of the pressurized fuselage structure.
- Specific goals are generally defined for structural repairs.

- Step 3 – Structural items to be considered

During the pre-development/development/design phase the major goal of the F&DT analyses is to determine the so-called allowable stresses for fatigue and damage tolerance aspects in order to consider these aspects during the early design phases. Allowable stresses for fatigue & damage tolerance:

- are defined for specific conditions of operational or static load cases
- may not be exceeded for these load cases to ensure adequate design
- are not pure material properties, but related to the specific design covering design goals, material behaviour, design implications, influence of manufacturing process and operational loads as well as design loads.

F&DT allowable stresses are to be defined for the airworthiness affected structure, i.e. primary structure and those secondary structures, which may affect the airworthiness of the aircraft. This includes:

- areas which contribute significantly to the weight of the aircraft due to their size (e.g. fuselage panels including skin, stringers and frames, wing panels, spars, ribs, etc.)
- areas which have pre-defined inspection targets and the operators would be penalized, if these targets are not met
- areas which are difficult and expensive to modify in case of insufficient F&DT behaviour (e.g. joints, door surroundings) Considering these criteria the structural items are selected for determination of the allowable stresses.

- Step 4 – Relevant input data

The F&DT analyses for determination of the allowable stresses require in principle the full set of input data. However, during early development phases not all data are available. Therefore preliminary data or assumptions and estimations, based on past experience, are used as far as necessary. The data required are:

- the loads and load spectra, which are converted into stresses and stress spectra
- the geometry
- stress concentration factors for fatigue life analysis

- stress intensity factors for crack growth and residual strength analysis
- the relevant material data.

Since the data required for F&DT analyses are in principle common to all industrial sectors and therefore not specific for the aeronautical application of the FFS procedure, no more details are presented here.

- Step 5 – Fatigue life analysis for single damage

FAR 25.571 Amendment 96 and AC 25.571 Issue 1C require fatigue life (crack initiation) analysis for the safe life structures only, since cracking in this type of structure would jeopardize the safety. The same regulations do not explicitly require the fatigue life analysis for the damage tolerant structures, since the safety of the structure is provided by the structural inspection program, which is based on crack growth and residual strength analysis. However, the majority of the manufacturers perform fatigue life analysis for two purposes:

- Demonstration of the reliability of the structure up to the design service goal or the extended service goal
- Determination of the inspection threshold instead of using the initial flaw concept for a certain type of “multiple load path and crack arrest ‘fail safe’ structure”.

According to AC 25.571-1C safe life and damage tolerance are defined as:

- Safe life of a structure is that number of events such as flights, landings, or flight hours, during which there is a low probability that the strength will degrade below its design ultimate value due to fatigue cracking.
- Damage tolerance is the attribute of the structure that permits it to retain its required residual strength for a period of use after the structure has sustained a given level of fatigue, corrosion, accidental or discrete source damage.

According to the AC, see [14.44], safe life structure is only allowed for the landing gear and its attachments.

The fatigue life analysis determines the period in time up to a detectable fatigue flaw, which is initiated and propagated due to cyclic loading. The detectable flaw size depends on the inspection method assumed, which is normally the visual inspection.

For all structural items first of all a single damage is assumed. The calculation method mainly used in the aeronautical field is the Palmgren-Miner rule, which is improved by most of the manufacturers by introduction of additional factors. These improvements lead to more realistic results which are comparable to test results. An overview of the analysis method, including correction factors to the Miner rule, is presented in [14.47].

- Step 6 – Scatter factor on fatigue life

The result of the fatigue life analysis is the mean fatigue life. To ensure the airworthiness of the aircraft (for safe life structure) or the economic usage (for damage tolerant structure) the mean fatigue life has to be reduced to the so-called safe fatigue life by application of a scatter factor. The following factors are to be applied for determination of the allowable stresses during the pre-development/development/design phase:

- Safe life structure: $N_E = N_F / 5$
- Damage tolerant structure: $N_E = N_F / 2$

with: N_E = safe fatigue life

N_F = calculated mean fatigue life based on SN data.

For demonstration of a sufficient inspection threshold (first inspection) the following is applied:

- Damage tolerant structure: $TH = N_F / 5$

The scatter factors given above are the minimum values to be applied. Higher factors may be used on a case-by-case basis due to specific reasons.

- Step 7 – Comparison of results with requirements

The safe fatigue life and the inspection threshold, both resulting from Step 6, have to be compared with the targets, i.e.:

- Safe life structure: $N_E \geq DSG$ (acc. to regulations)
- Damage tolerant structure: $N_E \geq DSG$ (acc. to manufacturer's requirement)
- $TH \geq TH_{MPD}$ (acc. to manufacturer's and customers' requirement)

with: TH_{MPD} = general threshold of frame inspection program of Maintenance Planning Document (MPD)

If the defined targets DSG and TH_{MPD} can be demonstrated, the procedure is continued with Step 8.

If the targets cannot be demonstrated the stress level for the structural item has to be reduced in order to obtain a longer fatigue life and the procedure is continued with Step 5. This iterative process is to be repeated until the targets are fulfilled.

- Step 8 – Classification of structural item (safe life vs. damage tolerant)

The complete structure is firstly distinguished into primary and secondary structure, where:

- Primary structure is that structure, which contributes significantly to carrying flight, ground and pressurization loads.
- Secondary structure is that structure, which carries only air or inertial loads generated on or within the secondary structure. All primary structure and those items of secondary structure, which may affect the airworthiness of the aircraft, is the so-called airworthiness affected structure. This structure is categorized into safe life and damage tolerant structure. As mentioned in chapter 3.5 the design of structure as safe life structure is only allowed for the landing gear and its attachments.

Because of the airworthiness of the safe life structure is based on sufficient fatigue life (crack initiation life), the following steps are not applicable and the procedure is continued with Step 15.

For damage tolerant structure the procedure is continued with Step 9.

- Step 9 – Susceptibility to MSD / MED

The issue of widespread fatigue damage (WFD), which may develop from multiple site damage (MSD) or multiple element damage (MED) is one of the major concerns for an aging airplane fleet, because MSD and MED have a significant influence of the structural behavior. Since the introduction of Amendment 96 of FAR 25 a widespread fatigue damage evaluation has to be performed for new certifications too. WFD, MSD and MED are defined according AC 25.571-1C as:

- Multiple Site Damage, MSD, is a source of widespread fatigue damage characterized by the simultaneous presence of fatigue cracks in the same structural element (i.e. fatigue cracks that may coalesce with or without other damage leading to a loss of required residual strength).
- Multiple Element Damage, MED, is a source of widespread fatigue damage characterized by the simultaneous presence of fatigue cracks in similar adjacent structural elements.
- Widespread Fatigue Damage, WFD, in a structure is characterized by the simultaneous presence of cracks at multiple structural details that are of sufficient size and density whereby the structure will no longer meet its damage tolerance requirement (i.e., to maintain its required residual strength after partial structural failure).

MSD and MED are illustrated in Figure 14.65.

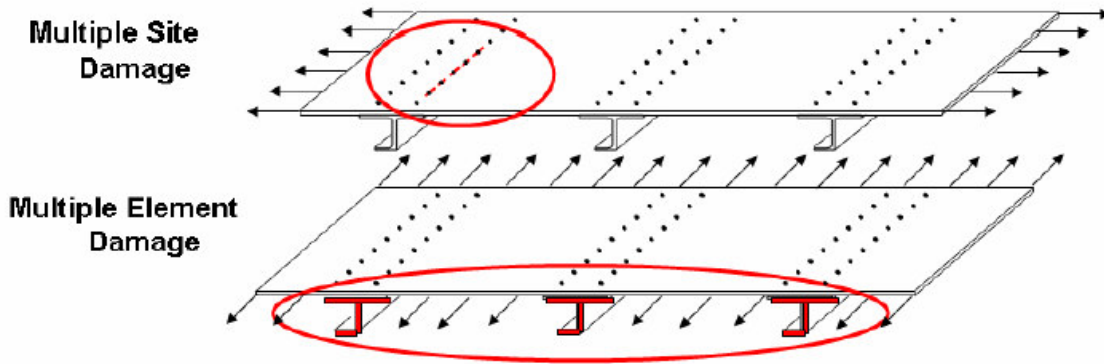


Figure 14.65 – Multiple site damage (MSD) and multiple element damage (MED) schemes.

The effect of MSD on the crack growth behavior and the residual strength is shown in Fig. 14.66.

[14.48] includes a list of structural items which are potentially susceptible to MSD and/or MED. The selection of these items is based on the experience of the major airframe manufacturers, who collected their experience from full scale fatigue tests and in-service during several international working groups on the issue of aging airplanes.

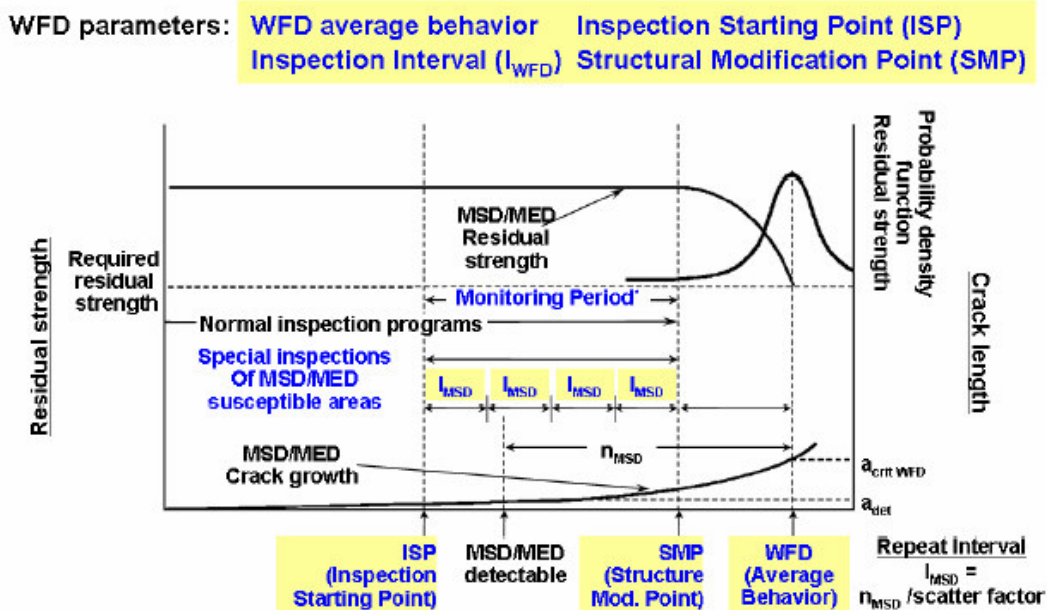


Figure 14.66 – Determination of WFD parameters and monitoring period.

- Step 10 – Fatigue life analysis of structure assuming MSD / MED

For analysis of structural items susceptible to MSD/MED, specific methods have been developed by the major manufacturers. There is general agreement throughout the literature that MSD and its subsequent phenomenon WFD largely depend on probabilistic effects. These effects can be derived from parameters which influence the development of MSD and WFD and which themselves show a probabilistic character. The major parameters are the initial design of a structural part, the loading (e.g. high tension, high induced bending or high load transfer), the manufacturing process, the material properties and to a certain degree the environment. These parameters obviously have a great influence on the fatigue life (MSD behaviour) of a structure. Therefore, any approach to assess MSD has to consider the probabilistic nature of these parameters.

For example, in one approach developed the probabilistic nature is taken into account by a Monte-Carlo simulation. The analysis model consists of two parts, a probabilistic and a deterministic part. Within the probabilistic algorithm the initial damage scenario is determined, while the subsequent steps, such as damage accumulation, crack growth and residual strength are calculated in a deterministic approach. The process is performed for a pre-defined number n of simulations. When calculating MSD scenarios it is essential to estimate the link-up process of these relatively small cracks. More details about the approach are given in [14.47].

The results of n iterations are evaluated statistically to obtain probability distributions, mean values and standard deviation for “Time to Initiation”, “Time to Detectable” and “Total Fatigue Endurance”. The final outputs of a complete Monte-Carlo simulation are crack and failure distributions associated with the structural configuration specified. The results are generally presented graphically, e.g. the cumulative probability versus the number of cycles.

- Step 11 – Scatter factor for MSD / MED susceptible structure

For aircraft to be certified according to the current regulation FAR 25.571 Amendment 96 it has to be demonstrated, that WFD will not occur within the DSG of the aircraft. This means, that the so-called Structural Modification Point (SMP), beyond which the airplane may not be operated without repair, modification or replacement, has to be greater than the DSG. Special inspections to detect MSD or MED may be performed starting at the Inspection Starting Point (ISP).

Both, the ISP and the SMP, are derived from the mean life up to WFD, which is obtained by a specific analysis method such as described in chapter 3.10. The following scatter factors should be applied on the so-called $WFD_{\text{average behavior}}$:

- Inspection Starting Point: $ISP = WFD_{\text{average behavior}} / 3$
- Structural Modification Point: $SMP = WFD_{\text{average behavior}} / 2$

These scatter factors are the minimum values and may only be applied, if the result of the analysis has the same reliability as full scale fatigue test results.

- Step 12 – Comparison of results with requirements

According to the current regulations the ISP may be below the DSG. However, since the specific inspections to detect MSD/MED generally have to be performed in short intervals, the manufacturer defines a minimum value for the ISP in order to satisfy his customers. Therefore the ISP received has to be checked against this requirement. If the ISP is lower than the required minimum, the stress level of the structural part has to be reduced to obtain a higher $WFD_{\text{average behavior}}$ and the procedure is continued with Step 10. This iterative process is to be repeated until the targets are fulfilled.

- Step 13 – Allowable stresses to reach required ISP

This step is only applicable to damage tolerant structure, which is susceptible to MSD/MED. The result of Step 11 and Step 12 is the allowable stress, which may not be exceeded in order to fulfil the manufacturer's requirements regarding WFD. Generally the allowable stresses are given for one or a few representative load cases. These may be e.g. for fuselages the internal pressure during cruise plus the steady load condition (1g) during cruise, depending on the location of the structural item and the major principal stresses.

- Step 14 – Allowable stresses to reach required inspection threshold

This step is only applicable to all damage tolerant structure assuming a single damage.

The result of Step 6 and Step 7 is the allowable stress, which may not be exceeded in order to fulfil the manufacturer's requirements regarding the inspection threshold. Generally the allowable stresses are given for one or a few representative load cases. These may be e.g. for fuselages the internal pressure during cruise plus the steady load condition (1g) during cruise, depending on the location of the structural item and the major principal stresses.

- Step 15 – Allowable stresses to reach required safe fatigue life

This step is applicable to damage tolerant structure and safe life structure.

The result of Step 6 and Step 7 is the allowable stress, which may not be exceeded in order to fulfil the requirements regarding the safe fatigue life considering the relevant scatter factors according to chapter 3.6. Generally the allowable stresses are given for one or a few representative load cases. These may be e.g. for fuselages the internal pressure during cruise plus the steady load condition (1g) during cruise, depending on the location of the structural item and the major principal stresses.

- Step 16 – Categorization of structure (safe life vs. damage tolerant)

As mentioned above the airworthiness of the safe life structure is based on the crack initiation life, which has to be sufficiently high compared to the DSG of the aircraft. Consequently no damage tolerance analysis is necessary for this type of structure.

The procedure is continued with Step 34 for the safe life items.

- Step 17 – Residual strength and crack growth analysis for single damage

The current regulation, see [14.43], requires clearly a damage tolerance analysis for the damage tolerant structure. Furthermore, based on these evaluations, inspections or other procedures must be established, as necessary, to prevent catastrophic failure and must be included in the Airworthiness Limitations Section of the Instructions for Continued Airworthiness required by § 25.1529, see [14.49].

The damage tolerance evaluation comprises a residual strength analysis with the result of the critical crack length and the crack growth analysis providing the crack growth curve between an initial flaw or the detectable crack length and the critical crack length. The residual strength analysis is based on the static limit loads, which are the loads occurring maximum once per life (for more details see FAR 25, e.g. FAR25.571, see [14.43]). The crack growth is determined under the spectrum of the operational loads.

The damage tolerance analysis has to consider different types of damages depending on the type of structure. Figure 14.67 shows as an example the damage types in principle to be considered during the damage tolerance evaluation of a fuselage shell.

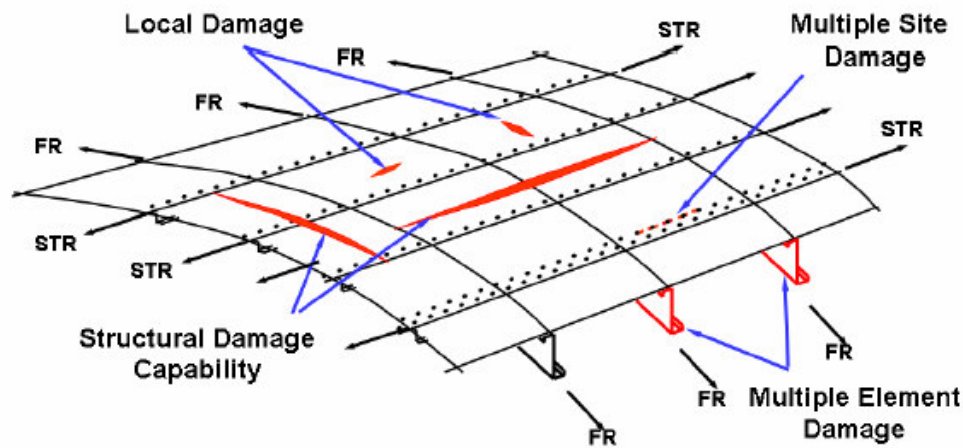


Figure 14.67 – Damage types to be considered during F&DT evaluation – fuselage examples

Step 17 considers the local damages only, the other types of damage are described in Step 24 and Step 27. Local damages occur in one or more elements of a principal structural element (PSE) at a single site and are not influenced by damages in adjacent locations. A PSE is defined as:

- Principal structural element (PSE) is an element that contributes significantly to the carrying of flight, ground, or pressurization loads, and whose integrity is essential in maintaining the overall structural integrity of the airplane.

The purpose of the residual strength analysis is to determine the maximum allowable crack length a_c (last point of stability), which corresponds to the static limit stress $\sigma_{c,l}$ as required by FAR 25.571. This allowable crack length is also called maximum tolerable crack length or critical crack length. For fuselage structure the conventional procedure based on stress intensity factor solutions and fracture toughness data is generally sufficient, see Figure 14.68. For other types of structures more complex methods may be necessary.

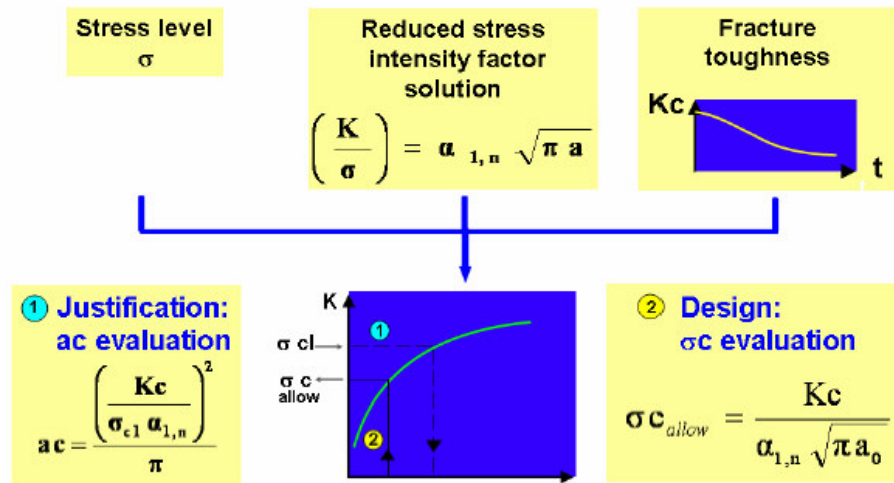


Figure 14.68 – Residual strength analysis

The goal of the crack growth analysis is to determine the crack growth curve between detectable damage size and the critical crack length. Again a conventional linear analysis procedure is generally applied to the fuselage structure as shown in Figure 14.69. Most often the Forman equation is used, in exceptional cases Paris or Walker equation may be chosen. For other types of structures more complex methods may be necessary, e.g. using a retardation model.

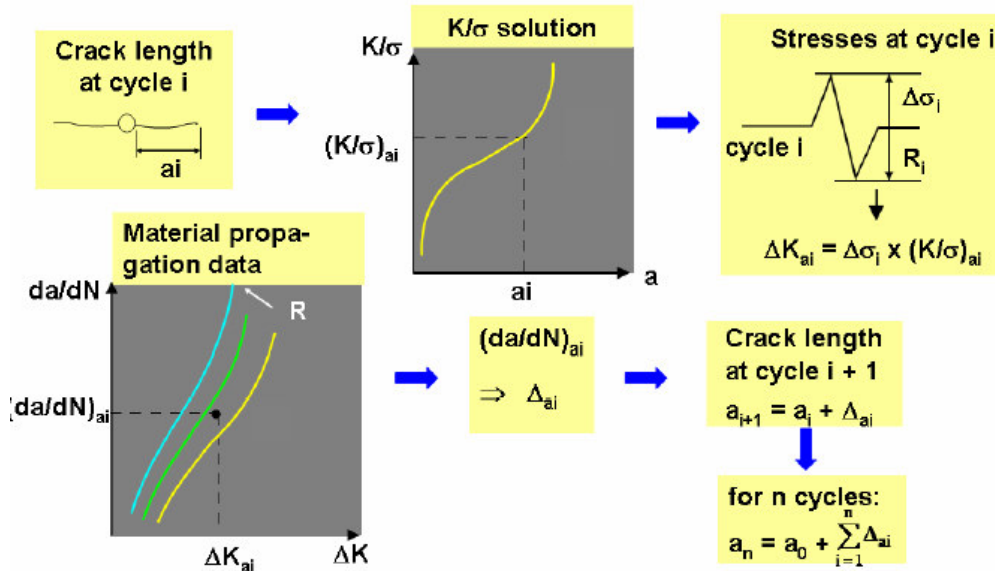


Figure 14.69 – Crack growth analysis

- Step 18 – Scatter factor on crack growth period

The result of the crack growth analysis is the mean crack growth curve between the detectable crack length and the critical crack length. To ensure the airworthiness of the aircraft for damage tolerant structure the mean crack growth period has to be reduced to by a scatter factor to obtain the inspection interval. The following factors are to be applied for determination of the allowable stresses during the pre-development/development/design phase:

- Single load path structure: $l = n / 3$
- Multiple load path structure with low scatter of operational loads: $l = n / 2$
- Multiple load path structure with larger scatter of operational loads: $l = n / 2.5$

where n is the crack growth period between detectable and critical crack length .

The scatter factors described above are the minimum values to be applied. Higher factors may be used on a case-by-case basis due to specific reasons.

Single load path structure and multiple load path structure are defined as follows acc. to [14.44]:

- Single load path is where the applied loads are eventually distributed through a single member, the failure of which would results in the loss of the structural capability to carry the applied loads.
- Multiple load path is identified with redundant structures in which (with the failure of individual elements) the applied loads would be safely distributed to other load-carrying members.

The detectable crack length depends on the inspection level and method envisaged. In general three inspection levels are possible acc. to the general inspection program planning. These are:

- General visual inspection (GVI)

- Detailed visual inspection (DET)
- Special detailed inspection (NDI/NDT)

The detectable crack length decreases with the inspection level, i.e. general visual inspection leads to relatively large detectable crack length (e.g. approx. 75 mm for undisturbed fuselage skin) compared with a detailed visual inspection (e.g. approx. 25 mm for the same location).

- Step 19 – Comparison of inspection interval with requirements

The inspection interval resulting from Step 18 has to be compared with the target, i.e.:

- $I \geq I_{MPD}$ (acc. to manufacturer's and customers' requirement)

where I_{MPD} is the general interval of frame inspection program of Maintenance Planning Document (MPD).

It is always the goal to use firstly the lowest inspection level, i.e. general visual inspection. If the resulting interval does not fit with the I_{MPD} for GVI, the next level is chosen, i.e. detailed visual inspection and so on. It has to be considered, that not all inspection levels are applicable to all kind of structure, e.g. because the item to be inspected is hidden by other structure and is therefore not visually inspectable. In this case only NDI is applicable and the most suitable method has to be selected. The most common NDI methods for aeronautical structure are Eddy Current (EC) or Ultra Sonic (US). X-ray is less often used, mainly because of the relatively long detectable crack length and necessity to gain access to both sides of the structural item.

If the defined target I_{MPD} can be demonstrated, the procedure is continued with Step 20.

If the target cannot be demonstrated the stress level for the structural item has to be reduced in order to obtain a longer crack growth period and the procedure is continued with Step 17. This iterative process is to be repeated until the target is fulfilled.

- Step 20 – Classification of structure (single load path, multiple load path)

The current regulation, see [14.43], requires "for single load path structure and multiple load path "fail-safe" structure and crack arrest "fail-safe" structure where it cannot be demonstrated that load path failure, partial failure, or crack arrest will be detected and repaired during normal maintenance, inspection, or operation of an airplane prior to failure of the remaining structure", that the inspection threshold is also derived from the results of the damage tolerance analysis, i.e. the application of the initial flaw concept (IFC) is required. For these types of structure the inspection threshold is the crack growth period between an initial flaw and the critical crack length, divided by an appropriate scatter factor.

The length of the initial flaw may be taken from the experience of the manufacturer. If no data are available, the proposals made by T. Swift may be used, see [14.50].

For other structure the manufacturer has the choice to use either the fatigue life approach or the initial flaw concept described above for determination of the inspection threshold.

- Step 21 – Crack growth period from initial flaw

The crack growth period between the initial flaw size and the critical crack length is derived from the results of Step 17. Since the classification of the structural item is known before starting the crack growth calculation, the starting crack length for this type of structure is set to the initial flaw size.

- Step 22 – Scatter factor on crack growth period for threshold determination

The scatter factor for the threshold determination by crack growth is:

- $TH_{IFC} = n_i / 2$

where n_i is the crack growth period between initial flaw and critical crack length .

The scatter factor is the minimum value to be applied. A higher factor may be used on a case-by-case basis due to specific reasons.

- Step 23 – Comparison of inspection threshold with requirements

The inspection threshold resulting from Step 22 has to be compared with the target, i.e.:

- $TH_{IFC} \geq TH_{MPD}$ (acc. to manufacturer's and customers' requirement)

where TH_{MPD} is the general threshold of frame inspection program of Maintenance Planning Document (MPD).

If the defined target TH_{MPD} can be demonstrated, the procedure is continued with Step 24.

If the target cannot be demonstrated the stress level for the structural item has to be reduced in order to obtain a longer crack growth period and the procedure is continued with Step 17. This iterative process is to be repeated until the target is fulfilled.

- Step 24 – SDC requirement

The structural damage capability (SDC) will be required by the forthcoming regulation, see [14.45]. It is the characteristic of the structure which permits it to retain sufficient static load capability in the presence of damage equivalent to the complete failure of a load path or partial failure of the load path between damage containment features. The AC draft, see [14.46], contains a more detailed interpretation of the structural damage capability.

The interpretation of this new requirement would lead to a minimum structural damage capability of one stiffener bay, i.e. "partial failure between damage containment features", which may be the stringers or frames. However, the major airframe manufacturers, e.g. Boeing and Airbus, interpret this SDC requirement as a two-bay crack for the general (undisturbed) fuselage skin.

A two-bay-crack is defined as a skin crack of a length of two stiffener bays, i.e. two stringer bays or two frame bays of the fuselage, see Figure 14.67. This crack in either circumferential or longitudinal direction may in principle occur above an intact central stiffener or above a broken central stiffener. The relevant application has to be decided based on the detailed circumstances for the structural item, e.g. the inspection program for the internal stiffeners and the risk of an impact due to discrete source damage resulting from engine rotor failure, etc. The two-bay-crack criterion requires that the structure is able to withstand this crack length under specified residual strength loads.

The idea of the two-bay-crack criterion was raised due to the fact, that the aerospace industry experienced several cases of long cracks, which occurred in service due to fatigue, accidental damage or discrete source damage. A long critical crack length of the structure has maintained in several cases the structural integrity of the airplane. Therefore the application of the two-bay-crack criterion was mainly promoted by the FAA, namely Tom Swift, the former national research specialist on fracture mechanics. This has significantly been supported by the TOGAA (Technical Oversight Group Aging Aircraft), which was established by the FAA. The ability of the structure

containing a two-bay crack to withstand residual strength loads provides the ultimate safety to the airframe in addition to the damage tolerance requirements.

Step 25 – Comparison of critical crack length with SDC requirement

The critical crack length is one result of Step 17. If this critical crack length is equal or greater as the SDC requirement (two-bay crack or other length), the procedure is continued with Step 26. Otherwise the stress level of the structural item is to be reduced in order to obtain a longer critical crack length and the procedure is continued with Step 17. This iterative process is to be repeated until the target is fulfilled.

- Step 26 – Susceptibility to MSD / MED

See chapter 3.9.

- Step 27 – Crack growth and residual strength analysis of structure containing MSD / MED

Structure assumed to develop MSD/MED cracking has to be analyzed by a specific analysis tool. Since this tool has to combine probabilistic and deterministic parts, there is in general one common tool for evaluation of the crack initiation life, the subsequent crack growth and the residual strength. For more details see chapter 3.10.

- Step 28 – Scatter factors for MSD / MED susceptible structure

The following scatter factors have to be applied for structure containing MSD/MED:

- Interval for structure with low scatter of operational loads: $I_{MSD} = n_{MSD} / 2$
- Interval structure with larger scatter of operational loads: $I_{MSD} = n_{MSD} / 2.5$
- Structural Modification Point: $SMP = WFD_{\text{average behavior}} / 2$

where n_{MSD} is the crack growth period between detectable and critical crack length for structure containing MSD cracks .

The scatter factors are the minimum values to be applied. Higher factors may be used on a case-by-case basis due to specific reasons.

- Step 29 – Comparison of results with requirements

According to the current regulations the ISP is allowed to be below the DSG, i.e. an interval is to be defined. This interval needs to fulfil the customers' expectations. For aircraft to be certified according to the current regulation it has to be demonstrated, that WFD will not occur within the DSG of the aircraft. This means, that the Structural Modification Point (SMP) has to be greater than the DSG. Furthermore, it should be considered, that aircraft are generally not retired at the DSG. Consequently, a life extension program will be launched, which should allow operation up to the so-called Extended Service Goal (ESG). Therefore, the allowable stresses for structure susceptible to MSD/MED should consider an estimated ESG instead of the DSG.

If the requirements for the interval and/or SMP are met, the procedure is continued with Step 30. If one or both values do not meet the requirements, the stress level for the structural item has to be reduced to obtain a longer crack growth period and/or higher $WFD_{\text{average behavior}}$ and the procedure is continued with Step 27. This iterative process is to be repeated until the targets are fulfilled.

- Step 30 – Allowable stresses to reach required IMSD and SMP

This step is only applicable to damage tolerant structure, which is susceptible to MSD/MED.

The result of Step 27 and Step 28 is the allowable stress, which may not be exceeded in order to fulfil the requirements regarding WFD. Generally the allowable stresses are given for one or a few representative load cases. These may be e.g. for fuselages the internal pressure during cruise plus the steady load condition (1g) during cruise, depending on the location of the structural item and the major principal stresses.

- Step 31 – Allowable stresses to reach SDC

This step is only applicable to damage tolerant structure, for which a SDC requirement is established.

The result of Step 24 and Step 25 is the allowable stress, which may not be exceeded in order to fulfil the requirements regarding structural damage capability. Since SDC is related to the residual strength, the allowable stress is given for the relevant static limit load case.

- Step 32 – Allowable stresses to reach required inspection threshold based on IFC

This step is only applicable to “single load path structure and multiple load path “fail-safe” structure and crack arrest “fail-safe” structure where it cannot be demonstrated that load path failure, partial failure, or crack arrest will be detected and repaired during normal maintenance, inspection, or operation of an airplane prior to failure of the remaining structure”.

The result of Step 17, Step 21 and Step 22 is the allowable stress, which may not be exceeded in order to fulfill the requirements regarding the inspection threshold based on the initial flaw concept. Generally the allowable stresses are given for one or a few representative load cases. These may be e.g. for fuselages the internal pressure during cruise plus the steady load condition (1g) during cruise, depending on the location of the structural item and the major principal stresses.

- Step 33 – Allowable stresses to reach required inspection interval

This step is applicable to all damage tolerant structure assuming local damage.

The result of Step 17 and Step 18 is the allowable stress, which may not be exceeded in order to fulfil the requirements regarding the inspection interval in case of a single damage. Generally the allowable stresses are given for one or a few representative load cases. These may be e.g. for fuselages the internal pressure during cruise plus the steady load condition (1g) during cruise, depending on the location of the structural item and the major principal stresses.

- Step 34 – Allowable stresses for other configurations

During the pre-development/development/design phase different structural configurations and/or materials may be investigated in order to define the optimum design solution. Therefore it is necessary to define allowable stresses for the concerned structural item for different design configurations and/or different materials. If this is required the procedure is repeated starting with Step 4.

- Step 35 – Comparison of allowable stresses with FEM results

The major objective of the F&DT analysis during the pre-development/development/design phase is to give an input to the design and dimensioning of the aircraft. This is done by the determination of the allowable stresses for all relevant criteria, see above, for the selected structural items. The allowable stresses are then compared with the results of the finite element

(FEM) calculations. FEM calculations are performed for static ultimate load cases and in addition for the F&DT representative load cases.

- Step 36 – Allowable stresses similar to FEM stresses

If the allowable stresses are approximately equal to the stresses determined by the FEM analysis, the structure is adequately dimensioned with respect to F&DT.

- Step 37 – FEM stresses higher than allowable stresses

If the FEM stresses are higher than the allowable stresses for F&DT, one or more F&DT targets described above (safe fatigue life, inspection threshold, inspection interval, SDC, etc.) will not be reached. This means either the regulations and/or the manufacturer's / customers' requirements are not fulfilled with the current design.

If the FEM stresses are less than the allowable stresses for F&DT, the F&DT targets are completely or partly exceeded and there is a reserve for one or more targets.

- Step 38 – Adapt design for adequate F&DT behaviour

If the F&DT targets are (partly) not fulfilled as described in chapter 3.37, the design has to be adapted. This may be done by changing the geometry, e.g. increase of thickness and cross sections, or the choice of another material with better properties for the relevant parameter (fatigue, crack growth, residual strength).

Generally, the FEM analysis is repeated several times during the pre-development/development/design phase due to refinement of loads, which provides the opportunity to check the adapted design against the F&DT targets.

- Step 39 – Adapt design to reduce reserve in F&DT behaviour

FEM stresses less than the allowable stresses for F&DT indicate a reserve for one or more F&DT targets. If no other criteria are dimensioning for the structure, e.g. static strength, stability, minimum thickness requirements, etc., the design may be adapted and the reserves on the F&DT target are reduced or eliminated. The adaptation may be done by reduction of thickness and cross sections or by the choice of another material.

Again, this adaptation should be checked by a new FEM analysis.

- Step 40 – Analysis of further items

If further items need to be analyzed, the whole procedure is continued with Step 4 to Step 39.

If no further items are to be analyzed, the procedure is completed and the results should be summarized.

14.13.6. FFS procedure for certification phase

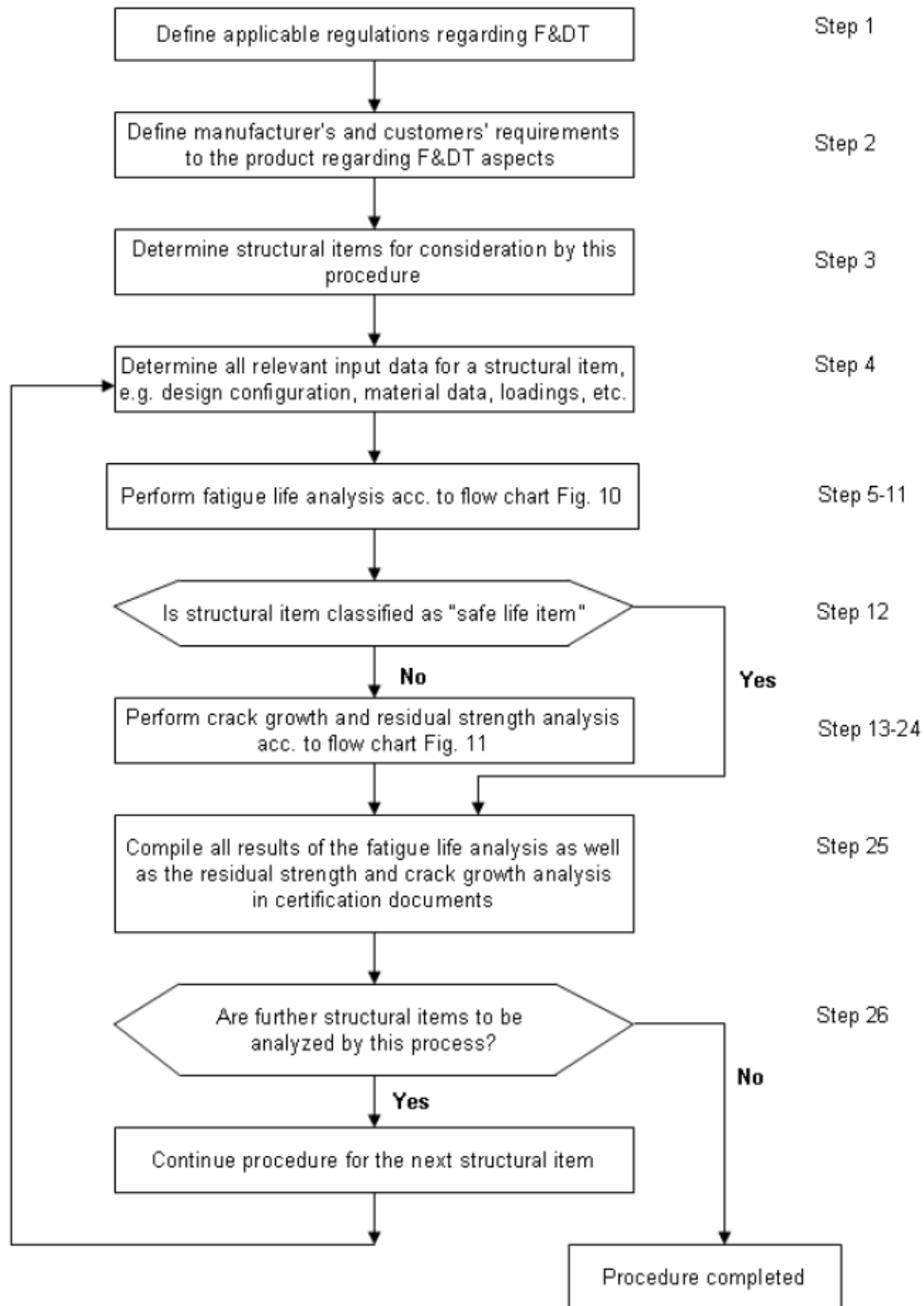


Figure 14.70 – Flow chart for overall F&DT procedure during certification phase

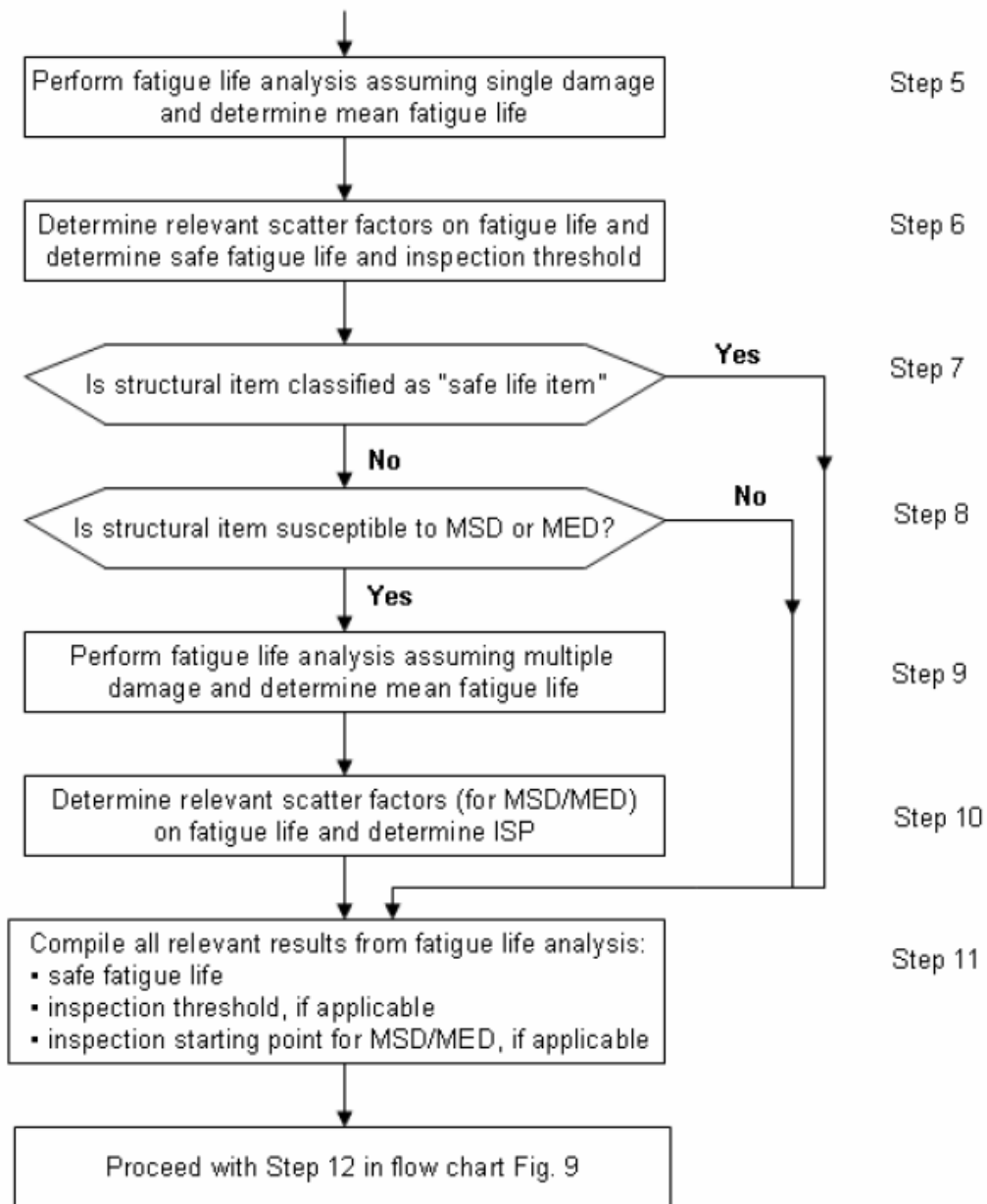


Figure 14.71 – Flow chart for fatigue life analysis during certification phase

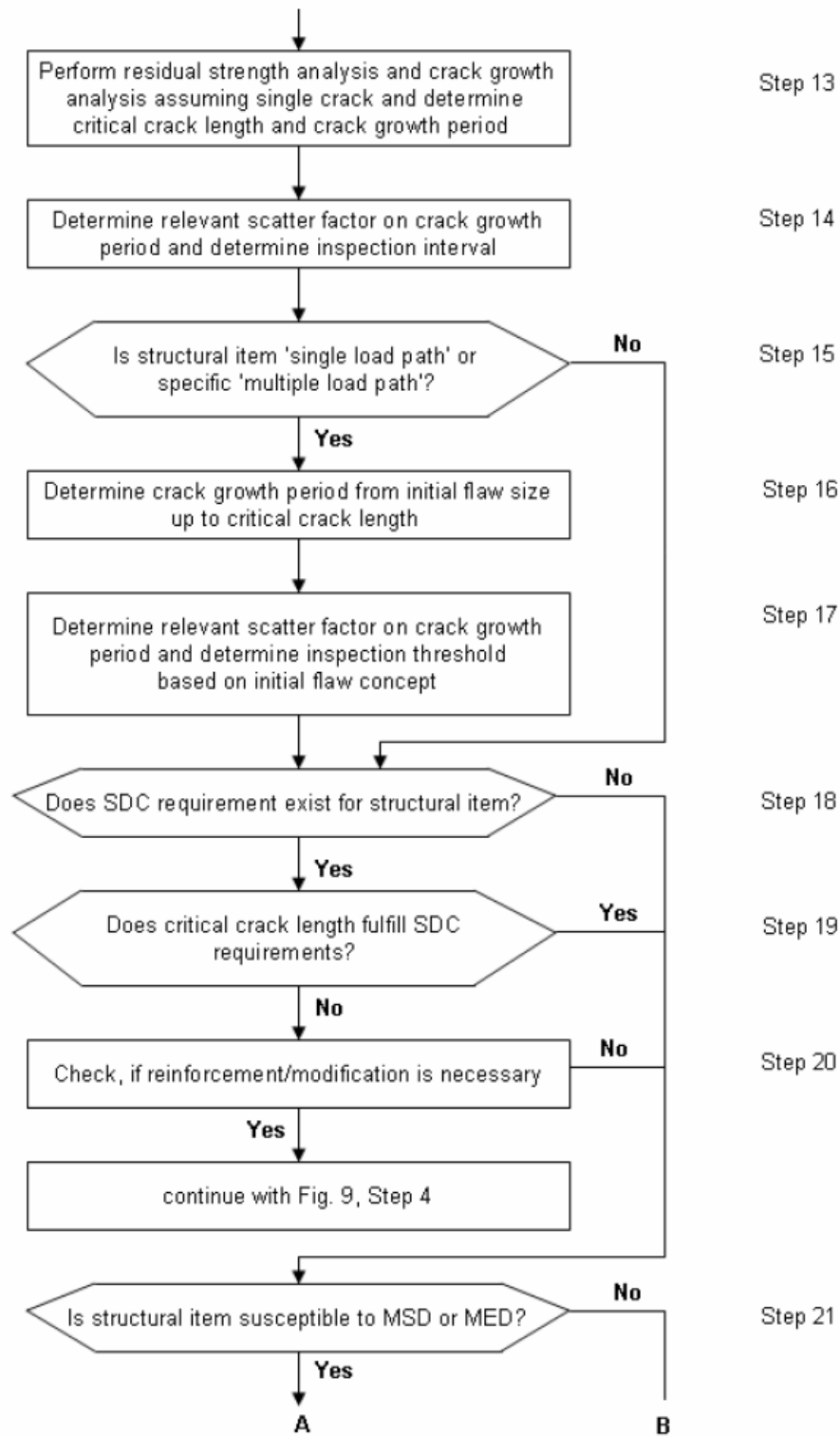


Figure 14.72 – Flow chart for residual strength and crack growth analysis during certification phase - part 1

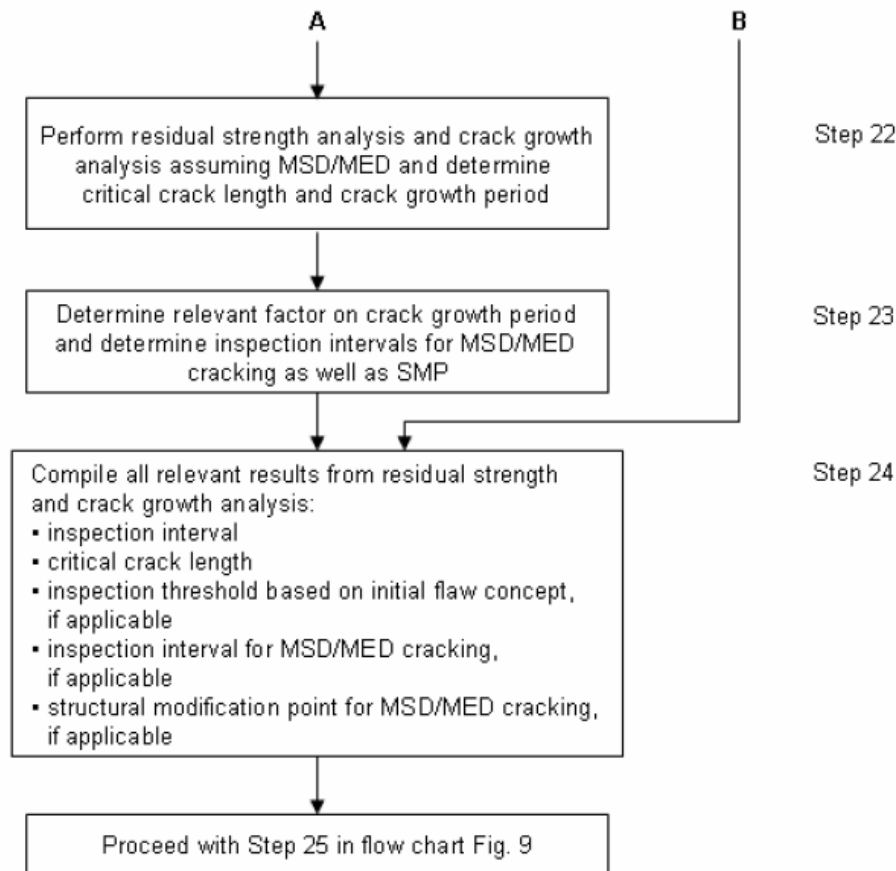


Figure 14.72 – Flow chart for residual strength and crack growth analysis during certification phase - part 2

The major objective of the F&DT analysis during the certification phase is to provide all F&DT relevant analysis results and justifications to demonstrate the airworthiness of the aircraft, to show compliance with the applicable regulations and finally to obtain certification.

In principle the same analyses are performed as during the pre-development/development/design phase. Since the design and dimensioning is completed prior to the certification phase, no iterative process is applied, but the analysis procedure is a straight forward procedure. As during the pre-development/development/design phase, the analyses during the certification phase are based on postulated damages. The analyses are performed considering the final design (design configuration, material, geometry, dimensions, etc.) as well as the final loads and load spectra provided for certification. The relevant results are compiled in the certification documents, which are presented to the airworthiness authorities.

Due to the fact, that the F&DT aspects are generally considered during the pre-development/development/design phase, the targets, which are defined for the structure (see chapter 3) will be met for the vast majority of the structural items. A few exceptions may be possible, e.g. due to significant increase of global or local loading. For these few exceptions the inspection program has to be adapted for damage tolerant structure or a modification / reinforcement is to be introduced to meet the original F&DT goals. Since most of the steps of the FFS procedure for the

certification phase are the same as for the pre-development/development/ design phase, only the changed/new steps are described in the following.

- Step 1 – Applicable regulations

See chapter 3.1.

- Step 2 – Manufacturer's and customers' requirements

See chapter 3.2.

- Step 3 – Structural items to be considered

As described above the major objective during the certification phase is to demonstrate the airworthiness of the aircraft. In contrast to the static strength analysis the F&DT analysis is not required for each single element of the structure, but for PSEs (principle structural elements) and AAS (airworthiness affected structure) only. To support the selection of the items reference [14.44] includes general guidance material for the selection as well as a list of PSE's to be considered.

In general the most F&DT sensitive areas of a PSE are analyzed, because these areas are important for the severity of the structural inspection program. According to Tom Swift, see [14.51], the following selection criteria may be applied when defining the structural areas for the F&DT analysis:

- Elements in tension or shear
- Low static margin
- High stress concentration
- High load transfer
- High spectrum density
- High stresses in secondary members after primary member failure
- Materials with high crack growth rates
- Areas prone to accidental damage
- Component test results
- Results of full scale fatigue test and in-service experience

- Step 4 – Relevant input data

The input data required for the F&DT analyses are described in chapter 3.4. During the certification phase the full set of data is available, since the design is completed and the loads are provided for all relevant load cases.

- Step 5 – Fatigue life analysis for single damage

See chapter 3.5.

Fatigue life analysis assuming a local damage are performed also for structural items susceptible to MSD/MED, since a local damage may occur at any time in the life, also in areas susceptible to MSD/MED.

- Step 6 – Scatter factor on fatigue life

See chapter 3.6.

Instead of using the fatigue life N_F (calculated fatigue life based on SN data) during certification phase also results from major full scale fatigue tests may be available. Therefore N_F may be substituted by:

N_T = Justified fatigue life in full scale fatigue test with no detectable crack

When using N_T the inspection threshold for damage tolerant items is:

Damage tolerant structure: $TH = N_T / 3$

- Step 7 – Classification of structural item (safe life vs. damage tolerant)

See chapter 3.8.

For damage tolerant structure the procedure is continued with Step 8.

For safe life structure the procedure is continued with Step 11.

- Step 8 – Susceptibility to MSD / MED

See chapter 3.9.

- Step 9 – Fatigue life analysis of structure assuming MSD / MED

See chapter 3.10.

- Step 10 – Scatter factor for MSD / MED susceptible structure

See chapter 3.11.

- Step 11 – Compilation of results from fatigue life analysis

The following results are needed for the certification:

- Safe fatigue life – for damage tolerant structure and safe life structure
- Inspection threshold – for damage tolerant structure without single load path and multiple load path structure not adequately covered by normal maintenance
- Inspection starting point – for damage tolerant structure, which is susceptible to MSD/MED.

- Step 12 – Categorization of structure (safe life vs. damage tolerant)

See chapter 3.16.

The procedure is continued with Step 25 for the safe life items

- *Step 13 – Residual strength and crack growth analysis for single damage*

See chapter 3.17.

- *Step 14 – Scatter factor on crack growth period*

See chapter 3.18.

The scatter factors on the crack growth period to determine the inspection interval are unchanged for the certification phase compared to the pre-development/development/design phase.

- *Step 15 – Classification of structure (single load path, multiple load path)*

See chapter 3.20.

- *Step 16 – Crack growth period from initial flaw*

The crack growth period between the initial flaw size and the critical crack length is derived from the results of Step 13. Since the classification of the structural item is known before starting the crack growth calculation, the starting crack length for this type of structure is set to the initial flaw size.

- *Step 17 – Scatter factor on crack growth period for threshold determination*

See chapter 3.22.

- *Step 18 – SDC requirement*

See chapter 3.24.

- *Step 19 – Comparison of critical crack length with SDC requirement*

The critical crack length is one result of Step 13. If this critical crack length is equal or greater as the SDC requirement (two-bay crack or other length), the procedure is continued with Step 21. Otherwise the procedure is continued with Step 20.

- *Step 20 – Check for reinforcement / modification*

Although the SDC requirement is checked during the pre-development/development/design phase (see chapters 3.24 and 3.25), it may occur, that in exceptional cases the SDC requirement is not met according to the residual strength analysis during the certification phase. Reasons may be e.g. increase of static loads and/or late design changes.

Since the SDC requirement (including the two-bay-crack criterion) is not included in the regulations up to now, it is up to the manufacturer to decide, whether the calculated critical crack length can be accepted considering all circumstances. A relaxation of the manufacturer's design goal may be acceptable, if the structural integrity of the aircraft is not compromised and the SDC requirements are fulfilled. Otherwise structural actions have to be considered.

If a new analysis becomes necessary, the procedure is continued with Step 4.

- *Step 21 – Susceptibility to MSD / MED*

See chapter 3.9.

- *Step 22 – Crack growth and residual strength analysis of structure containing MSD / MED*

See chapter 3.27.

- *Step 23 – Scatter factors for MSD / MED susceptible structure*

See chapter 3.28.

- *Step 24 – Compilation of results from residual strength and crack growth analysis*

The following results are needed for the certification of the damage tolerant structure:

- Critical crack length
- Inspection interval
- Inspection threshold based on initial flaw concept – for single load path structure and certain type of multiple load path structure
- Inspection interval to detect MSD/MED cracking – for damage tolerant structure, which is susceptible to MSD/MED
- Structural modification point – for damage tolerant structure, which is susceptible to MSD/MED

- *Step 25 – Compilation of all results*

The results of the fatigue life analysis (see Step 11) and from the residual strength and crack growth analysis (see Step 24) are to be compiled in the required certification documents.

- *Step 26 – Analysis of further items*

See chapter 3.40.

14.13.7. FFS procedure for in-service phase

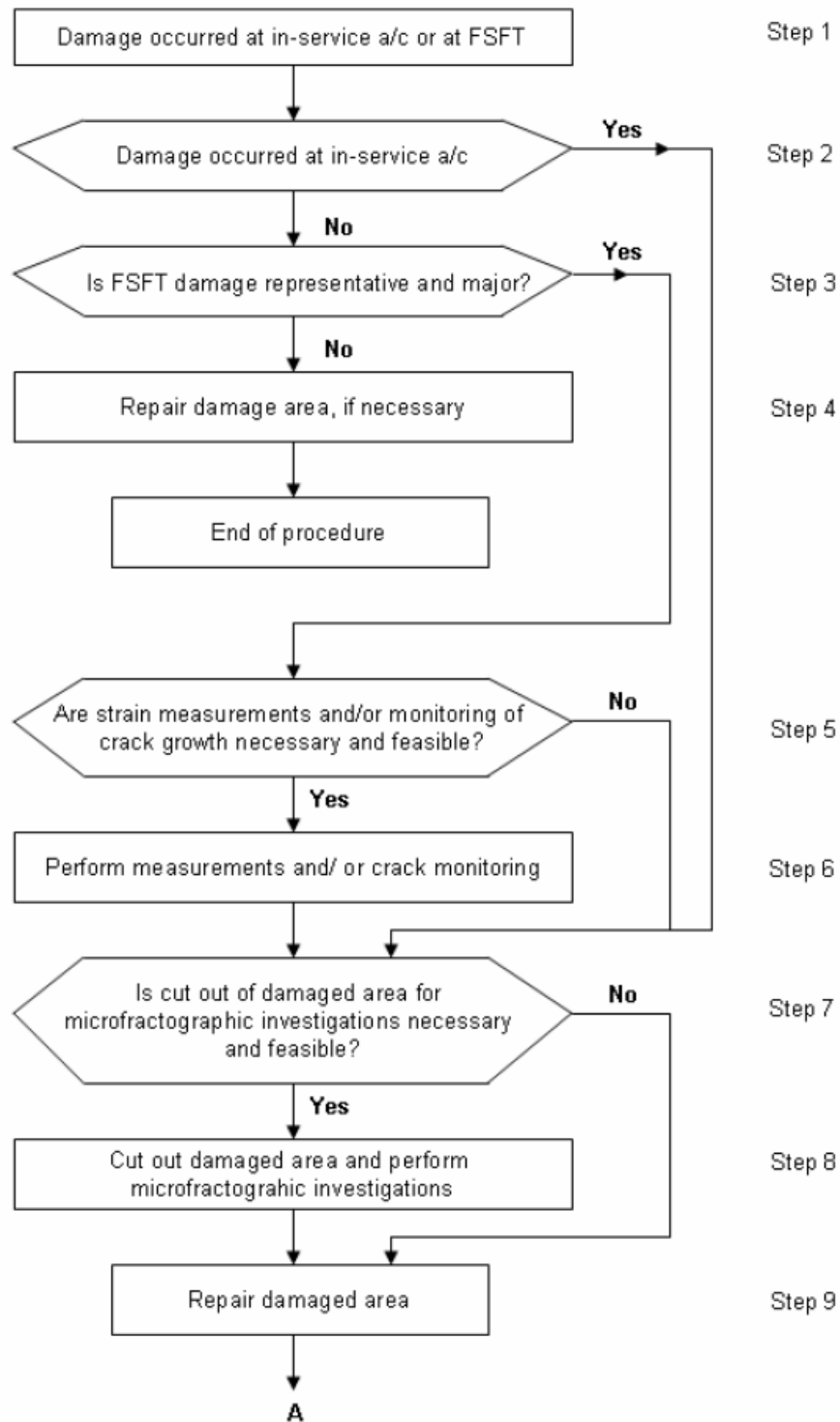


Figure 14.73 – Flow chart for overall F&DT procedure during in-service phase - part 1 -

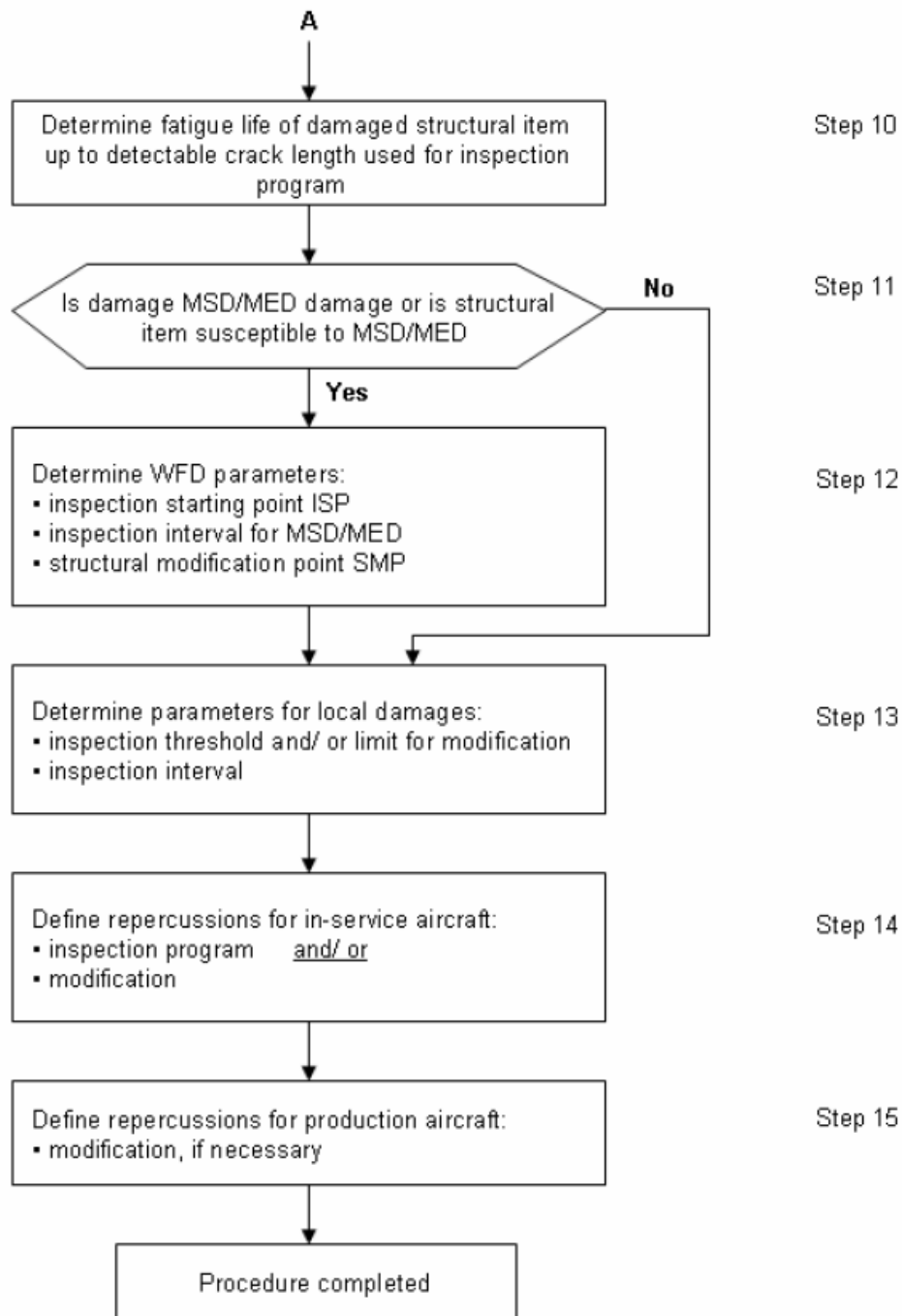


Figure 14.73 – Flow chart for overall F&DT procedure during in-service phase - part 2 –

F&DT evaluations are performed for areas with major damages detected at full scale fatigue test (FSFT) specimens and at in-service aircraft. The objective of these investigations is to define the repercussions on the in-service aircraft and on the production aircraft. The repercussions may be an update of the inspection requirements and/or structural modifications depending on the severity of the detected damage. In contrast to the pre-development/ development/design phase

and the certification phase the starting point for the procedure is a real damage instead of a postulated damage.

- Step 1 – Occurrence of damage

Damages may be detected at in-service aircraft as well as during the FSFT. Different types of damages occur at in-service aircraft, such as scratches, dents, corrosion and cracks. The procedure described by this chapter is applicable mainly to cracks or similar damages, which occur due to fatigue. Damages, which are clearly resulting from accidental events, e.g. ground handling, runway debris, etc., are repaired and not treated according to the described procedure. Corrosion damages are also not treated by this procedure, but require a specific one. At FSFT specimens the damages are generally resulting from fatigue.

As far as the FSFT is concerned, the phase described in this chapter starts already prior to time of certification. Generally the FSFT starts prior to certification of the aircraft, and it is agreed between the manufacturer and the Airworthiness Authorities to simulate a certain number of flights prior to certification. In praxis this are the number of flights, which are accumulated in a two-year's operation for the aircraft type tested, multiplied by a scatter factor of five. The scatter factor of five is applied, since during the first two years of operation no detailed inspections for fatigue purposes are planned at the in-service aircraft. Therefore the scatter factor for threshold determination based on fatigue life is applied, see chapter 3.6.

- Step 2 – Damage occurred at in-service a/c or at FSFT

Besides the damages, which occur at aircraft during in-service operation, the results of full scale fatigue tests are important information about the F&DT behaviour of the structure. FSFTs are performed with the structure of a complete aircraft or in several parts as a so-called multi-section test. An example of such a test is shown in Figure 14.74.

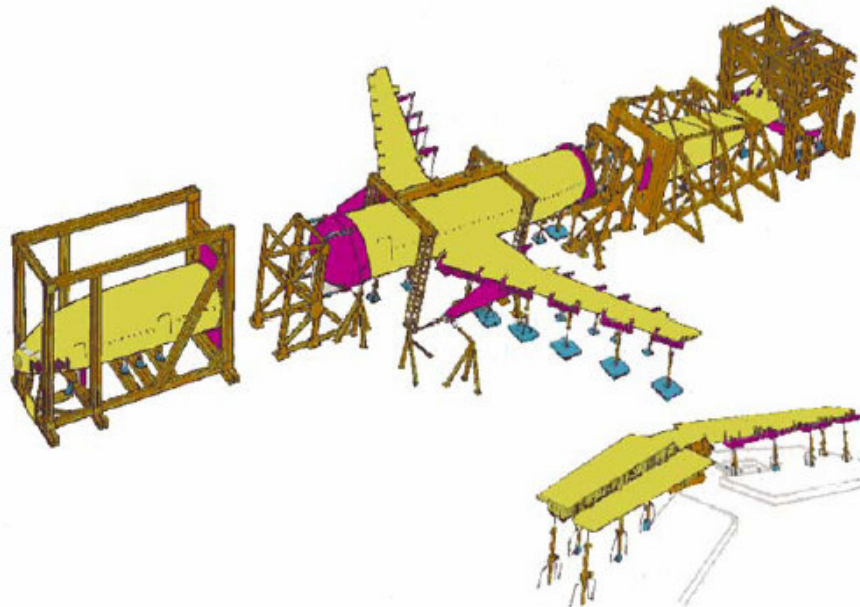


Figure 14.74 – Example of multi-section full scale fatigue test (Airbus A300)

The major goals of a FSFT are:

- Validation of crack initiation life
- Validation of the predicted fatigue and crack growth behaviour
- Establishment of in-service structural inspection program
- Detection of areas of early local cracking
- Demonstration that the structure is free from significant MSD/MED up to the DSG
- Validation of the structural damage capability
- Validation of the global and local stresses
- Validation of NDI procedures
- Validation of fatigue lives of typical major repair solutions, reworks and dents

For damages occurred at FSFT the procedure is continued with Step 3.

For damages occurred at in-service aircraft the procedure is continued with Step 7.

- Step 3 – Classification of FSFT damage

The procedure described in this chapter is applied to representative, major FSFT damages. First of all it has to be checked, if the damaged structure is representative for the series aircraft. FSFT specimens include non-series structure, e.g. for load introduction purposes. Damages occurring at the non-series structure do not need to be treated by the procedure described. Furthermore, some damages may be classified as minor damage, because they are of low importance to the structural integrity, e.g. small damages. Examples of minor damages are single broken rivet heads and small cracks with negligible crack growth, which do not degrade the strength of the structure below the required limit. All other damages are classified as major. For representative major damages the procedure is continued with Step 5.

- Step 4 – Repair of non-representative damages

Even if a damage is classified as non-representative, a repair may be necessary in order to allow continuation of the test, e.g. to allow load introduction.

- Step 5 – Check for measurements / monitoring at FSFT

In order to gain more information about the damaged structure strain measurements and/or crack monitoring may be performed at the FSFT specimen. In the majority of the cases the structure is available twice at the specimen, e.g. LH and RH side of fuselage, LH and RH wing. If one side is still undamaged, strain measurements could be performed at the intact structure for validation or adaptation of the local FEM analysis. If no strain measurements are possible, the local FEM analysis has to be checked for applicability or a refinement has to be performed. Furthermore, crack growth monitoring provides important information, especially in case of complex structure. The results allow the validation or adaptation of the crack growth analysis, especially the stress intensity factor solution.

- Step 6 – Measurements / monitoring at FSFT

The strain measurements are generally performed for a few selected load cases, e.g. fuselage differential cabin pressure, steady load conditions (1g) and representative incremental loads of the spectrum (gust, manoeuvre, landing, etc.). In some cases it might be useful to measure also strains in structure adjacent to the damaged area in order to get information about load redistribution after cracking.

Crack monitoring is done by inspections in defined intervals and/or by application of crack sensors such as crack wires. The crack monitoring has to be stopped sufficiently before the crack could reach the critical crack length, in order not to jeopardize the specimen.

- Step 7 – Check for microfractographic investigations

In order to gain more information about the damaged structure microfractographic investigations may be good means, especially to get information about the origin of the fatigue crack and the crack growth behaviour.

In general microfractographic investigations are necessary in case of MSD cracking. The investigation allows the detection of small cracks, which have not been detected by the inspection methods applied at the in-service aircraft or the FSFT specimen. This leads to the full information about the MSD status of the damaged area. For areas of local damages the microfractographic investigations are necessary in exceptional cases only.

Furthermore, it has to be checked, that the cut-out the damaged area may complicate the subsequent repair.

- Step 8 – Microfractographic investigations

In case of an in-service damage the operator has to be approached for delivery of the damaged part. The microfractographic investigation is performed mainly by the manufacturer.

- Step 9 – Repair

In general all damaged structure has to be repaired. This is done under all circumstances at in-service aircraft using the instructions available in the Structural Repair Manual (SRM) or according special instructions provided by the aircraft manufacturer.

Major damages at FSFT are either repaired immediately after damage detection or after completion of strain measurements and/or crack monitoring, see Step 6. Non-critical damages occurring late in the test are not repaired. For damaged area at the FSFT specimen SRM instructions are only available for selected locations. For other locations the manufacturer provides the repairs instructions and/or performs the repair.

- Step 10 – Fatigue life up to detectable crack length

In Steps 12 to 15 the repercussions of the damage on the in-service aircraft and on the production aircraft are defined. The interpretation of the damages includes F&DT evaluations, which are similar to FFS procedure applied during the certification phase. The test fatigue life of the damaged structure needs to be extrapolated to the detectable crack length. The detectable crack length is defined as that crack length, which may be detected when using the relevant inspection method of the structural inspection program (SIP) for the structural item under consideration.

The recalculation of the life up to detectable crack length is done using the F&DT methods described in chapter 3. Furthermore, the results of the strain measurements, the crack growth monitoring and the microfractographic investigation are considered as far as available.

- Step 11 – Susceptibility to MSD / MED

See chapter 3.9.

Furthermore, if the damage detected is of MSD/MED nature, the structural item should be categorized as susceptible to MSD/MED.

- Step 12 – Determination of WFD parameters

In order to define the repercussions of the damage the WFD parameters have to be determined, if the structural item is susceptible to MSD/MED or this damage type has been detected:

- Inspection starting point ISP
- Inspection interval for MSD/MED $I_{MSD/MED}$
- Structural modification point SMP

The calculation of the WFD parameters is done using the method described in chapter 3. Furthermore, the results of the strain measurements, the crack growth monitoring and the microfractographic investigation are considered as far as available. The scatter factors to be applied are the same as given in chapter 3:

- Inspection Starting Point: $ISP = WFD_{\text{average behavior}} / 3$
- Inspection interval for MSD/MED:
 - Structure with low scatter of operational loads: $I_{MSD} = n_{MSD} / 2$
 - Structure with larger scatter of operational loads: $I_{MSD} = n_{MSD} / 2.5$
- Structural Modification Point: $SMP = WFD_{\text{average behavior}} / 2$

In addition to the three parameters given above the inspection method has to be defined, which is used to fulfil the inspection interval.

- Step 13 – Determination of parameters for local damages

In order to define the repercussions of local damages the following parameters have to be defined:

- Safe life structure:
 - Life limit for introduction of modification or replacement
- Damage tolerant structure:
 - Inspection threshold or limit for introduction of modification
 - Inspection interval

The application of the different parameters and the possibilities for repercussions are explained in detail in chapter 5.14 and 5.15.

The calculation of these parameters is done using the F&DT method described in chapter 3. Furthermore, the results of the strain measurements, the crack growth monitoring and the

microfractographic investigation are considered as far as available. The scatter factors to be applied are:

- Safe life structure – life limit:
$$N_{\text{limit}} = N_{\text{test}} / SF$$

where N_{test} is fatigue life obtained in FSFT and SF is the scatter factor for safe life item according to AC 25.571-1C, see [14.44]

- Damage tolerant structure:
$$TH_{\text{mod}} = TH_{\text{insp}} = N_{\text{det}} / 3$$

where N_{det} is the fatigue life up to detectable crack length resulting from damage at in- service aircraft or FSFT specimen.

Inspection interval:

- Single load path structure:
$$I = n / 3$$
- Multiple load path structure with low scatter of operational loads:
$$I = n / 2$$
- Multiple load path structure with larger scatter of operational loads:
$$I = n / 2.5$$

where n is the crack growth period between detectable and critical crack length.

In addition to the parameters given above the inspection method, which is to be used to fulfil the inspection interval, has to be defined (if inspection is applicable). The parameters for local damages are also determined for structural items susceptible to MSD/MED, since a local damage may occur at any time, also in areas susceptible to MSD/MED.

- Step 14 – Repercussion for in-service aircraft

As a consequence of major damages occurred at in-service aircraft or representative, major damages detected at FSFT specimen, repercussions for the fleet in operation have to be defined by the manufacturer in agreement with the Airworthiness Authorities (AA). Depending on the type of structure the following possibilities exist:

Safe life structure:

- The airworthiness of safe life structure is based on the safe fatigue life. Damage tolerance characteristics and inspections do (by definition) not contribute to the airworthiness. Therefore the structural item has to be replaced by a new part latest at the defined life limit N_{limit} , see chapter 5.13.
- If an improvement of the fatigue life is possible by an easy modification such as cold expansion, interference fit of bolts and bushes, etc., is possible, this action has to be performed in the first phase of the life to limit the pre-fatigue damage. This may prevent the establishment of a life limit for the original structure.

Damage tolerant structure – susceptible to local damages:

- Mandatory retro-modification to be installed latest at TH_{mod} .

This alternative is generally chosen by the manufacturer, if one or more of the following conditions apply:

- Failure of the structural item has a significant impact on the structural integrity of the airplane.
- Damage occurred relatively early during FSFT or during in-service.

The modification is defined by the manufacturer. The manufacturer recommends to the AA to render the modification as mandatory. The AA classifies the retro-modification as mandatory. The documentation for the modification is issued in a so-called Service Bulletin (SB), also called Modification Service Bulletin (MSB).

- Recommended retro-modification to be installed latest at TH_{mod} or mandatory inspection program to be started latest at TH_{insp} . and to be performed in intervals I.

This alternative is chosen by the manufacturer, if the conditions described above do not apply. Since inspections are an additional burden for the operators and the necessary repairs may cause unscheduled down times, the manufacturer offers an alternative retro-modification. The airworthiness of the aircraft can be ensured by inspections, but it is probably more economic to perform the modification. It is up to the operators to choose either the modification or the inspections.

The modification is defined in a SB or MSB. The documentation for the inspections is either given in a so-called Inspection Service Bulletin (ISB) or given in the MPD. The ISB is classified by the AA as mandatory. If the inspection is defined in the MPD, the task has also to be listed in the Airworthiness limitation Section (ALS) of the Instructions for Continued Airworthiness (ICA), i.e. status of the inspection requirement is also mandatory.

- Mandatory inspection program to be started latest at TH_{insp} . and to be performed in intervals I.

This alternative is chosen by the manufacturer, if the risk of damage within the DSG is low. Therefore the installation of a modification would not be adequate from the economic point of view. Also in this alternative the airworthiness of the aircraft is ensured by mandatory inspections, documented in an ISB or in the MPD as described for the previous alternative.

Damage tolerant structure – susceptible to MSD/MED:

- Mandatory inspection program to be started latest at ISP and to be performed in intervals IMSD and mandatory repair, modification or replacement latest at SMP.

This procedure is required by regulation and the AC 91-56A, see [14.48]. The inspection program and the modification will be classified as mandatory by the AA.

Furthermore the manufacturer may recommend a modification to be performed at $TH_{mod} \leq ISP$, which leads to the deletion of further maintenance actions. If this is preferable from the economic point of view the operator could choose this alternative.

- Step 15 – Repercussion for production aircraft

It is common standard to launch production modifications to improve the F&DT characteristics of the structure in order to reduce the burden on the operators for inspection and retro-modification activities at in-service aircraft.

In cases, where the damage occurred very late during a FSFT requiring only one or a few inspections at the in-service aircraft, or if the inspections are covered by inspection tasks already defined in the MPD, no modification is introduced in the production line.

14.13.8. FFS procedure for in-service—Life extension phase

The DSG established during the development of a new aircraft type is no operational limit for in-service aircraft. However, the original structural inspection program is only valid up to the DSG. It is common practice to allow a further operation beyond DSG to a certain extent.

During life extension activities the FFS procedure is similar to that of the certification phase, since the objective is to extend the operation of the aircraft beyond the design service goal, while maintaining the reliability of the structure. This objective is reached by defining the structural inspection and maintenance program for the operation beyond the DSG up to the envisaged extended service goal (ESG). The tasks of the existing maintenance program are validated or modified and new tasks are defined as far as necessary.

For determination of the relevant parameters, such as threshold, intervals, ISP and SMP, the same procedures and methods as described in chapters 3 and 4 are applied. However, more experience is available from FSFTs, which are generally completed after type certification, and from in-service. So-called tear down inspections (dismantling of the structure with subsequent NDI inspections) at the end of FSFT provide significant information about the F&DT behavior of high-time aircraft. This experience is considered when defining the updated maintenance program. Furthermore the results of the certification analyses are available. If necessary, new F&DT tests are performed.

The application of this information is presented in Figure 14.75 for postulated and real local damages and in Figure 14.76 for postulated and real MSD/MED.

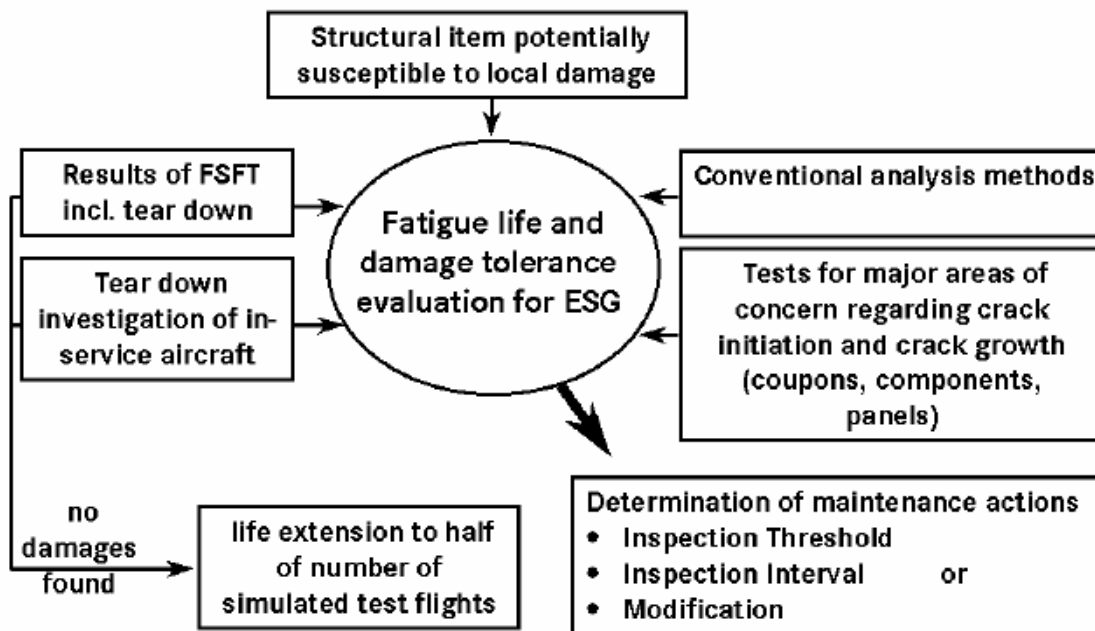


Figure 14.75 – Evaluation of structure susceptible to local damages for life extension

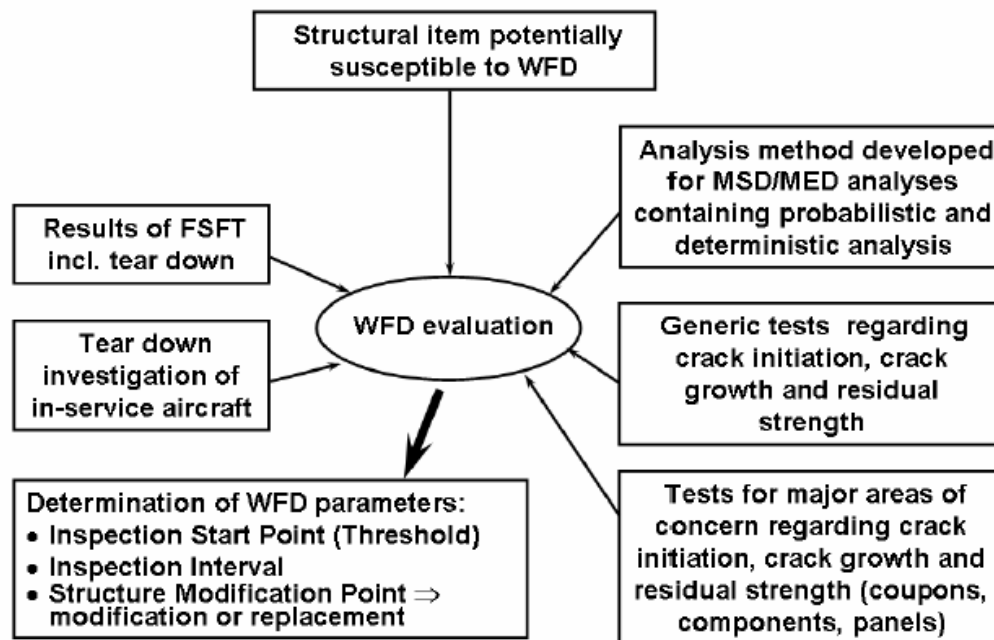


Figure 14.76 – Evaluation of structure susceptible to MSD/MED for life extension

14.13.9. Bibliography

- [14.42] Material supplied by H.J. Schmidt and B. Schmidt-Brandecker.
- [14.43] N.N., Damage tolerance and fatigue evaluation of structure, FAR 25.571 Amendment 96
- [14.44] N.N., Damage tolerance and fatigue evaluation of structure, AC 25.571-1C
- [14.45] N.N., Damage tolerance and fatigue evaluation of structure, draft rule 25.571
- [14.46] N.N., Damage tolerance and fatigue evaluation of structure, Draft AC 25.571-1x
- [14.47] Schmidt, H.-J., Damage tolerance technology for current and future aircraft structure, Plantema Memorial Lecture presented to the 23rd ICAF Symposium, Hamburg, Germany, June 2005
- [14.48] N.N., Continuing structural integrity program for large transport category airplanes, AC 91-56A
- [14.49] N.N., Instructions for continued airworthiness, FAR 25.571 Amendment 54
- [14.50] Swift, T., Verification of methods for damage tolerance evaluation of aircraft structures to FAA requirements, presented to 12th ICAF Symposium, Toulouse, France, May 1983
- [14.51] N Swift, T., Course in damage tolerance technology – stress analysis oriented fracture mechanics, Phase I & II, Federal Aviation Administration (unpublished)